Alma Mater Studiorum – Università di Bologna

DOTTORATO DI RICERCA IN

INGEGNERIA BIOMEDICA, ELETTRICA E DEI SISTEMI

Ciclo 33°

Settore Concorsuale: 09/E4 - MISURE

Settore Scientifico Disciplinare: ING-INF/07 – MISURE ELETTRICHE ED ELETTRONICHE

DEVELOPMENT AND METROLOGICAL CHARACTERIZATION OF MEASURING INSTRUMENTS FOR LOW-VOLTAGE NETWORKS MONITORING

Presentata da: Lorenzo Bartolomei

Coordinatore Dottorato

Prof. Michele Monaci

Supervisore

Prof. Lorenzo Peretto

Co-supervisore

Prof. Carlo Alberto Nucci

Esame finale anno 2021

Abstract

This thesis, written at the end of a 3-year PhD course, collects the main results about my research and the work related to the designing of monitoring systems of low-voltage distribution networks. In fact, my PhD course was industrial type and totally supported and financed by REPL Italia srl, that employed me with a high apprenticeship contract.
Despite the very applicative nature of my course, there were several scientific results which provide a small contribution in the development of innovative techniques and new standards for the metrological characterization of monitoring instruments and energy meters for low-voltage applications.
The first three chapters provide an overview on different topics. The first one describes the main concepts contained in the guide for the evaluation of measurement uncertainty (also called GUM), since some of them are recalled in the next sections.
Chapter 2 provides the main notions on the smart grid concept, the new generation of distribution networks characterized by a high degree of automation, and on the main power quality problems affecting the grids. Therefore, the following standard, connected to the above topics, are presented:

- EN 50160 on the voltage waveform.
- IEEE 519 on the assessment of the harmonics.
- IEC 61000-4-7 on the minimum requirement for the power quality monitoring instruments.

Finally, chapter 3 presents a general description of the main sensors suitable for the LV monitoring systems for the acquisition of voltage and current waveforms, providing information on the working principles, the metrological performances and recalling the related standards (as the IEC 61869).
Chapter 4 gets to the heart of the work done in my PhD course; in fact, the two monitoring devices specifically developed to meet the needs of the future smart grids are presented: the Guardian Meter and the Network Monitoring Unit. Hence, information is provided on the purposes of each device, on their technical characteristics, on the tests conducted for the metrological characterization and on the results related to measurement performance.
It is noteworthy that the testing activity has led to the development of procedures, some of which innovative, for the metrological evaluation of monitoring devices. In fact, the last chapter collects the scientific outcomes deriving from the R&D activity which, as already mentioned above, can be the starting points for the updating of current standards related to monitoring systems and for the development of new procedures to evaluate the metrological performance of the energy meters.

Index

	page
1. The basis of metrology: the "GUM"	6
1.1 From error to uncertainty	6
1.2 standard uncertainty	6
1.2.1 Statistical evaluation of uncertainty	7
1.2.2 Combining standard uncertainty	8
1.3 Indirect measurements	8
1.4 Monte Carlo Method	9
2. Smart grids and power quality	11
2.1 What is a smart grid	11
2.1.1 Overview	11
2.1.2 Automation features of a smart grid	11
2.2 the importance of the measurements on power networks	12
2.2.1 Low cost measurement systems for LV grids	14
2.3 Power quality	16
2.3.1 IEEE 514 standard	16
2.3.2 EN 50160 standard	19
2.3.2.1 Nominal values	19
2.3.2.2 Phenomena	19
2.3.3 IEC 61000-4-30 standard	24
2.3.3.1 Interruption evaluation	25
2.3.3.2 Voltage harmonics evaluation	26
3. Sensors for LV monitoring systems	27
3.1 Current sensors	27
3.1.1 Shunt	27
3.1.2 Current transformer	28
3.1.3 Rogowski coil	30
3.1.4 Hall effect current sensor	32
3.2 Voltage sensors	34
3.2.1 Dividers	34
3.2.2 Hall effect voltage sensor	35
4. Design and Development of Measurement instruments	38
4.1 The Guardian Meter	39
4.1.1 Purpose of the instrument	39
4.1.2 Instrument description	41
4.1.2.1 A brief overview on power line communication	44
4.1.3 Metrological characterization	46
4.1.3.1 Measure of instantaneous parameters	46
4.1.3.2 Measure of energies	49
4.1.3.3 Evaluation of the results	50

4.2 The Network Monitoring Unit 51
4.2.1 Purpose of the instrument 51
4.2.2 Instrument description 52
4.2.3 Metrological characterization 58
4.2.3.1 Measure of instantaneous parameters 58
4.2.3.2 Measure of energies 63
4.2.3.3 Metrological performance vs temperature 64
4.2.3.4 metrological performance with realistic distorted voltages and currents 66
4.2.3.5 evaluation of the results 67
5. Experimental activities and Scientific results (scientific outcomes from the developed products) 68
5.1 Accuracy verification of a Low cost PLL-Based Acquisition System 68
5.1.1 Introduction 68
5.1.2 Spectral leakage 69
5.1.2.1 Definition 69
5.1.2.2 Methods for leakage error reduction 71
5.1.3 Acquisition board 71
5.1.4 System evaluation tests 73
5.1.4.1 Setup 73
5.1.4.2 Amplitude characterization 74
5.1.4.3 Amplitude vs. frequency characterization 75
5.1.4.4 Amplitude vs. harmonic components characterization 75
5.1.4.5 Windowing test 75
5.1.5 Results 75
5.1.5.1 AS evaluation 76
5.1.5.2 Data acquisition systems comparison 78
5.1.5.3 Economic analysis 83
5.1.6 Conclusions 84
5.2 Performance evaluation of an energy meter for low-voltage system monitoring 85
5.2.1 The energy meter 85
5.2.2 Measurement setup 86
5.2.3 Results and discussion 87
5.2.4 Conclusions 89
5.3 Testing of electrical energy meters in off-nominal frequency conditions 90
5.3.1 Introduction 90
5.3.2 Regulatory context 91
5.3.3 Measurement system description 94
5.3.4 Experimental tests 95
5.3.4.1 Sinusoidal current and voltage-calibration measurement 95
5.3.4.2 Fixed random harmonics 96
5.3.4.3 Random time-varying harmonic distorsion 97

5.3.5 Experimental results 97
5.3.5.1 Sinusoidal current and voltage-calibration measurement 97
5.3.5.2 Fixed random harmonics 98
5.3.5.3 Random time-varying harmonic distorsion 99
5.3.6 Conclusions 100
6. Conclusions 101
7. Bibliography 103
8. List of figures 110
9. List of tables 113
10. List of acronyms 115

1. The basis of metrology: the “GUM”

One of the most important references for metrologists is the "Guide to the expression of uncertainty in measurement" [1] . Issued to cover the lack of international consensus, the document provides the basis for the assessment of uncertainty and the comparison of measurement results.
The goal of this chapter is to recall the basic concepts reported in the guide, that will be fundamental in understanding the metrological aspects mentioned and treated in the next sections.

1.1 From error to uncertainty

As it is well known, it is mandatory to express the result of a measurement together with an indication about its quality and reliability, so that a comparison can be made with other measures carried out, for example, with a different equipment.
For a long time, this parameter has been identified with the concept of "error of measurement", that presupposed theoretically the knowledge of the "true value" on which to calculate the deviation; since this is not knowable in almost all cases, the scientific community has moved on to the probabilistic concept of "uncertainty", which defines a confidence interval in which we have a certain probability of finding the real value of the measurand.

A list of contributions to uncertainty is provided by the GUM. Some of these are:

- Incomplete definition of the measurand
- Imperfect realization of the definition of the measurand
- Measured sample not representative of the measurand
- Lack of knowledge of environmental conditions
- Bias in the reading of analogic instruments
- Variation of the measurand during repeated measurements with apparent identical conditions
- Finite resolution of the instrumentation
- Not perfect instruments calibration

1.2 Standard uncertainty

The GUM treats uncertainty in a probabilistic way defining the "standard uncertainty" (expressed as a standard deviation). This has two contributions:

- Type A standard uncertainty: quantity calculated with classical statistic method, using the concepts of average and variance.
- Type B standard uncertainty: expressed as standard deviation but obtained with a scientific evaluation of all available information about measurand variability. For instance, they are considered:
    - Past measurement results
    - Personnel experience
    - Instruments specification

Considering the traditional subdivision of the contributions to the measurement error composed of random errors and systematic errors, it can be affirmed that the former contribution is evaluated through type A uncertainty and the latter through type B uncertainty.

1.2.1 Statistical evaluation on uncertainty

In order to evaluate the type A uncertainty, it is necessary to repeat the measurements a certain number of times applying the statistical concept of "standard deviation", which estimates the dispersion of the samples.
Assuming to have n values of a certain quantity (for example, n measures of the same measurand), their standard deviation is defined as:

$$s(x) = \sqrt{\frac{\sum_{i=1}^{n}(x_i - \bar{x})^2}{n-1}} \tag{1.1}$$

- x_i : sample of the quantity
- $\bar{x}$: average value.

Although the distribution of the values is not Gaussian, considering the central limit theorem it can be assumed that the distribution of the sample averages will follow a normal PDF and, therefore, its standard deviation can be estimated according to the following relationship:

$$s(\bar{x}) \sim \frac{s(x)}{\sqrt{n}} \tag{1.2}$$

- *s:* standard deviation
- *n:* number of values

Regarding the contributions to type B uncertainty, the GUM requires that they are treated as random variables, although they are often generated by systematic effects. In case the associated PDFs are not known (most frequent case), uniform distributions must be considered by virtue of the principle of maximum entropy, calculating the standard deviation in this way:

$$s(x) = \frac{\Delta G}{\sqrt{3}} \tag{1.3}$$

- ΔG: half-amplitude of the variability interval.

Generally, the manufacturers of the instruments provide some indexes that allow to evaluate the error on the measurement caused by the equipment itself (and which composes the type B uncertainty). The most used indexes are:

- Reading error index (or gain error) % L: component proportional to the size of the measurand
- Non-linearity (or full scale) error index % FS: constant component, independent from the measurand, which allows to calculate the maximum deviation (given by the

instrumentation) between the input quantity and the output reading. This is generally normalized according to the full-scale value.

Considering the previous relation, the standard uncertainty of type B can be expressed in most cases as (G is the measurand):

$$s_b(x) = \frac{\frac{(\%L*G)}{100} + \frac{\%FS*G_{FS}}{100}}{\sqrt{3}} \tag{1.4}$$

- s_b : standard uncertainty of type B

1.2.2 Combining standard uncertainty

To consider all components, the uncertainty associated with each measure is given by the sum of the type A and type B uncertainty.
Furthermore, considering that the PDF of the sample average is Gaussian for the central limit theorem, a "confidence interval" with a certain probability of finding the average values of the measurand's estimation can be defined. Therefore, The GUM introduces the concept of "extended uncertainty", given by the product between the total standard uncertainty and a coverage factor k, which can usually vary between 1 and 3 (for confidence intervals ranging from 68% to over 99%).
Hence, the correct way to describe the result of a measurement is:

$$G = \bar{x} \pm k\sqrt{({s_a}^2 + {s_b}^2)} \tag{1.5}$$

- G : quantity considered
- $\bar{x}$: average value of the repeated measures
- k : coverage factor
- s_a : standard uncertainty of type A
- s_b : standard uncertainty of type B

1.3 Indirect measurements

If a quantity Y is calculated indirectly through the measurement of others, a function *f* describing their relationship can be defined.

$$y = f(x_1, x_2, x_3, x_4, \ldots . x_n) \tag{1.6}$$

- x_i : measurements

In order to associate an uncertainty to y, it is possible to combine the various uncertainties evaluated on the quantities $x_1 \ldots x_n$. In some cases the combination is easy calculable:

- Indirect quantity calculated by adding or subtracting quantities

$$s_y = \sqrt{{s_{x1}}^2 + {s_{x2}}^2 + {s_{x3}}^2 + \ldots + {s_{xn}}^2} \tag{1.7}$$

  - s_i : standard uncertainty

- Indirect quantity calculated by product or quotient of quantities

$$s_y = y * \sqrt{\left(\frac{{s_{x1}}^2}{x_0}\right) + \left(\frac{{s_{x2}}^2}{x_2}\right) + \left(\frac{{s_{x3}}^2}{x_3}\right) + \ldots + \left(\frac{{s_{xn}}^2}{x_n}\right)} \tag{1.8}$$

For all other cases, the GUM defines a general formula which presupposes to know precisely, in addition to f, also the distributions of the quantities on which y depends and the correlations each other:

$$s_y = \sqrt{\sum_{i=1}^{n} \left(\frac{\partial f}{\partial x_i}\right)^2 {s_{xi}}^2 + 2 \sum_{i=1}^{n-1} \sum_{j=i+1}^{n} \frac{\partial f}{\partial x_i} \frac{\partial f}{\partial x_j} \; r(x_i, x_j) \, s_{xi} \, s_{xj}} \tag{1.9}$$

  - r : covariance.

If the quantities are not correlated each other, the formulation is reduced to:

$$s_y = \sqrt{\sum_{i=1}^{n} \left(\frac{\partial f}{\partial x_i}\right)^2 {s_{xi}}^2} \tag{1.10}$$

1.4 Monte Carlo Method

Often it is complicated to evaluate the uncertainty associated with an indirect quantity through the propagation law described in the previous paragraph, for example due to the difficulty of representing the measurement model or if the PDFs associated with the quantities are very different from a Gaussian curve. In these cases, it is possible to apply the prescriptions of GUM Supplement 1 [2], which describes the "Monte Carlo" method based on the concept of propagation of distributions.
For its application, the steps to follow are:

- Defining the output quantity y and the input quantities x_i
- Developing a model that relates y to x_i
- Assigning the PDF to the x_i, on the base of the available information
- Through the developed model, propagating the PDF of the variables to obtain the PDF of y
  - Generating *m* samples of each x_i
  - Through the model, calculating *m* values of y
  - Ordinating the obtained values in ascending order

- Thought estimated PDF, calculating average value, standard deviation and coverage interval of y

Before applying this method, it is necessary verifying the following hypothesis:

- The number of extracted values must be sufficiently high (it is recommended to consider a number much greater than 1/(1-p), where p is the coverage probability)
- The PDF of y must be continuous in the interval where it is strictly positive, unimodal, strictly increasing to the left of the mode and strictly decreasing to the right of the mode
- The expected value and the variance exist
- Distribution function of y continuous and strictly increasing

At operative level, it is possible to use an adaptive procedure for *m* calculation, repeating the Monte Carlo method more times increasing gradually *m* until the results do not differ each other more than a quantity reputed acceptable.

2. Smart grids and power quality

The first part of this chapter provides some basic information on new generation distribution networks, of which LV networks and their monitoring systems are an integral part.
Then, the second part is dedicated to the description of the main power quality problems affecting the distribution networks and how to monitor and to assess these phenomena.

2.1 What is a smart grid

2.1.1 Overview

In recent years we have witnessed a large increase in electrical energy production systems from sustainable and renewable sources, mainly to reduce the atmospheric emissions of pollutants. Due to the different nature of these sources and especially for their low programmability, active power grids that can adapt themselves automatically to optimize their contribution are necessary. Mainly for this reason are rising the "smart grids, which are defined as (by the "Smart Grid European Technology Platform"): "an electrical network that can intelligently integrate the actions of all users connected to it. Generators, consumers and those that do both, in order to efficiently deliver sustainable, economic and secure electricity supply". [4]
To implement these networks is necessary to support the traditional power grid with a capillary monitoring system, a telecommunication infrastructure, and an automation system.
The objectives of the smart grids are [3]:

- Increase the reliability of the system
- Facilitate the integration of distributed generation (generally from renewable sources)
- Provide a better service and a greater control to the customers

Furthermore, in a scenario where a progressive increase of electric mobility is expected, the technological evolution of the network becomes indispensable.

2.1.2 Automation features of a smart grid

The smart grid is active especially in the automatic management of distributed generation, through the help of the so-called "active network management system", which take advantage of real-time communication and the automation infrastructure in order to manage in every moment the setting of the network.
The main automation features that can be attributed to smart grids are:

- Fault and Stability Diagnosis: it is possible to analyse faults automatically and locate them more easily, in order to better plan maintenance on the network, speed up interventions and increase the stability.

- Reactive power control: the constant control on the reactive power allows to act automatically for its reduction, in order to decrease the losses due to the greater circulating currents.
- Distributed Generation for Emergency: the complete management of the distributed generators allows to connect and disconnect them dynamically, to make up for any shortcomings of the traditional generation systems.
- Network Reconfiguration: in case of need, the smart grids can quickly reconfigure thyself through the control of all the circuit-breakers and disconnectors installed, allowing, for example, the rapid re-powering of an isolated section (for example, due to a fault).
- System Restoration: in the event of transient faults, the network is able to automatically restore the electrical energy distribution.
- Demand Side Management: customers management is entrusted to smart meters, energy meters with advanced control and measurement functions connected to the communication infrastructure through, normally, PLC technology (power line communication).

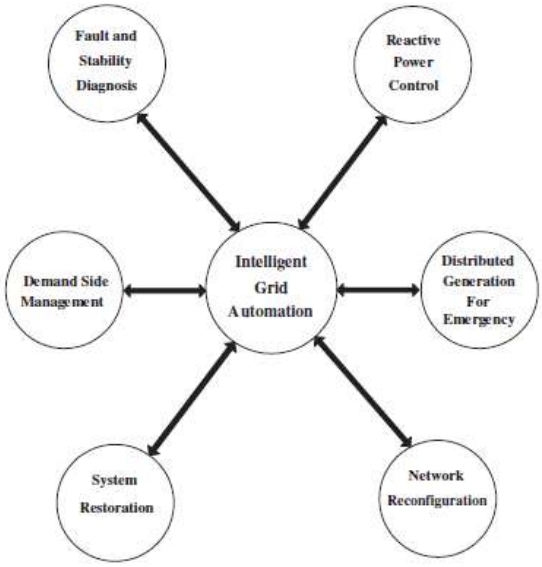

Figure 2.1 – automation functions of a smart grid

2.2 The importance of the measurements on power networks

The correct operation of a smart grid needs a huge dissemination of sensors and measurement systems to maintain control over itself [5][6].
For this reason, many utilities over the world are investing in remote smart meters, that permit to have in real-time:

- a correct knowledge of the energy flows
- a monitoring of the energy purchased by the distributed generators and sold to customers

However, to reach the objective to develop a real smart grid it is not enough to have these devices installed exclusively at the users, but it is necessary to install part of them in the key nodes of the network, also implementing some functions that allow them to measure all the main electrical parameters (in addition to the active energy).
Furthermore, to increase the reliability and keep to minimum the service interruptions, it is possible to use the measurement instrumentation for the "automatic power line fault location"; In fact, due to the capillarity of the grids (especially with regard to the low-voltage one), very often the outages can last for many hours with huge economic losses. A reduction of these times has then two main benefits:

- Saving of the money that utilities must pay to the authority or to the customers for fines imposed in proportion to the outages
- Lower human costs for "manual" fault location

Moreover, sometimes the outages are caused by transient phenomena which, after a short time, disappear. These phenomena occur randomly several times over time and, with classical fault location methods, it is very difficult to intervene to avoid them.
Monitoring systems capable to locate a fault at the time it occurs are, therefore, of strategic importance to prevent a high number of interruptions.
Hence, we can affirm that the reliability of the distribution system is strongly related to the quality, accuracy, and capillarity of the measurements.
Considering the availability of the service defined as

$$A(t) = \frac{MTBF}{MTBF+MTTR} \tag{2.1}$$

the new generation real-time monitoring systems can strongly intervene increasing the MTBF (mean time between failures) and reducing the MTTR (mean time to repair).
It is estimated that, with the adoption of this instrumentation, the price of energy could drop by up to 30 %.
The metrology experts become hence fundamental in the transition between traditional networks and smart grids, as they can provide a substantial contribution to increasing the efficiency of the networks.
In this way, some European utilities are investing in the installation of tools that allow fault location, such as the Italian RGDM ("rilevatore di guasto direzionale e misura", Figure 2.2) which has also voltage control and regulation functions at the delivery point. In this case, the communication between similar equipments and with the control room is managed through the IEC 61850 protocol, specifically designed for networks management.
As sensors, in case of installation in MV grids, this type of devices can work with the new generation LPIT ("low power instruments transformer", generally capacitive or resistive divider for voltage measurements and Rogowski coils for current measurements), very often fully integrated in the cable terminations (Figure 2.3). This solution allows to save the space that in the past had to be occupied by the traditional voltage and current transformers (Figure 2.4).

Figure 2.2 – RGDM

Figure 2.3 – smart terminations

Figure 2.4 – Smart termination installed in a MV/LV substation

2.2.1 Low-cost measurement systems for LV grids

To guarantee the huge dissemination of monitoring instruments needed for the management of the smart grids, it is necessary that their cost is acceptable. This concept is valid especially for the LV network, being the most widespread.
The lack of low-cost instrumentation makes that, even today, there are only few monitoring systems installed in the LV distribution grid, and normally these are located only in the secondary substations.
Considering that these networks were the first developed in the last century, often their exact topology is unknown, and the only secondary substations monitoring is not sufficient.
Fortunately, nowadays some companies (as REPL Italia) are investing in the development of low-cost systems that are suitable for installation in the electrical cabinets (preferably without putting these out of service), considering these objectives during the design:

- "non-technical losses" verification: often the DSOs do not know which customers are supplied from each secondary substation. Therefore, a widespread energy metering system is necessary to carry out the appropriate comparisons with the revenue energy meters data, to detect these unwanted losses.

- identification of the line involved in a fault.
  The low-voltage network is characterized by a very high number of branches for powering the various users.
  Taking for example the case illustrated in Figure 4, a failure on the line number 3 triggers the protection installed in the secondary substation, leaving all the users connected to the other lines without power supply. In the absence of better systems, the fault is now resolved empirically, sectioning the various trunks one by one and attempting more times to manually reset the circuit breaker, causing the outage to persist for several hours.

Therefore, adding the "fault passage indicator" function (with the possibility of a remote alarm in case of overcurrent) to these devices, it can achieve a huge reduction in the intervention times.

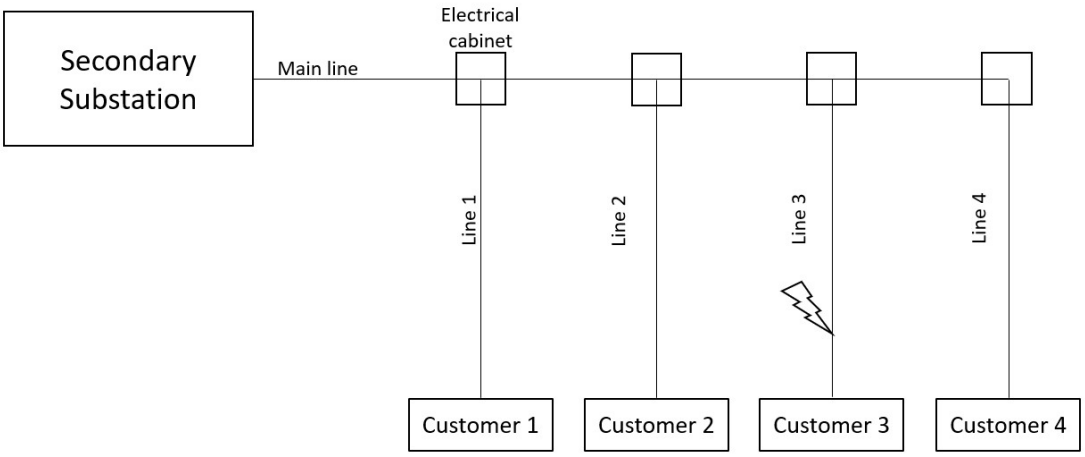

Figure 2.5 – example of a fault in the LV network

- assessment of the power quality, for example implementing the calculation of the total harmonic distortion indexes (THDv and THDi) and recording the unwanted phenomena described in the EN 50160 standard

- monitoring of the neutral conductor potential, to avoid losing control of the voltage supplied to the users (in case, for example, of interruption of the neutral conductor)

- improvement of the network safety, monitoring the real state of closure of the cabinets where these instruments are installed, since non-insulated conductors with dangerous voltage are normally located inside them.

2.3 Power quality

Mainly due to the spread of the distributed generators, the electrical mobility, etc., the power network is becoming more and more complex every day, forcing Distributor System Operators (DSOs) and utilities to invest on systems aimed at improving the quality of the energy supplied, hence providing benefits for the customers.
In this regard, the Council of European Energy Regulators (CEER) [7] issues a report every three years that focuses on (i) the continuity of service and (ii) the power quality.
One of the reasons for the growing interest in power quality is the large use in the last decades of equipment capable of generating harmonics. The wide use of drivers for electric motors, switching power supplies and in general all the electronic loads that have a non-linear absorption, cause harmonics that are introduced into the electric system "polluting" the voltage supplied to the customers. Furthermore, many of the electronic devices in use today are very sensitive to disturbances, which often cause malfunctions or decreases in efficiency.
Over time, the Institute of Electrical and Electronics Engineers (IEEE) has issued various standards relating to power quality, including the 519 of 2014, called "Recommended Practice and Requirements for Harmonic Control in Electric Power Systems". In the same way, also the International Electrotechnical Commission (IEC) has redacted some documents regarding this argument.
The most important standards on power quality evaluation [8] are hence illustrated below.

2.3.1 IEEE 519-2014 Standard

This standard [9] describes a series of requirements for the design of electrical networks containing both linear and non-linear loads, and, therefore, able to generate harmonic distortion. To keep the harmonics below a certain limit, it is necessary that:

- All customers limit their absorption of harmonic currents
- The DSOs intervene to reduce the levels of distortion by modifying, if necessary, the impedance of the power supply system

The measurements shall be done at the common coupling points (PCC), which are defined as: "Point on a public power supply system, electrically nearest to a particular load, at which other loads are, or could be, connected. The PCC is a point located upstream of the considered installation". [10]
The standard defines two ways of measuring harmonics:

- Very short time harmonic measurements, based on 3 seconds of acquisition, aggregating 15 consecutive windows of 10 signal periods (considering 50 Hz systems). The harmonic components are calculated according to the following formula:

$$F_{n,vs} = \sqrt{\frac{1}{15}\sum_{i=1}^{15} F_{n,i}^2} \tag{2.2}$$

"F" is the voltage or current (in RMS value) and "n" the harmonic order

- Short time harmonic measurements, calculated in an interval of 10 minutes which aggregates 200 "very short time" values. The quantity is computed in this way:

$$F_{n,sh} = \sqrt{\frac{1}{200}\sum_{i=1}^{200} F_{(n,vs),i}^2} \tag{2.3}$$

For voltage (at PCC), the recommended limits are shown in table 2.1

Bus voltage V at PCC	Individual harmonic (%)	THD (%)
V ≤ 1.0 kV	5.0	8.0
1 kV < V ≤ 69 kV	3.0	5.0
69 kV < V ≤ 161 kV	1.5	3.5
161 kV < V	1.0	1.5

Table 2.1 – Voltage harmonic limit values

The standard also adds that:

- 99 % of the very short time values must be less than 1.5 times the quantities shown in the table 2.1
- Weekly, 95 % of short time values must be below the quantities shown in the table 2.1

Turning to the current, considering the systems with nominal voltage between 120 V and 69 kV, the values recommended at the PCC are the following (table 2.2):

Maximum harmonic current distortion in percent of I_L						
Individual harmonic order (odd harmonics)						
I_{SC}/I_L	**3 ≤ h <11**	**11≤ h < 17**	**17 ≤ h < 23**	**23 ≤ h < 35**	**35 ≤ h ≤ 50**	**TDD**
< 20	4.0	3.0	1.5	0.6	0.3	5.0
20 < 50	7.0	3.5	3.5	1.0	0.5	8.0
50 < 100	10.0	4.5	4.0	1.5	0.7	13.0
100 < 1000	13.0	5.5	5.0	3.0	1.0	15.0
> 1000	15.0	7.0	6.0	3.5	1.4	20.0

Table 2.2 – Current harmonic limit values
Isc = maximum short-circuit current at PCC
I_L = maximum demand load current at PCC

Furthermore, it is suggested to respect the values reported according to the following criteria:

- 99 % of the very short time harmonic currents must be below 2 times the values shown in the table 2.2
- Weekly, 99 % of the short time harmonic currents must be below 1.5 times the values shown in the table 2.2
- - Weekly, 95 % of the short time harmonic currents must be below the values shown in the table 2.2

There are also recommendations for the control of voltage interharmonics, i.e. those disturbances that do not have a frequency multiple of the nominal frequency of the system.
The standard (referring to the 60 Hz typical of American systems) imposes for 95 % of the short time harmonic voltages the maximum values collected in table 2.3 and shown graphically in figure 2.6 (considering the frequencies between 0 and 120 Hz), since the low frequency interharmonics are responsible for the phenomenon called "Flicker" (described in the next paragraph).

Frequency (Hz)	Magnitude (%)	Frequency (Hz)	Magnitude (%)	Frequency (Hz)	Magnitude (%)	Frequency (Hz)	Magnitude (%)
16	5.00	27	1.78	38	0.81	49	0.28
17	4.50	28	1.64	39	0.78	50	0.25
18	3.90	29	1.54	40	0.71	51	0.23
19	3.45	30	1.43	41	0.64	52	0.25
20	3.00	31	1.33	42	0.57	53	0.27
21	3.77	32	1.26	43	0.50	54	0.29
22	3.53	33	1.20	44	0.48	55	0.35
23	3.30	34	1.13	45	0.43	56	0.40
24	3.15	35	1.05	46	0.38	57	0.58
25	3.03	36	0.95	47	0.34	58	0.77
26	1.90	37	0.85	48	0.31	59	0.95

Table 2.3 – interharmonic limit values

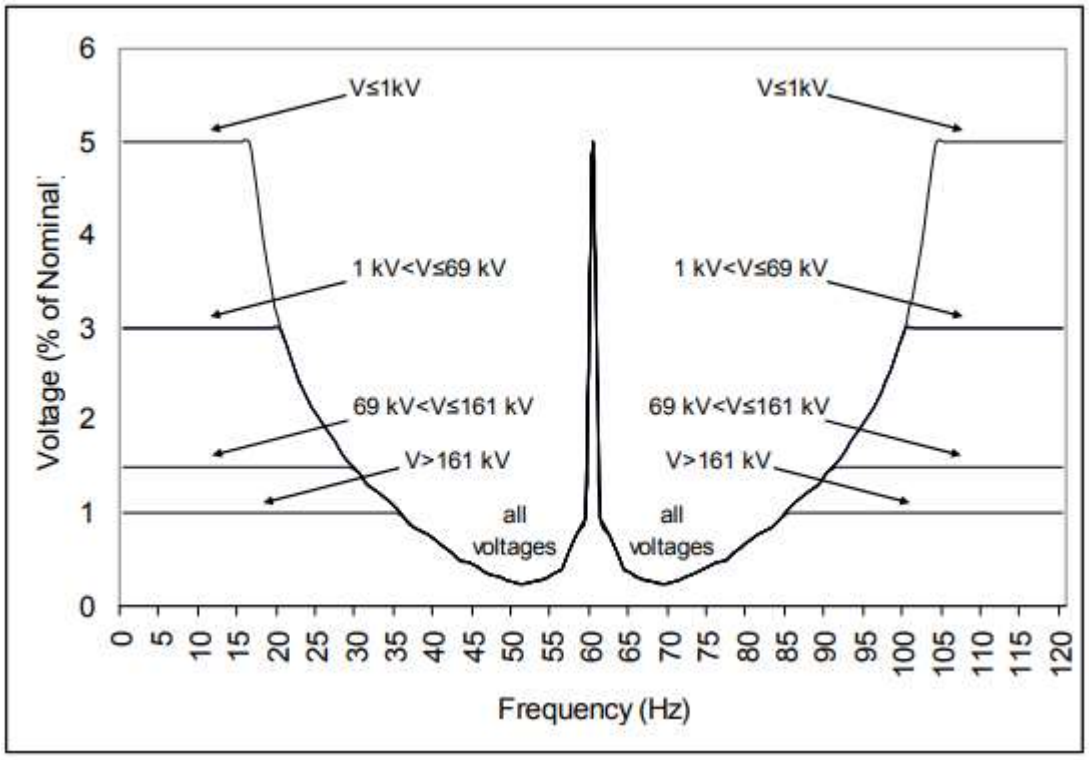

Figure 2.6 – interharmonic limit values

2.3.2 EN 50160 Standard

In Europe, the standard for the power quality evaluation is the EN 50160 [11], which describes the characteristics that must have the voltage supplied in the public distribution networks providing prescriptions for:

- Frequency
- Amplitude
- Waveform
- Symmetry of the voltages

In fact, these characteristics vary over time and they must be checked in order to guarantee an efficient service.
Furthermore, the standard describes the most common phenomena that affected the voltage waveform and it impose limits for some of these.

2.3.3.1 Nominal values

The nominal frequency of European electrical networks is 50 Hz. Due to the continuous variation of loads and the not perfect balance between consumption and production, the frequency is subject to variations. To ensure proper system operation, the standard provides that:

- The frequency shall be 50 Hz ± 1 % for the 95 % of the year
- The frequency shall be 50 Hz +4 % / -6 % for the 100 % of the year

Amplitude limits are also imposed at 230 V, and the nominal RMS value shall remain in these intervals:

- U_n ± 10 % for the 9 5% of the year
- U_n + 10 % / - 15 % for the 100 % of the year

2.3.3.2 Phenomena

The standard describes the most common phenomena dividing them into:

- CONTINUOUS PHENOMENA: a deviation from the nominal values that occurs continuously over time (due, for example, to non-linear loads)
- TRANSIENT EVENTS: sudden and temporary deviation from the nominal values (due for example to line faults)

The following are the most relevant:

- FLICKER: it is defined as a low frequency fluctuation of the voltage RMS value. This can lead to an instability of the light sources connected to the network, which can generate unwanted somatic phenomena to people directly exposed to these sources (such as headaches or epileptic seizures).

The short-term severity of the flicker, indicated by the Pst parameter, is determined through a model of the human reaction to light changes and through a statistical analysis of the instant annoying sensation.
A long-term severity can also be defined, considering the sequence of 12 short-term severities over a two-hour interval

$$P_{lt} = \sqrt[3]{\sum_{i=1}^{12} \frac{P_{st}^3}{12}} \tag{2.4}$$

The 50160 standard imposes that the Plt severity shall remain below the unit value for 95 % of each week.

- VOLTAGE UNBALANCE: Since the energy distribution and transmission takes place via three-phase networks, the standard impose that the inverse sequence component must be less than 2 % of the direct sequence component for 95 % of each week.

- HARMONIC DISTORSION: How explained initially, due mainly to the currents absorbed by the electronic loads present in the network, the voltage waveform often contains harmonic components.
  The index most used to quantify harmonic distortion is the THD (total harmonic distortion index), calculated in this way:

$$THD_V = \frac{\sqrt{\sum_2^{+\infty} V_i}}{V_1} \tag{2.5}$$

  - V_i is the voltage harmonic of "i" order

The standard defines that this parameter, considering the harmonics up to the 40th order, shall remain below 8 % for the 100 % of each week. Furthermore, limits are also imposed for the maximum RMS values of each harmonic (table 2.4) for the 95 % of each week.

Odd harmonics				Even harmonics	
Not multiples of 3		Multiples of 3			
Order h	Relative amplitude U_h	Order h	Relative amplitude U_h	Order H	Relative amplitude U_h
5	6.0 %	3	5.0 %	2	2.0 %
7	5.0 %	9	1.5 %	4	1.0 %
9	3.5 %	15	1.0 %	6 …… 24	0.5 %
11	3.0 %	21	0.75 %		
13	2.0 %				
17	1.5 %				
19	1.5 %				
23	1.5 %				
25	1.5 %				

Table 2.4 – harmonic limit values

- VOLTAGE DIPS, SWELLS AND NOTCHING: the voltage dip is defined as a transient reduction of the RSM voltage between 10 % and 90 % of the rate value, with a duration between 10 ms and 60 s. Normally, they are generated by faults in the public or private networks.

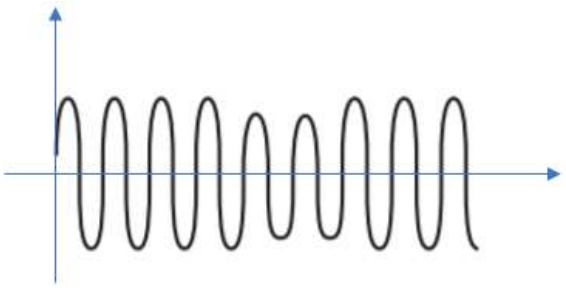

Figure 2.7 – voltage dip

Inversely to the dips, the swells are transient increases (with a duration between 10 ms and 60 s) of the RMS value of the voltage between 110 % and 180 % (Figure 2.8).

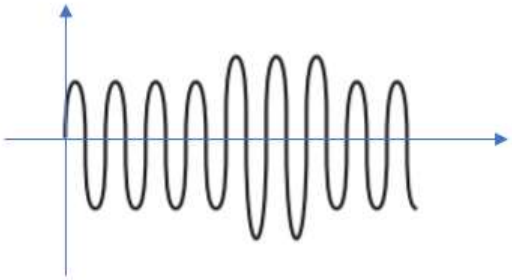

Figure 2.8 – voltage swell

Finally, the notching is a phenomenon caused by the current switching of the circuits containing rectifiers, represented by very fast impulsive variations of the RMS voltage (Figure 2.9)

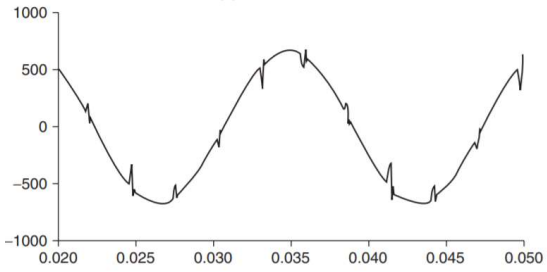

Figure 2.9 – notching

- INTERRUPTION: they are defined as reductions of the RMS voltage below 10 % of the nominal value, generally caused by the opening for a fault of the circuit breakers installed in the network (Figure 2.10)

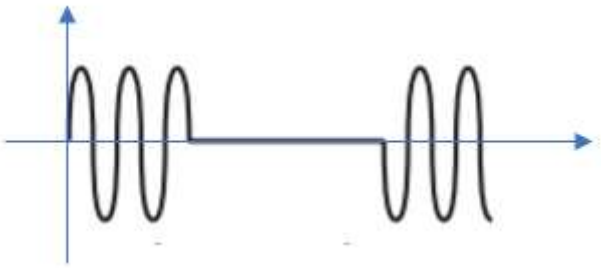

Figure 2.10 - interruption

According to their duration, they can be divided into:

- Short interruption: < 1 minute
- Long interruption: ≥ 1 minute

The authorities that check the operation of the networks monitor particularly the interruption, as they affect the continuity of service.
To allow objective evaluations and comparisons between different utilities, it is useful to define some indexes [12]:

- **SAIDI (System Average Interruption Duration Index)**

$$SAIDI = \frac{\Sigma U_i N_i}{N_T}$$

N_i: number of customers in the area "i"
U_i: annual outage time in the area "i"
N_T: total number of customers

- **SAIFI (System Average Interruption Frequency Index)**

$$SAIDI = \frac{\Sigma \lambda_i N_i}{N_T}$$

λ_i: failure rate in the area "i"
U_i: annual outage time in the area "i"
N_T: total number of customers

- **ENS (Energy Not Supplied)**

$$\text{ENS} = \Sigma P_i D_i$$

P_i : electrical power interrupted at "interruption i"

D_i : time of the "interruption i"

- **MAIFI (Momentary Average Interruption Duration Index)**

$$\text{MAIFI} = \frac{\text{n}}{N_T}$$

n: total number of short customer interruption (<3 min)
N_T: total number of customers

Authorities can dispose of compensation to customers or fines to the DSOs that do not comply with the minimum service continuity requirements.
For example, in Italy the Authority for Electricity and Gas (AEEG), with resolution 333/07, expects an automatic compensation for customers who in a year suffer of a number of outages greater than a certain threshold.
Considering the users connected to the medium voltage distribution network, an indicator is defined based on the number of long interruptions without notice (longer than 3 minutes and spaced more than 60 minutes) suffered in the year for reasons not attributable to subjects other than the distributors. The threshold values are the following:

- 2 long interruptions, for customers in high concentration areas
- 3 long interruptions, for customers in medium concentration areas
- 4 long interruptions, for customers in low concentration areas

The compensation is calculated with this formula

$$\sum_{j=1}^{m} \sum_{i=s(j)+1}^{\min(n(j),2s(j))} \left(V_p * PMI_{ij}\right) \quad (2.6)$$

- m: customers whose continuity of service has not been respected
- n: interruptions suffered by each customer
- s: specific level of continuity
- PMI: average interrupted power (interruption i, customer k)
- Vp: multiplicative coefficient (2,5 € / kW for the first 500 kW, 2 € / kW for the following)

Considering these possible outlays, it is clear that is of primary importance for the DSOs to invest in systems capable of improving the reliability of the managed network, trying to guarantee the best possible service continuity.

2.3.3 61000-4-30 Standard

The following standard [13] defines the minimum requirements and measurement methods for the evaluation of each power quality parameter, to ensure comparability between the results provided by different instruments.
The quantities considered are the following:

- Power frequency
- Magnitude of the supply voltage and current
- Flicker
- Supply voltage dips and swells
- Voltage interruptions
- Transient voltages
- Supply voltage and current unbalance
- Voltage and current harmonics
- Rapid voltage change

For each quantity, the procedures for two performance classes are described, according to the purpose of the measurements:

- Class A: *This class is used where precise measurements are necessary, for example, for contractual applications that may require resolving disputes, verifying compliance with standards, etc. Any measurements of a parameter carried out with two different instruments complying with the requirements of Class A, when measuring the same signals, will produce matching results within the specified uncertainty for that parameter[13].*

- Class S: *This class is used for statistical applications such as surveys or power quality assessment, possibly with a limited subset of parameters. Although it uses equivalent intervals of measurement as Class A, the Class S processing requirements are much lower. Some surveys may assess power quality parameters of several measurement sites on a network; other surveys assess power quality parameters at a single site over a period of time, or at locations within a building or even within a single large piece of equipment[13].*

There is also an additional class, called class B, which was present in the first version of the standard and then deleted. Therefore, it is not recommended for new generation instruments.
The basic time interval considered for the measurements timing is, for 50 Hz networks, equivalent to the duration of 10 signal periods. For class A measurements, a resynchronization of the intervals is required every UTC 10-min tick, as shown in figure 2.11.

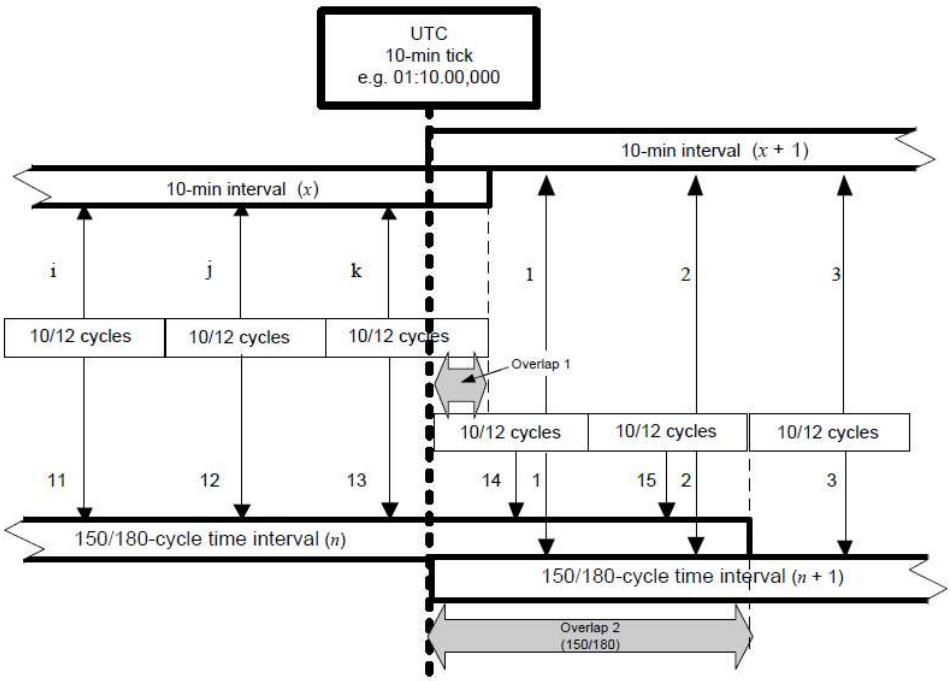

Figure 2.11 – time management for power quality monitoring systems

The measures can be aggregated into three intervals:

- 150 consecutive periods
- 10 minutes
- 2 hours (only for Plt calculation, related to the flicker)

The standard also defines the maximum uncertainty allowed for the real-time clock, which can have different values according to the chosen class:

- Class A: the uncertainty must not exceed ± 20 ms in the entire measurement interval. If an external synchronization source (such as a GPS) is not available, the maximum tolerance must be better than ± 1 s for each 24 h period
- Class S: the uncertainty must not exceed ± 5 s for each 24 h period

By way of example, considering the complexity of the standard, we report below the methods for evaluating voltage interruptions and harmonics, as the following measurements represent two of the most interesting parameters in distribution networks monitoring.

2.3.3.1 Interruption evaluation

As reference value, the standard defines U_{din} as the value obtained multiplying the declared supply voltage with the voltage transducer ratio, on which the threshold is calculated (which is then set as a percentage of U_{din}, typically 5 % or 10 %).
The interruptions are recorded in this way:

- Single-phase systems: the interruption begins when the RMS value of the voltage falls below the threshold and ends when it rises above the threshold plus the hysteresis.
- Polyphase systems: the interruption begins when the RMS values of all the phases fall below the threshold and end when at least one rises above the threshold plus the hysteresis.

Typically, the hysteresis is set at 2 % of U_{din}.
The saving of the event shall contain the absolute start timestamp and the absolute end timestamp. The duration of the event is defined as the difference between the two absolute timestamps.
About the accuracy, being essentially a temporal measure, reference is made to the requirements for the real-time clock illustrated above.
In this case, there are no differences between measures in class A and measures in class B

2.3.3.2 Voltage harmonics evaluation

For the harmonic calculation, the specific sub-standard 61000-4-7 [14] is recalled. In this case, there is a differentiation of the methods according to the reference class.

- CLASS A

The calculation must be made considering cycles of 10 periods without gaps, reaching up to the 50th order in the FFT calculation. The formula used for the THD, considering a certain group of harmonics, must be the following:

$$THDS_V = \sqrt{\sum_{h=h_{min}}^{h_{max}} \left(\frac{V_{sg,h}}{V_{sg,1}}\right)^2} \tag{2.7}$$

- h_{min} normally is 2
- h_{max} if not specified, is 40

With steady state signals and the nominal operating conditions indicated by the manufacturer, the prescribed accuracy shall be (U_m: measured value; U_{nom} : rated value):

- for $U_m \geq 1\ \%\ U_{nom}$ → ± 5 % U_m
- for $U_m < 1\ \%\ U_{nom}$ → ± 0,05 % U_{nom}

- CLASS S

Unlike class A, gaps between groups of 10 periods are allowed and the calculation must be done at least up to the 40th order.

3. Sensors for LV monitoring systems

The main types of current and voltage sensors used in monitoring and measurement systems for low-voltage networks are presented below. Therefore, those types that are used exclusively in systems with voltage levels above 1000 V, as the voltage transformer, are neglected. [15] [16] [17].

3.1 Current sensors

3.1.1 Shunt

The goal of current sensors is to provide an output signal proportional to the current (that we want to measure) that is suitable for the acquisition. The simplest transducer, and widely used in single-phase energy meters, is the shunt.
This is composed by a resistor of such value as to affect only minimally the impedance of the system, placed in series with the line. Therefore, the transduction takes place by exploiting Ohm's law, providing the resistor voltage drop to the acquisition system (Figure 3.1).

$$V_{sh} = R_{sh} I_{line} \tag{3.1}$$

- V_{sh}: voltage drop on the shunt
- R_{sh} : shunt resistance
- I_{line}: current

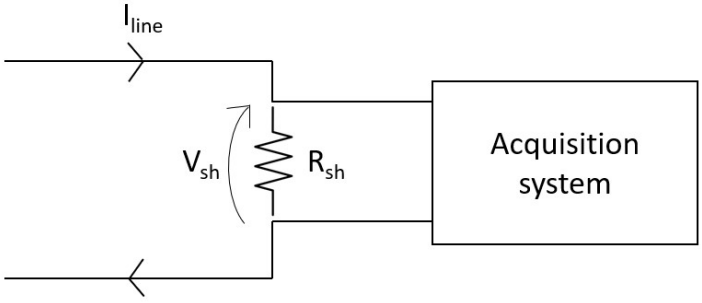

Figure 3.1 – scheme for current measurement through a shunt

Although it is a simple, reliable sensor with potential high accuracy (uncertainty can be less than 1%), it is not very often used, due to the following problems:

- It is not always possible to interpose components in series to a line
- They affect, even if minimally, the value of the circulating current
- It is difficult to protect them in case of fault over-currents

Therefore, sensors that exploit the magnetic induction properties of the current are more widely used.

3.1.2 Current transformer

The current transformer (CT) for low-voltage applications consists generally of a toroidal ferromagnetic core on which the secondary winding is mounted. Normally, the primary winding consists of the line conductor itself, which passes through the toroid (Figure 3.2).

Figure 3.2 – Commercial current transformer

The magnetic flux generated by the primary current is used to develop a secondary current proportional to it. Considering the magnetic circuits laws, this equation can be written:

$$N_1 I_1 - N_2 I_2 = R\Phi \tag{3.2}$$

- R: reluctance
- N_1, N_2 : number of turns
- Φ: magnetic flux
- I_1, I_2 : currents

Thanks to the ferromagnetic core, the reluctance is very low, and the term to the right of the equal can be neglected, obtaining (in absolute terms):

$$I_2 = \frac{N_1}{N_2} I_1 \tag{3.3}$$

To also consider the parasitic phenomena, the circuit schematization proposed in Figure 3.3 can be taken, where the following components can be distinguished:

- Z_1 e Z_2: they are the longitudinal parameters of the transformer, composed of two resistances (R1 and R2) which collect the losses due to the joule effect in the windings, and of two dispersion inductive reactances (X1 and X2) that take into account of the dispersed magnetic flux.
- Y_0: it is the transversal parameter of the transformer, composed of a resistance R0 (which consider the joule losses due to eddy currents in the core) and of an inductive reactance X0, also called magnetization inductance.

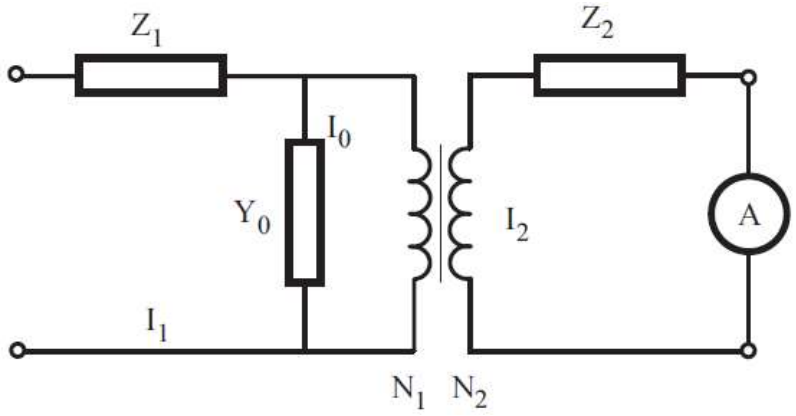

Figure 3.3 – equivalent scheme of a transformer

Therefore, this equation must always be vectorially satisfied:

$$N_1\overline{I_1} = N_2\overline{I_2} + N_1\overline{I_0} \tag{3.4}$$

- $\overline{I_1}$: primary current
- $\overline{I_2}$: secondary current
- $\overline{I_0}$: magnetizing current

Dividing every term by N1, the parameter k can be defined as the transformation ratio N2/N1.

$$\overline{I_1} = k\overline{I_2} + \overline{I_0} \tag{3.5}$$

The direct linearity between primary and secondary current is hence lost due to the magnetizing current I_0.
In the Figure 3.4 there is an example of possible vector diagram, where is notable that the quantity $-kI_2$ does not correspond to I_1 (as would be desirable), but differs from it in magnitude and phase.

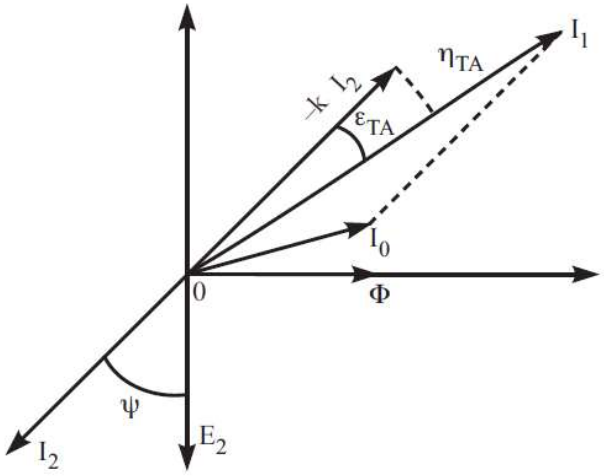

Figure 3.4 – CT vectorial diagram

A ratio error η and a phase error ε can be hence defined, that the designer must try to minimize:

$$\eta = \frac{kI_2 - I_1}{I_1} \qquad (3.5) \qquad\qquad \varepsilon = -\varphi_2 - \varphi_1 \qquad (3.6)$$

Usually, the industrial CTs have a normalized secondary rated current to standardize the acquisition systems, and the value can be generally 1 A, 2 A or 5 A.
When this type of sensor is chosen for protection purpose, the transducer must be able to withstand very high currents for short periods (normally 1 s is considered). Hence, each of these is characterized by a rated thermal current and a rated dynamic current (which can be even over 100 times the rated current).
The accuracy class is defined as the maximum possible ratio error that can occur when the primary current is between 25% and 100% of the nominal value, with a minimum cos (φ) of 0.8. Like other parameters, the accuracy class is standardized, and the typical values are: 0.1, 0.2, 0.5, 1, and 3.
By way of example, table 3.1 shows the limits related to the accuracy classes described by the IEC standards for normal applications CTs (not protection).

CLASS	**Ratio error %**				**Phase error [crad]**			
	5%	**20%**	**100%**	**120%**	**5%**	**20%**	**100%**	**120%**
0.1	0.4	0.2	0.1	0.1	0.45	0.24	0.15	0.15
0.2	0.75	0.35	0.2	0.2	0.9	0.45	0.3	0.3
0.5	1.5	0.75	0.5	0.5	2.7	1.35	0.9	0.9
1.0	3.0	1.5	1.0	1.0	5.4	2.7	1.8	1.8

Table 3.1 – Current transformer ratio and phase errors

3.1.3 Rogowski coil

The Rogowski sensors are essentially composed of an insulating toroidal support on which is winded a coil that covers the entire lateral area (Figure 3.5). The current to be measured shall flow in a conductor that pass through the toroid (like the toroidal current transformers).

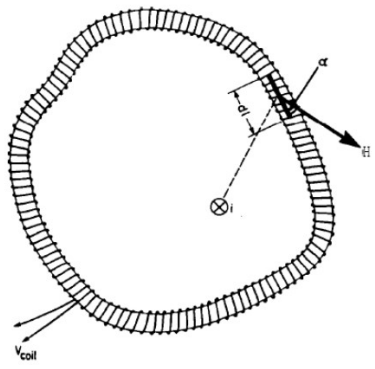

Figure 3.5 – schematization of a Rogowski coil

If n is the number of turns per unit of length, the infinitesimal unit of flow related to each dl is equal to (where A is the section of the toroid):

$$d\varphi = \mu_0 HAn \cos(\alpha)\, dl \tag{3.7}$$

To obtain the total concatenated flow, the following integration must be carried out

$$\varphi = \mu_0 An \int H \cos(\alpha)\, dl \tag{3.8}$$

Thanks to Ampere's law, the integral can be replaced with the current

$$\oint H \cos(\alpha)\, dl = i \quad \rightarrow \quad \varphi = \mu_0 A\, n\, i \tag{3.9}$$

Therefore, the output voltage is easily computable with the Faraday-Neumann-Lenz's law:

$$v_{coil} = -\frac{d\varphi}{dt} = -\mu_0 A\, n\, \frac{di}{dt} \tag{3.10}$$

As we can observe, the output voltage is proportional to the derivative of the current input.
Hence, for classical applications, it is necessary to add an analogic integrator circuit in cascade to the transducer (essentially composed of an operational amplifier in a low pass filter configuration) or a digital integration system.
Rogowski coils are characterized by a very great linearity (thanks to the absence of ferromagnetic materials) and high dynamics (which makes it suitable for the measurement of transient currents).
However, on the other hand, a design not in a workmanlike manner with, for example, a not constant density of turns or a not negligible section of the secondary conductor can increase the influence of the external fields to the output and the dependence of the measure from the position of the conductor inside the toroid.
Furthermore, considering the very low output voltage that generally these sensors provide, they are not indicated for low current measurements (<5 A).
By accepting slightly lower metrological performances (as the perfect respect of Ampere's law is lacking), it is possible to design openable Rogowski coils (Figure 3.6), characterized by high transportability and ease of installation (very useful for temporary installations and for portable instruments designed to carry out in-field measurements).

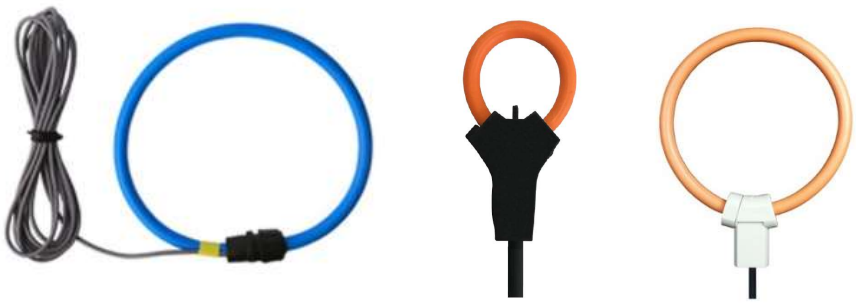

Figure 3.6 – Commercial openable Rogowski coils

On standard level, the Rogowski coils are considered "low power passive current transformers" and are described by the IEC 61869-1 [19] and IEC 61869-10 [20] standards, which define the requirements for their construction, accuracy classes, test setups, etc.
For their low-power and consequent resistance to high currents, this type of transducer is widely used in the new generation protection systems. In fact, their important point of strength is the very small footprint that makes them suitable for integration in cable accessories (for example joints and terminals).

3.1.4 Hall effect current sensor

The Hall effect sensors [18] are widely used in power plants, for their ability of transduce both DC and AC signals and for their very good metrological characteristics.
Their operating principle is based on a metal plate (Figure 3.7) subjected to a magnetic field B (produced by the current to be measured) in the z-direction and crossed by a constant current in the x-direction.

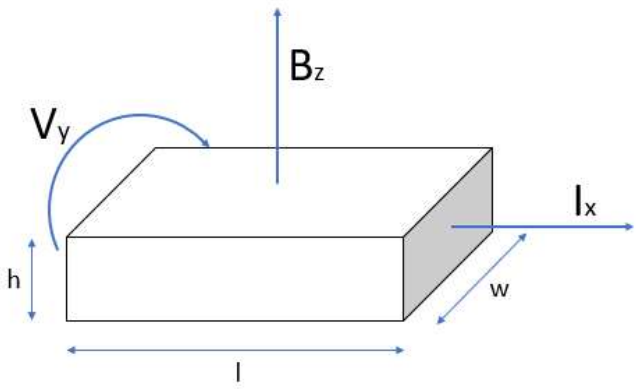

Figure 3.7 – Hall element

During the functioning, the current is subjected to the Lorentz force $\bar{F} = q\,\bar{v} \wedge \bar{B}$, which deflect the electron flux in the y-direction.
In the two faces orthogonal to y-direction a potential difference can be measured, due to the densification of electrons on one side and an emptying on the other; this voltage, called "Hall voltage", is proportional to the magnetic field and then to the current intensity.
The deviation of the charges is gradually balanced by the resulting electric field and, in steady state conditions (when is verified the equation $qE = qvB$), the Hall voltage is

$$V_h = E\,w = \frac{F}{Q}\,w \tag{3.11}$$

Considering that $F = Q\,v\,B$ and that the speed of charges depends on the material and it is equal to (qn is the charge density)

$$v = \frac{I}{qn\,w\,h} \tag{3.12}$$

This equation can be written:

$$V_h = \frac{B\,I}{h} k_h\, w \tag{3.13}$$

Where K_h is the Hall constant and corresponds to the quantity 1/qn, intrinsic of the conductor material used.
Constructively, the transducer can be realized using a toroidal ferromagnetic core on which is made a small air gap for the insertion of the Hall element (Figure 3.8).

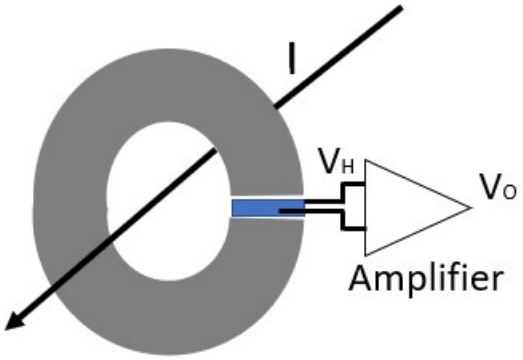

Figure 3.8 - scheme of the open-loop Hall effect current sensor

The conductor is positioned inside the toroid so that the Hall element is subjected to a magnetic field proportional to the current

$$B \approx \frac{\mu}{2\pi r} I \tag{3.14}$$

This simple set up, called "open-loop", is not widely used because saturation of core can occur.
The field compensation solution is then often preferred (Figure 3.9)

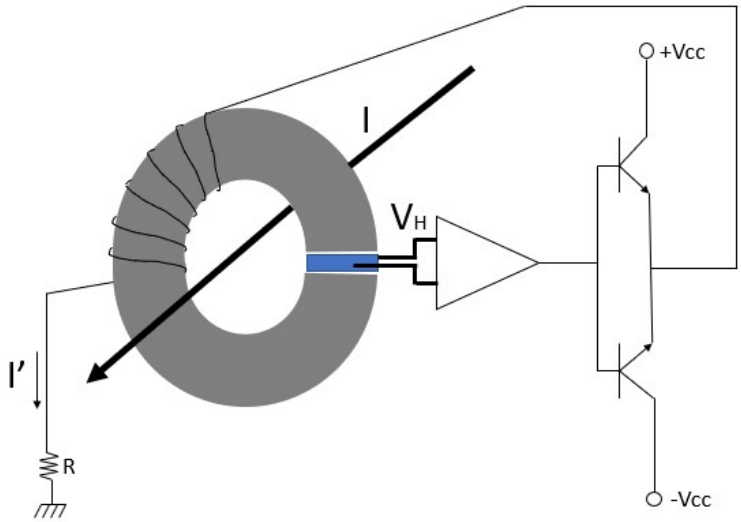

Figure 3.9 – scheme of the closed-loop Hall effect current sensor

The highly amplified Hall voltage drives an analogic "push-pull" stage which, in turn, generates a current proportional to it. The winding balances the magnetic flux inside the core avoiding the risk of saturation.
At equilibrium, when both the Hall voltage and the magnetic field have a value close to zero, we have that

$$I = I'N \tag{3.15}$$

Considering the voltage across the resistor, the input current can be derived through the relationship

$$I = N\frac{V_R}{R} \tag{3.16}$$

About their use, Hall effect sensors are suitable when very accurate measurements are required (usually the uncertainty of these systems is below 1%) and, for their high bandwidth, when the frequency of the input signal can reach some MHz.

3.2 Voltage sensors

3.2.1 Dividers

Regarding the voltage measurements in the low-voltage networks, the most used transducers are the dividers composed of resistors, capacitors, or a mix of the two components.
They allow to reduce the nominal system voltage to one proportional to it and suitable to be directly acquired by electronic systems. In the Figure 3.10 are shown the four configurations expected and covered by the standard 61869-11 [21] ("requirements for low-power passive voltage transformers")

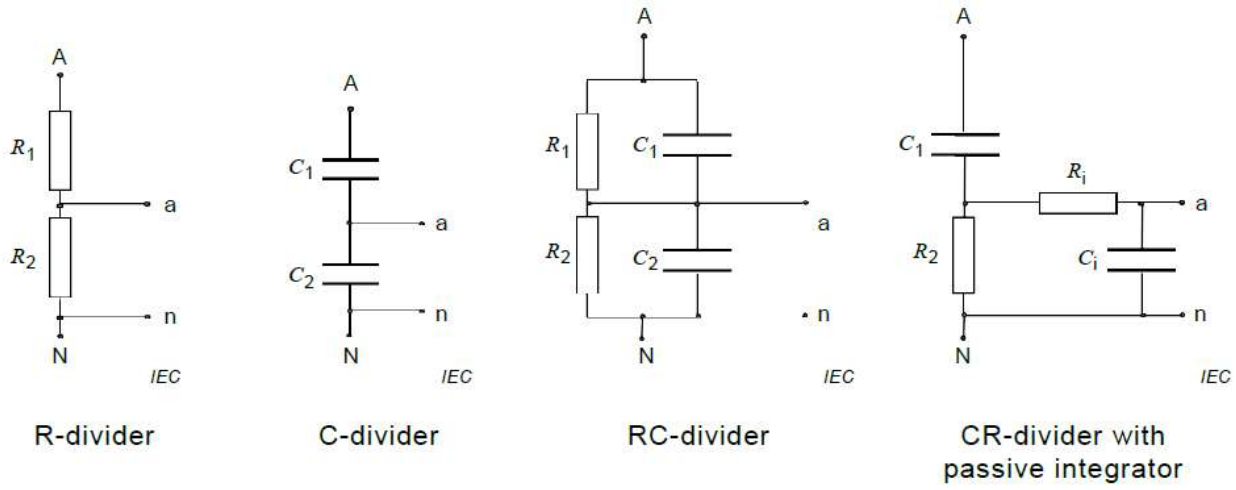

Figure 3.10 – types of dividers expected by the IEC 61869-11 standard

By briefly analysing the first two types, which are the most used, the following I/O relationships can be written:

- R divider $V_{an} = V_{AN} \frac{R_1}{R_1+R_2}$ (3.17)

- C divider $V_{an} = V_{AN} \frac{C_2}{C_1+C_2}$ (3.18)

In low-voltage equipments the most used divider are the resistive type, for the greater accuracy and bandwidth. Capacitive dividers are instead mostly used in medium and high voltage systems, due to their very low energy dissipation (due exclusively to parasitic phenomena).
According to the 61869-1 standard, it is possible to associate a percentage ratio error to each of these devices, which defines the deviation of the real transformation ratio to the nominal one.

$$\varepsilon = \frac{K_r U_s - U_p}{U_p} * 100 \quad (3.19)$$

- K_r : nominal ratio
- U_s : secundary RMS voltage
- U_p : primary RMS voltage

Therefore, it is possible to introduce a correction factor " CF_U ", evaluated at the nominal frequency and with the nominal load, which allows the divider to reach the specified accuracy class.
The formulation of ratio error can be modified in this way:

$$\varepsilon = \frac{CF_u K_r U_s - U_p}{U_p} * 100 \quad (3.20)$$

On the technological level, considering the not excessive values of the voltages in the LV systems, very often the dividers are realized directly on the electronic boards where the signal acquisition and processing system are mounted (preferably with surface-mounted components, Figure 3.11), by placing attention on:

- Tolerance on the component value
- Temperature variation coefficients
- Stability

Figure 3.11 – surface-mounted resistors

3.2.2 Hall effect voltage sensor

Hall effect voltage sensors [18] are less common because they are more expensive, but in general they have better metrological characteristics than the dividers. Their operation is based on the same

principle as the counterpart for the current measurements, naturally with some circuital differences. In fact, a primary winding is added to apply the voltage to be measured (Figure 3.12).

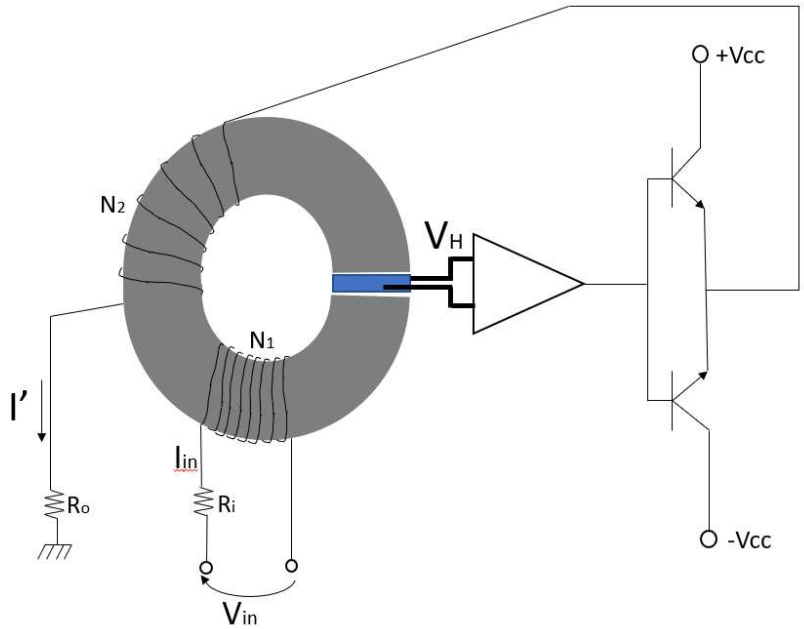

Figure 3.12 – scheme of Hall effect voltage sensor

The primary current, limited to a small value by the series resistance Ri, produce a magnetic flux inside the core. The system composed by the Hall element, the amplifier, the push-pull stage and the secondary winding will perform the field compensation, generating a current I' proportional to Vin.
Therefore, after reaching equilibrium:

$$I_{in}N_1 = I'N_2 \quad \rightarrow \quad I_{in} = \frac{N_2}{N_1}\frac{V_{Ro}}{R_o} \tag{3.21}$$

Considering that $I_{in} = \frac{V_{in}}{R_{in}}$, the input voltage can be calculated according to the following relationship:

$$V_{in} = \frac{N_2}{N_1}\frac{R_i}{R_o}V_{Ro} \tag{3.22}$$

Like the current counterpart, they reach good accuracy (with uncertainties less than 1%) and can work in a wide range of frequencies (up to several MHz).
Finally, we can observe in Figure 3.13 how this type of transducer is can be made at the industrial level.

Figure 3.13 – commercial Hall effect voltage sensor

4. Design and Development of Measurement instruments

In this chapter are described the two monitoring systems for LV networks designed during the PhD course for REPL Italia (with the collaboration of the University of Bologna). In both cases, the procedure followed for the development has been the following:

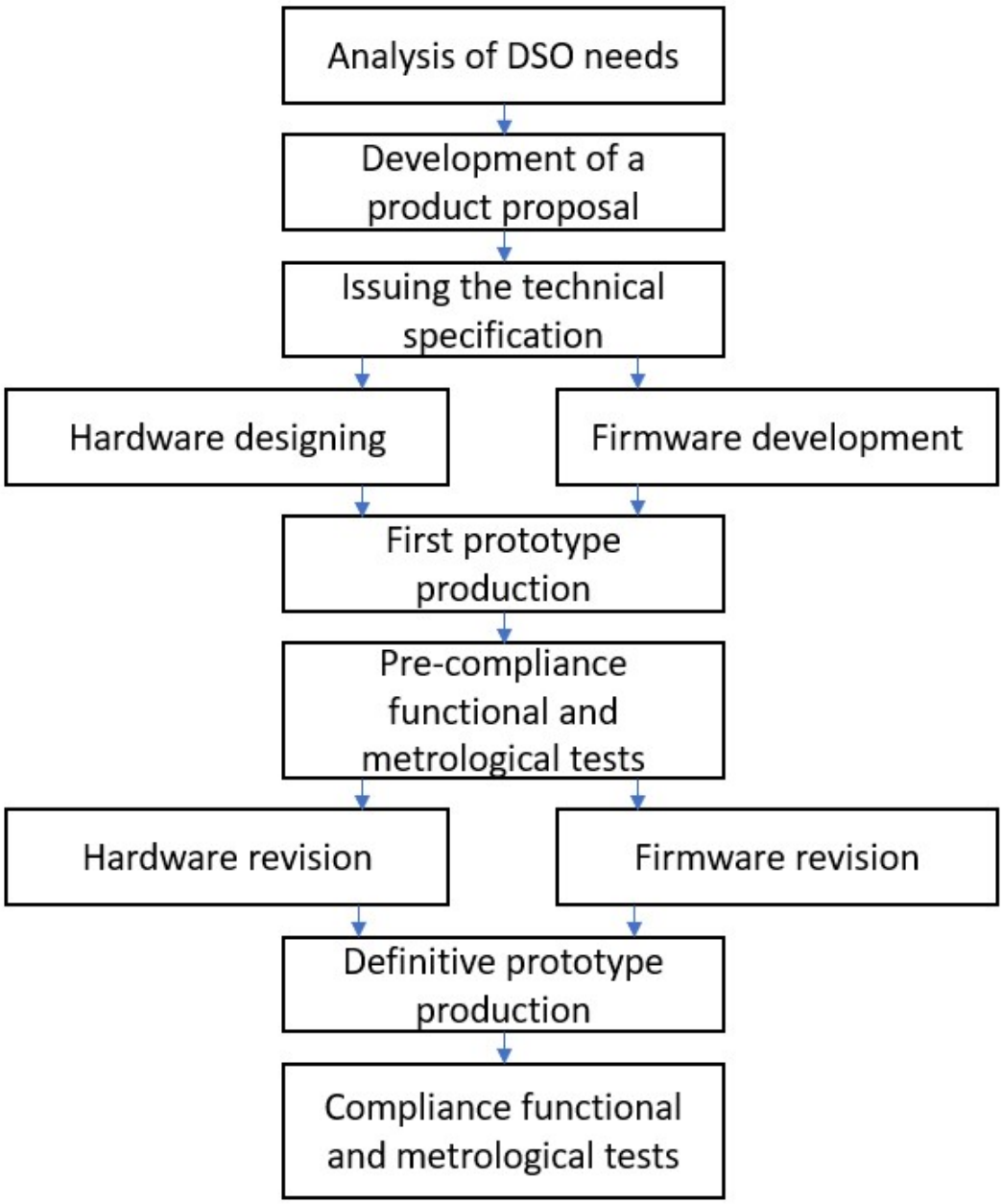

Figure 4.1 – development procedure

The chapter provides some general information on how these instruments are made (several specific particulars are omitted to protect the REPL Italia industrial secrets), what are their purposes and how I have evaluated the metrological performance.

4.1 The Guardian Meter

4.1.1 Purposes of the instrument

The guardian meter is a monitoring unit suitable for the installation in the LV street electrical cabinets (Figure 4.2), where are located the connections with the branches for customers powering (Figure 4.3).

Figure 4.2 – street electrical cabinets

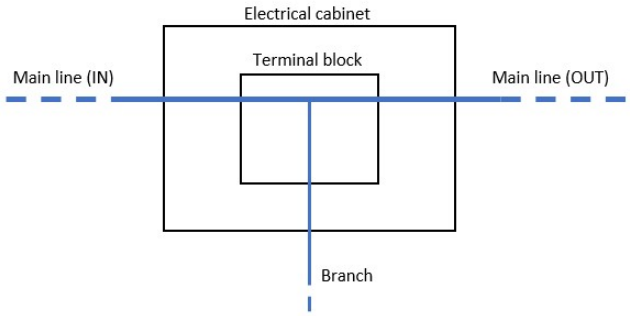

Figure 4.3 – "inside" an electrical cabinet

To use the instrument, it shall be connected to the cabinet terminal block (both for powering and for measuring the voltages). The current signals acquisition has been made through three Rogowski coils (one for each phase). The choice of this type of sensor is due to its cheapness and easy handling, although the output proportional to the current derivative (as explained in chapter 4, in this case 100 mV/kA @50Hz) could be more complex to elaborate than the output of a shunt of a current transformer, because the design shall include a digital or analogic integrator.
The computed values by the meter are the following:

- RMS values (voltages and currents)
- Phase displacements
- Active powers
- Reactive powers
- Power factors
- Active energies
- Reactive energies

The small dimensions of the device (Figure 4.4) and the possibility to install it without interruption of the electrical energy supply (thanks to the openable Rogowski coils, Figure 4.5), allow the DSO technicians to install it quickly, also in the smaller electrical boxes.
Furthermore, the low cost of the device (around 200 €) aims to a big spread of it, helping the DSOs to have a better general knowledge of the real state of the grids (since the instrument monitor all the main electrical parameters).
In particular, it is possible to check how much each single line is charged, verifying if it is underloaded or overloaded (monitoring, for examples, the circulating currents or the voltage drops).

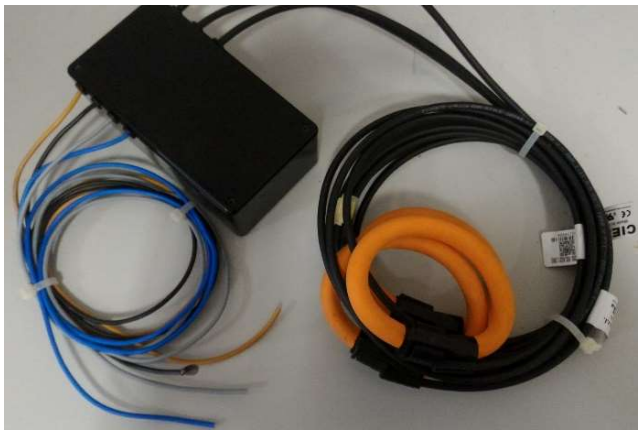

Figure 4.4 – Guardian Meter

Figure 4.5 – Openable Rogowski coil

Another important objective which led to the development of this equipment, it is the "non-technical losses" individuation (losses that occur due to unidentified energy flows that, in the most cases, are caused by energy thefts).
Currently, the only monitoring unit installed in LV networks are the secondary substation energy meters and they are, unfortunately, insufficient to locate the non-technical losses. In fact, the LV grids were the first developed in the last century and, surprisingly, their topology is often not perfectly known.
In big cities, it is common to find a situation like that described in Figure 4.6, which the DSO does not know if the customers 3 and 4 are powered by the secondary substation A or B.

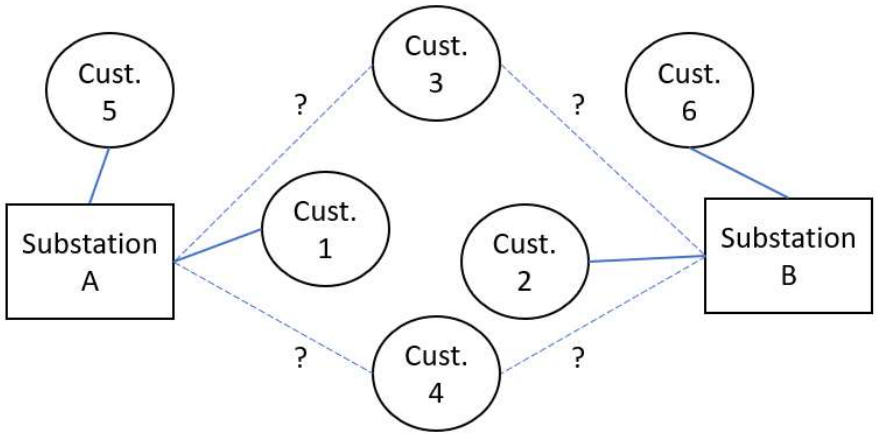

Figure 4.6 – hypothetical situation of connections between customers and substations

In this situation, it is impossible to check if the balance described by the equation 4.1 is verified and, hence, if there are non-technical losses.

$$E_{Sout} = \sum_{i=1}^{n} E_{Cin\,i} + \sum_{j=1}^{m} L_j \tag{4.1}$$

- E_{Sout} : output energy from the secondary substation
- $E_{Cin\,i}$: input energy (customer "i")
- L_j : know losses "j"
- n: number of customers
- m: number of losses

Furthermore, often the huge number of customers connected to a single substation makes very difficult to locate the responsible of a non-technical lost also if the network topology is well known. Hence, monitoring the energy flows through the branches (that generally powering only a few users) with the Guardian Meters and comparing the measures with the data of the standards revenue energy meters could be the best solution to resolve this type of problems.
Furthermore, the high portability and the ease of installation make that, for this purpose, it is not necessary to install a Guardian Meter in all electrical cabinets, but it is sufficient to move some of these periodically in more point of the network when the DSO has the founded suspect of the presence of unidentified losses.

4.1.2 Instrument description

The main characteristics considered for the designing of the Guardian Meter are the following:

- Power supply: 5 W three-phase switching power supply (admitted voltage range: 100 – 400 V)
- Accuracy:
  - 2 % (active and reactive energy)
  - 0.4 % (voltage RMS)
  - 1.5 % (current RMS)
- Rated voltage: 230 V (RMS)
- Rated current: 200 A (RMS)
- Overvoltage category: CAT IV (compliant with IEC EN 61010-1 [27] [28])
- Insulation: double

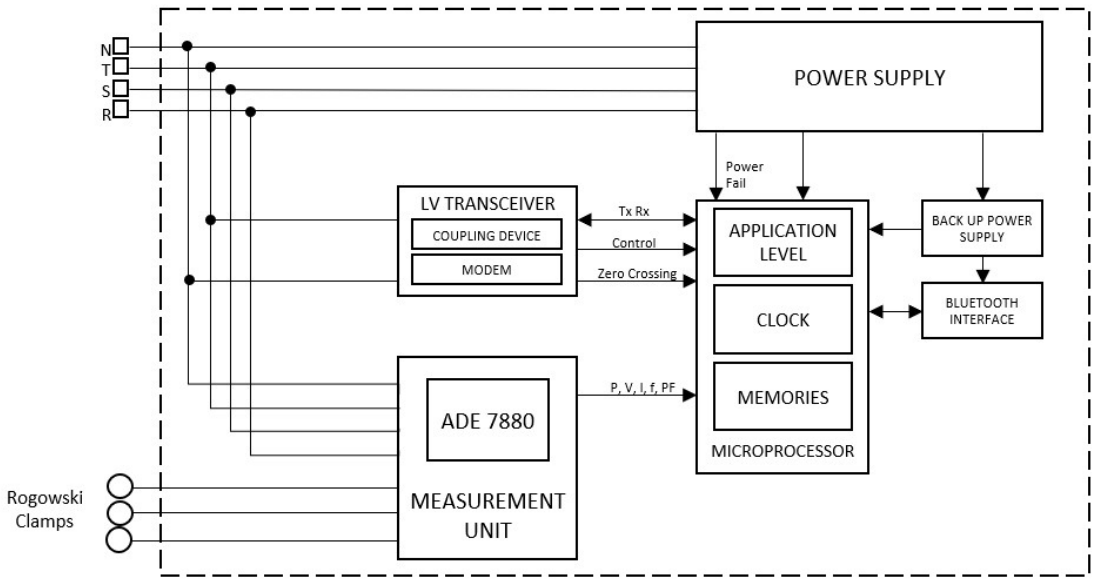

Figure 4.7 – Block diagram

The microcontroller chosen for the device management is the STMicroelectronics STM32F101 [22] (Arm Cortex M3, 36 MHz, 512 kB Flash, 48 kB Ram), that communicate with the DSP deputed to signal acquisition and elaboration though an I2C bus. The latter is the Polyphase Multifunction Energy Metering IC Analog Device ADE7880 [23], with the following characteristics:

- 6 second-order sigma-delta converters (24 bits, 8 kSA/s)
- Less than 0.1 % error in active and fundamental reactive energy
- Less than 0.1 % error in voltage and current rms
- Integrated digital integrator for derivative current sensors
- Supports IEC 61000-4-7 Class I and Class II accuracy specification

In this device, the DSP acquires the voltage signals from 1:2000 resistive dividers (installed directly on the circuit board) and the Rogowski signal (proportional to the current derivative), computing these parameters:

- Voltage RMS values
- Current RMS values
- Active energies
- Reactive energies

Each second, using the 1 Hz interrupt from the internal RTC (real-time clock) circuit, the microcontroller downloads the data from the ADE performing these operations:

- Multiply the RSM values for the calibration coefficients
- Multiply the active and reactive energies for the calibration coefficients
- Update the energy totalizers (variables that contains the energy values, updated every seconds. There are 4 totalizers for each phase, E+,E-,R+,R-, divided according with the type of load and energy toward criteria. These variables reset automatically when they reach the value 999.999.999 Wh/VArh)

- Compute the powers, phase displacements and the power factors from the energy values

Periodically (with an interval settable in the range 1 minute / 24 hours) the Guardian Meter store locally in its flash memory (4 MB) the measurements, dividing them in two different profiles:

- Measurements profile: the frame contains the timestamp and all instantaneous electrical parameters (Figure 4.8). The user can select to store:
    - Instantaneous parameters computed in correspondence of the saving
    - Average values (in the interval between two savings)
    - Maximum values (in the interval between two savings)
    - Minimum values (in the interval between two savings)

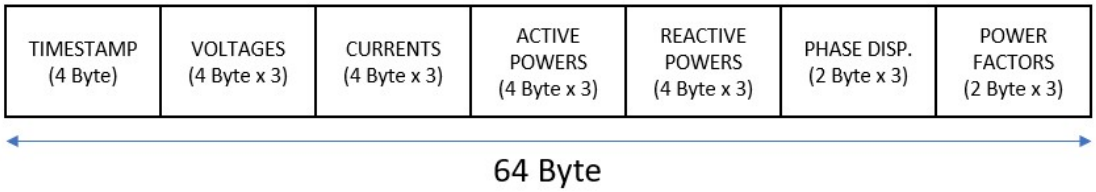

Figure 4.8 – Measurement profile

- Energies profile: the frame contains the timestamp and the values of the totalizers in correspondence of the saving (Figure 4.9)

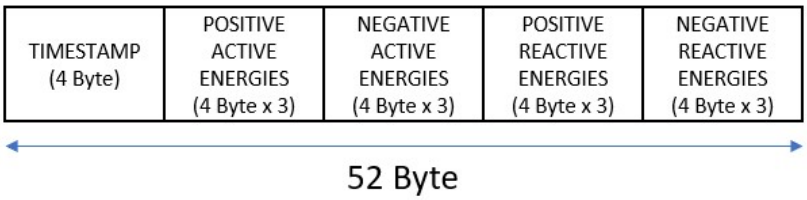

Figure 4.9 – Energy profile

To calibrate the meter, it was implemented a procedure as that expected by the DSP manufacturer and described in the AN-1711 [24] application note for the ADE 7880. This procedure is activable only by the manufacturer, using special commands sent through JTAG cable connection (used also for the first firmware programming), and it is composed by the following steps:

1) Connection of the meter to an electrical standard with accuracies at least 4 times better those declared for the DUT (Figure 4.10)
2) Application of the rated voltage and sending of the first calibration command. Hence, the device acquires 100 voltage values with a refresh time of 1 s and calculate the average calibration voltage coefficient.
3) Application of the rated current (PF = 1) and sending of the second calibration command. In this step, the meter evaluates the phase errors and adjust the ADE registers to minimize them.
4) Sending of the third calibration command. The meter acquires 100 current values and calculate the average current coefficient.

The calibration coefficients for powers and energies are computed from the currents and voltages coefficients.

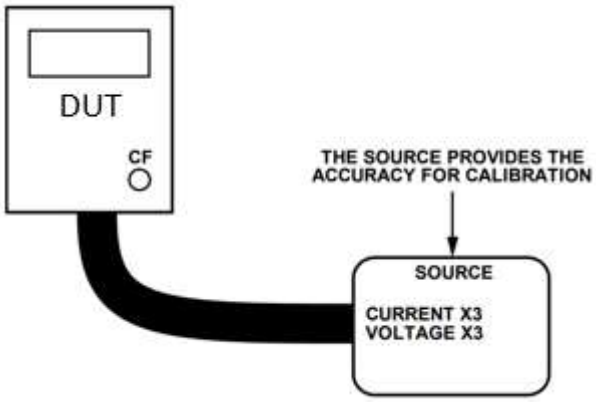

Figure 4.10 – Calibration setup

To manage the device, a series of commands have been implemented in the firmware, in order to:

- Set the device ID
- Synchronize the internal real time clock
- Visualize the alarms (from the auto-diagnosis systems)
- Visualize all the instantaneous parameters (with a refresh time of 1 s)
- Visualize the totalizers (with a refresh time of 1 s)
- Download the profiles
- Erase the internal memory
- Update the firmware

The Guardian Meter works as a slave device, and it answer only when a master sends it a command. The master can communicate thought two ways: (i) locally via Bluetooth, with an Android application developed specifically for these purposes or (ii) via power line communication. In fact, the device has a PLC modem compliant with the specification adopted by many DSOs in the world. In this case, the protocol implemented in the firmware is that developed by bigger Italian DSO and it permits the equipment to communicate with their data concentrators installed in the secondary substations. The phase chosen for the communication is the “T”.
Since the power line communication is not a standard communication method, but there is an increasing interest for this in the world of the network monitoring units, in the next paragraph is presented a very brief description on the main related concepts.

4.1.2.1 A Brief overview on power line communication

To allow remote information exchange, it is possible to take advantage of the connection to the electrical network using the "power line communication" (PLC) technology [25]. European legislation allows the use of the network for these purposes, using frequencies between 3 kHz and 148 kHz for the carrier, dividing the band into 4 ranges by type of user.

Band	Frequency range	Application
A	9 – 95 kHz	Electrical utilities
B	95 – 125 kHz	Consumer use without protocol
C	125 – 140 kHz	Consumer use with CENELEC protocol
D	140 – 148,5 kHz	Consumer use without protocol

Table 4.1 – frequency ranges for PLC communication

The simplest standard developed for this type of communication is the "X-10", which allows to reach rather low transmission speeds (50 bps on 50 Hz networks and 60 bps on 60 Hz networks). Communication takes place in a 1 ms window (Fig. 4.11) following the zero crossing of one of the 3 lines (the one designated for the communication). The value 1 will be represented by a carrier frequency burst, while the 0 by the not-presence of the carrier.

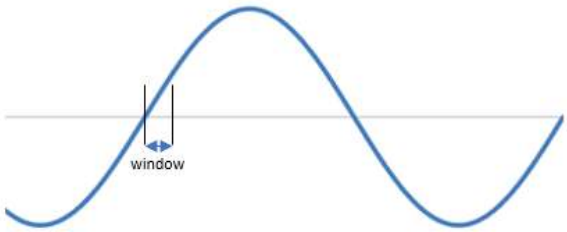

Figure 4.11 – window for PLC communication

To achieve higher transmission speeds, PSK (phase shift keying) numeric modulation is usually used. The technique consists in assigning a group of bits to a specific carrier starting phase (which is measured in conjunction with the zero crossing of the voltage at rated industrial frequency). Normally, 8 different phase displacements are considered for the carrier (Figure 4.12) with the 8-PSK modulation, communicating with 3-bit packets (tripling the transmission speed).

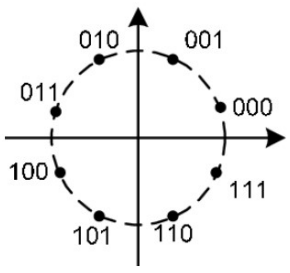

Figure 4.12 – possible phase displacement for the carrier in 8-PSK modulation

Regarding the high-level communication standards, protocols such as Euridis, DLMS / COSEM and IEC 60870-5-102 [26] are used.

In electrical networks, PLC communication is widely used for the management of revenue energy meters, realizing the AMR (automatic meter reading). A solution often implemented is shown in Figure 4.13.

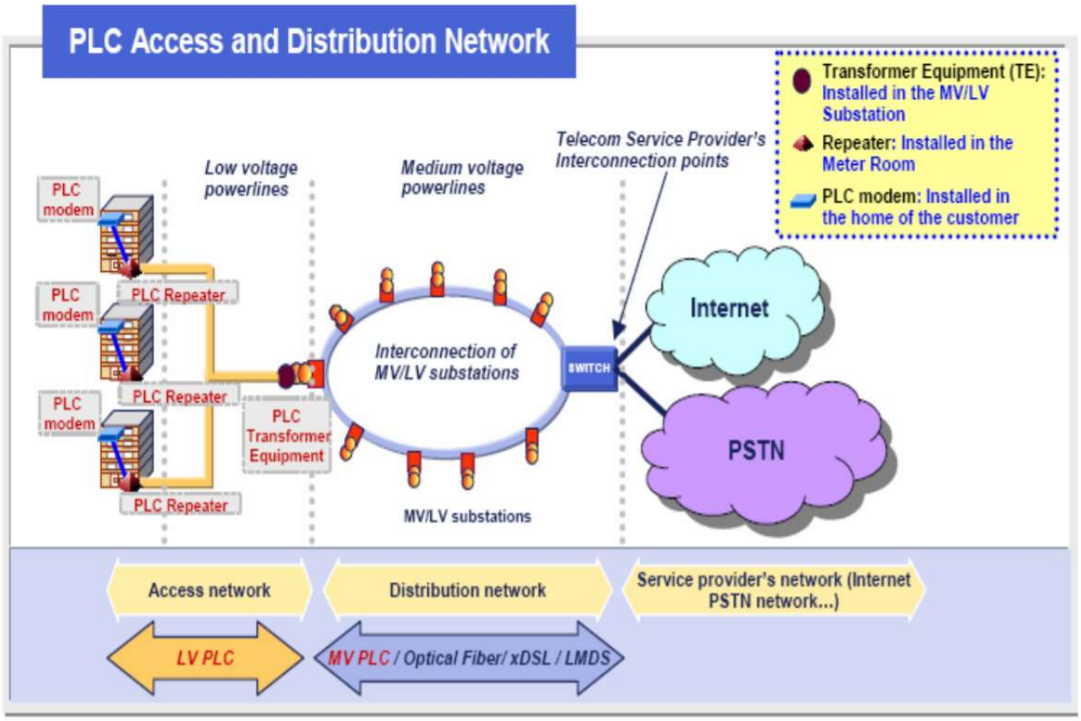

Figure 4.13 – Scheme of automatic system for meters reading

Therefore, usually PLC communication takes place between the customers and the data access points located in the secondary substations. These, through a network that can be either PLC (on MV lines) or traditional type (optical fibre, ADSL, etc.), transfer the data to the telecom service provider, so that they can be accessible by the DSO.

4.1.4 Metrological characterization

4.1.3.1 Measure of instantaneous parameters

The test setup used for the evaluation of the Guardian meter performance in the measurement of instantaneous parameters is described in detail in the chapter 5 (paragraph 5.2), where is described the procedure used for the evaluation of an intermediate version of this device.
Briefly, the test points considered are all the combination of:

- Voltage: 80%, 100% and 120% of rated voltage (230 V)
- Current: 5%, 20%, 100%, 120% of rated current (200 A)

- Frequency: 47 Hz, 49.5 Hz, 50 Hz, 50.5 Hz, 52 Hz
- Phase Angle: 60°, 36.87°, 25,842°,0°

For a total of 240 test points.
By way of example, 8 results are reported in the tables from 4.3 to 4.10, relating the combination described in table 4.2.

Test point	Voltage [V]	Current [A]	Power factor	Frequency [Hz]
1	230	200	1	50
2	230	200	0.8L	50
3	230	200	0.5L	50
4	184	200	0.9L	50
5	276	200	0.9L	50
6	230	40	0.9L	50
7	230	200	0.9L	51.5
8	230	200	0.9L	49.5

Table 4.2 – test points

TEST POINT 1										
	Voltage		Current		phase disp.		Active power		Reactive power	
phase	$\overline{x}$ [V]	$\sigma/\overline{x}$	$\overline{x}$ [A]	$\sigma/\overline{x}$	$\overline{x}$ [rad]	$\sigma/\overline{x}$	$\overline{x}$ [W]	$\sigma/\overline{x}$	$\overline{x}$ [VAr]	$\sigma/\overline{x}$
1	229.76	0.00041	198.34	0.00059	0.00327	0.0027	45570	0.00075	149.0	0.0027
2	229.57	0.00046	198.71	0.00062	0.00312	0.0027	45616	0.00076	142.4	0.0029
3	229.52	0.00048	200.46	0.00053	0.00407	0.0027	46008	0.00071	187.3	0.0028

Table 4.3 – results related to test point 1

TEST POINT 2										
	Voltage		Current		phase disp.		Active power		Reactive power	
phase	$\overline{x}$ [V]	$\sigma/\overline{x}$	$\overline{x}$ [A]	$\sigma/\overline{x}$	$\overline{x}$ [rad]	$\sigma/\overline{x}$	$\overline{x}$ [W]	$\sigma/\overline{x}$	$\overline{x}$ [VAr]	$\sigma/\overline{x}$
1	229.69	0.00041	198.54	0.00056	0.647	0.0027	36376	0.00150	27502	0.0024
2	229.59	0.00042	199.09	0.00055	0.645	0.0031	36514	0.00162	27497	0.0028
3	229.60	0.00048	200.00	0.00055	0.647	0.0030	36626	0.00158	27701	0.0027

Table 4.4 – results related to test point 2

TEST POINT 3										
	Voltage		Current		phase disp.		Active power		Reactive power	
phase	$\overline{x}$ [V]	$\sigma/\overline{x}$	$\overline{x}$ [A]	$\sigma/\overline{x}$	$\overline{x}$ [rad]	$\sigma/\overline{x}$	$\overline{x}$ [W]	$\sigma/\overline{x}$	$\overline{x}$ [VAr]	$\sigma/\overline{x}$
1	229.66	0.00045	200.28	0.00057	1.049	0.0028	22893	0.00523	39895	0.0018
2	229.63	0.00046	200.84	0.00055	1.048	0.0029	22989	0.00529	39982	0.0020
3	229.54	0.00043	198.50	0.00056	1.051	0.0029	22631	0.00530	39544	0.0019

Table 4.5 – results related to test point 3

TEST POINT 4										
	Voltage		Current		phase disp.		Active power		Reactive power	
phase	$\overline{x}$ [V]	$\sigma/\overline{x}$	$\overline{x}$ [A]	$\sigma/\overline{x}$	$\overline{x}$ [rad]	$\sigma/\overline{x}$	$\overline{x}$ [W]	$\sigma/\overline{x}$	$\overline{x}$ [VAr]	$\sigma/\overline{x}$
1	183.79	0.00045	199.36	0.00058	0.454	0.0029	32918	0.00104	16090	0.0028
2	183.47	0.00042	199.95	0.00055	0.453	0.0030	32969	0.00098	16066	0.0029
3	183.64	0.00043	199.48	0.00057	0.454	0.0028	32907	0.00106	16095	0.0026

Table 4.6 – results related to test point 4

TEST POINT 5										
	Voltage		Current		phase disp.		Active power		Reactive power	
phase	$\overline{x}$ [V]	$\sigma/\overline{x}$	$\overline{x}$ [A]	$\sigma/\overline{x}$	$\overline{x}$ [rad]	$\sigma/\overline{x}$	$\overline{x}$ [W]	$\sigma/\overline{x}$	$\overline{x}$ [VAr]	$\sigma/\overline{x}$
1	275.62	0.00043	198.53	0.00058	0.454	0.0030	49170	0.00099	24011	0.0028
2	275.55	0.00042	199.69	0.00061	0.454	0.0029	49442	0.00100	24145	0.0027
3	275.63	0.00043	200.73	0.00060	0.454	0.0030	49705	0.00098	24299	0.0029

Table 4.7 – results related to test point 5

TEST POINT 6										
	Voltage		Current		phase disp.		Active power		Reactive power	
phase	$\overline{x}$ [V]	$\sigma/\overline{x}$	$\overline{x}$ [A]	$\sigma/\overline{x}$	$\overline{x}$ [rad]	$\sigma/\overline{x}$	$\overline{x}$ [W]	$\sigma/\overline{x}$	$\overline{x}$ [VAr]	$\sigma/\overline{x}$
1	229.83	0.00044	40.53	0.00057	0.453	0.0028	8372	0.00095	4084	0.0027
2	229.50	0.00037	40.59	0.00057	0.453	0.0030	8371	0.00087	4075	0.0030
3	229.74	0.00045	39.61	0.00054	0.455	0.0027	8174	0.00096	3999	0.0026

Table 4.8 – results related to test point 6

TEST POINT 7										
	Voltage		Current		phase disp.		Active power		Reactive power	
phase	$\overline{x}$ [V]	$\sigma/\overline{x}$	$\overline{x}$ [A]	$\sigma/\overline{x}$	$\overline{x}$ [rad]	$\sigma/\overline{x}$	$\overline{x}$ [W]	$\sigma/\overline{x}$	$\overline{x}$ [VAr]	$\sigma/\overline{x}$
1	229.80	0.00043	200.19	0.00056	0.454	0.0030	41343	0.00097	20175	0.0028
2	229.46	0.00041	199.15	0.00058	0.453	0.0029	41084	0.00095	20010	0.0028
3	229.58	0.00046	200.50	0.00057	0.454	0.0029	41358	0.00106	20210	0.0027

Table 4.9 – results related to test point 7

TEST POINT 8										
	Voltage		Current		phase disp.		Active power		Reactive power	
phase	$\overline{x}$ [V]	$\sigma/\overline{x}$	$\overline{x}$ [A]	$\sigma/\overline{x}$	$\overline{x}$ [rad]	$\sigma/\overline{x}$	$\overline{x}$ [W]	$\sigma/\overline{x}$	$\overline{x}$ [VAr]	$\sigma/\overline{x}$
1	229.73	0.00046	198.69	0.00059	0.454	0.0028	41014	0.00090	20031	0.0028
2	229.58	0.00043	200.88	0.00058	0.454	0.0027	41437	0.00103	20248	0.0026
3	229.46	0.00042	200.90	0.00059	0.454	0.0029	41413	0.00100	20248	0.0027

Table 4.10 – results related to test point 8

4.1.4.2 Measure of energies

To evaluate the performance as energy meter of the Guardian meter, I have carried out 20 measurement for each point described in the table 4.11, with the same setup used for instantaneous measurement tests. Also in this case, the average values of measured quantity and the relative standard deviations have been computed.

Test point	Voltage [V]	Current [A]	Power factor	Frequency [Hz]	Time [h]
9	230 (RST)	160 (RST)	1	50	2
10	230 (RST)	160 (RST)	0.5L	50	2
11	230 (RST)	160 (RST)	0.8C	50	2

Table 4.11 – test points

The test results are collected in the following tables.

TEST POINT 1				
	active energy		**reactive energy**	
phase	$\overline{x}$ [Wh]	$\sigma/\overline{x}$	$\overline{x}$ [VArh]	$\sigma/\overline{x}$
1	73833	0.00074	238	0.0030
2	73342	0.00076	202	0.0029
3	73135	0.00071	319	0.0031

Table 4.12 – results related to test point 9

TEST POINT 1				
	active energy		**reactive energy**	
phase	$\overline{x}$ [Wh]	$\sigma/\overline{x}$	$\overline{x}$ [VArh]	$\sigma/\overline{x}$
1	36258	0.00532	63253	0.0019
2	36262	0.00527	63231	0.0019
3	36796	0.00558	64268	0.0020

Table 4.13 – results related to test point 10

TEST POINT 1				
	active energy		**reactive energy**	
phase	$\overline{x}$ [Wh]	$\sigma/\overline{x}$	$\overline{x}$ [VArh]	$\sigma/\overline{x}$
1	58484	0.00162	44151	0.0027
2	58545	0.00156	44130	0.0024
3	58809	0.00163	44510	0.0024

Table 4.14 – results related to test point 11

4.1.4.3 Evaluation of the results

To verify the accuracies declared in the 4.1.2 paragraph, the rated values are considered to calculate the maximum acceptable differences. To compute the uncertainty of the average measured values, the standard uncertainties have been multiplied for a coverage factor of 2, to obtain a 95% confidence interval.
Therefore, for each test point the result can be considered:

- Compliant with the specification: the average value and its confidence interval are entirely inside the acceptable range
- Undetermined: part of the confidence interval is inside the acceptable range and part it is outside
- Not compliant with the specification: the average value and its confidence interval are outside the acceptable range

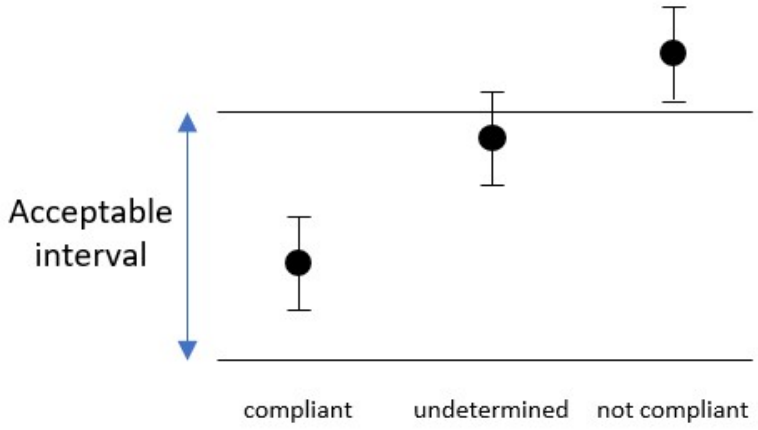

Figure 4.14 – evaluation of the results

In the table 4.15 are indicated all the reference values calculated considering the rated value and the accuracies declared.

Parameter	Rated value	Declared accuracy	Acceptable interval
Voltage	230 V	0.4 %	± 0.92 V
Current	200 A	1.5 %	± 3 A
Active power	46000 W	2 %	± 920 W
Reactive power	46000 VAr	2 %	± 920 VAr
Active energy	73600 Wh	2 %	± 1472 Wh
Reactive energy	73600 VArh	2 %	± 1472 VArh

Table 4.15 – reference values

All the measurements carried out by the Guardian Meter are compliant with the specification declared for the product, therefore, the accuracy classes for voltage, current, power and energy measurements are verified.

4.2 The Network Monitoring Unit (NMU)

4.2.1 Purposes of the instrument

As the Guardian Meter, the Network Monitoring Unit is designed for the installation in electrical street cabinet and it is essentially its evolution.
The main features that characterize the device are:

- Two triplets of Rogowski coil, to monitor both main line and branch
- GSM/GPRS model for sending SMS alarms and to connect with a MySQL server
- Light sensor to monitor the state of closure of the cabinet
- Fault passage indicator function
- Monitoring of the voltage unbalance
- THDv and THDi measurement
- Internal backup battery
- NFC tag

Figure 4.15 – NMU first prototype

Figure 4.16 – NMU final version

The device is installable without putting the cabinet out-of-service thanks to the openable Rogowki coils (Figure 4.17, 50mV/kA @50 Hz) and the CAT IV [27] [28] voltage plugs. Furthermore, to protect the equipment, in every plug is located a changeable fuse (500 mA ultra-rapid).

Figure 4.17 – openable Rogowski coil and voltage plug

The NMU is thought to provide a big amount of information about the quality of the electrical energy supplied in a specified point of the LV network. In particular:

1) Harmonic content: with the THDv and the THDi calculation, it is possible to have an estimation of the harmonic distortion of the voltage and current waveforms.
2) Interruption monitoring: saving periodically the electrical parameters, the continuity of service in the point of installation can be checked. The savings are guaranteed by the internal backup Li-Ion battery, that ensures the device operation without voltage input.
   This functionality is very important in the case the real topology of the network is not known (as described in the 4.1.1 paragraph) and the DSO wants to know which costumers are affected by an outage when a secondary substation circuit breaker intervene for a fault.
3) Under-load and over-load monitoring: as the Guardian Meter, the NMU is very useful to check if a line is under-loaded or over-loaded, measuring the powers, the currents flowing, and the voltage drops. In this way, for example, the DSO can program the update of a branch with higher section cables.
4) Voltage unbalance monitoring: computing the three differences between each couple of RMS voltages (V1-V2, V2-V3, V3-V1), the DSO can check if a line is more loaded of another. Furthermore, if at least one of the three difference overcome a settable threshold, the device suspect a neutral voltage displacement and it automatically sends an SMS alarm.

Furthermore, two more device functions are noteworthy, also if they are less related to the power quality:

1) The fault passage indicator function: if the current overcome a settable threshold, the instrument automatically sends an SMS alarm. This functionality is particularly useful to reduce dramatically the intervention time (how described in 3.1.3 paragraph) and, combined with the periodical storing of the electrical parameters, can provide the timestamp of an interruption beginning.
2) The monitoring of the state of closure of the cabinet, measuring the amount of light, allow to increase the safety of the grid. In fact, it is not uncommon that, for example due to car accident, the street electrical cabinets open making the terminal blocks easily accessible.
   The device sends an SMS when the measured light overcome a threshold, warning the DSO of the unauthorized cabinet opening or breaking.

Obviously, all the functions are available for both lines monitored (thanks to the two triplets of Rogowski coils).

4.2.2 Instrument description

The general characteristics of the device are:

- Power supply: 8 W single-phase linear power supply (admitted voltage range: 230 V ± 10%)
- Accuracy:
  - 2 % (active and reactive energy)

    - 0.4 % (voltage RMS)
    - 1.5 % (current RMS)
    - 5 % (current peak for FPI function)
- Rated voltage: 230 V (RMS)
- Rated current: 100 A (RMS)
- Maximum current for FPI function: 1000 A (peak)
- Over-current threshold range: 0 - 1000 A
- Voltage unbalance threshold range: 0 - 300 V
- Overvoltage category: CAT IV (compliant with IEC EN 61010-1)
- Insulation: double

Regarding the electrical parameters measurement, the microcontroller STM32F411 [29] (ARM Cortex M4, 100 MHz maximum, 512 kB Flash, 128 kB SRAM) do each second the same operation described in the 4.1.2 paragraph for the Guardian Meter (also regarding the creation of data frame and the storing), with these additions:

1) Calculation of the three differences between each couple of RMS voltages and checking if these overcome the settable threshold.
2) Downloading of the THDv and THDi values from the ADE 7880, to monitor the harmonic content of the waveforms.
3) Converting the signal coming the light sensor and checking if this overcome the threshold (the sensitivity is settable)

Regarding the last point, when the operator actives the light monitoring function (also called "anti-tampering" function), the device does a light measurement that will be used as reference.
Furthermore, every 20 ms (scheduled with an internal timer) the microcontroller converts the six voltages coming from the circuits for current peaks detection (schematized in Figure 4.18) multiplying them for the calibration coefficients, checking if there are any over-currents (for the Fault Passage Indicator function).

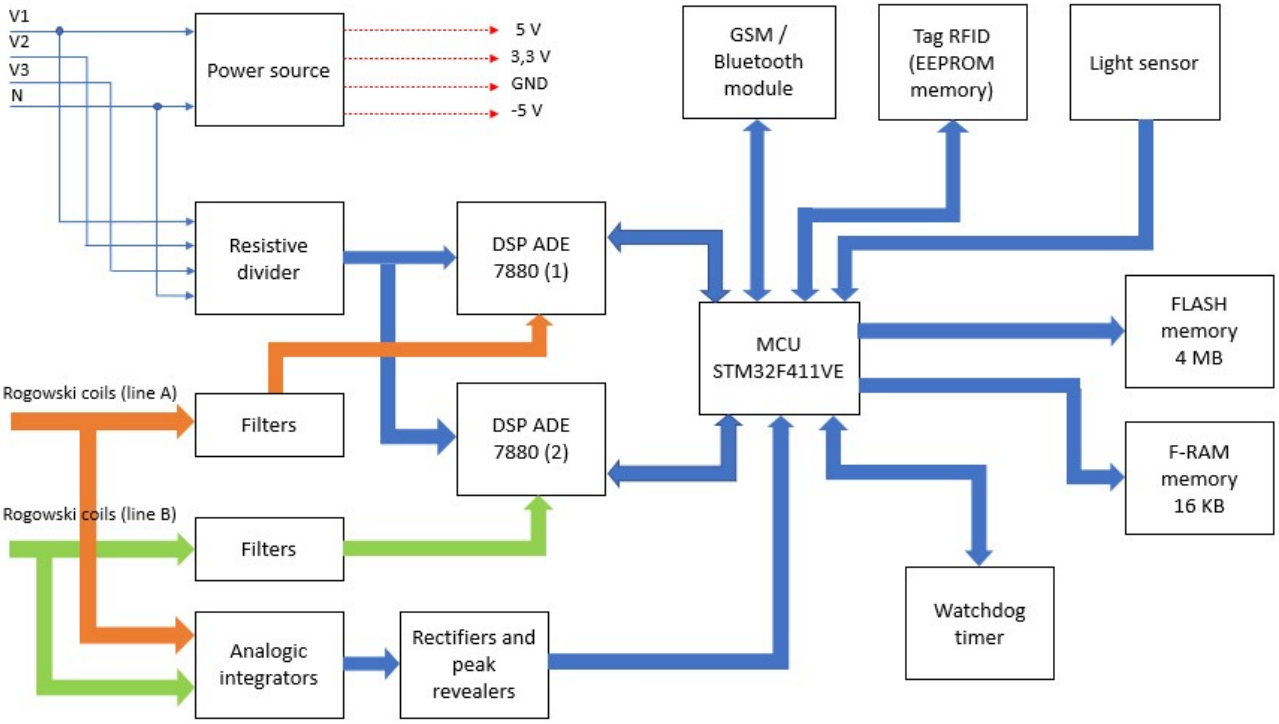

Figure 4.18 – Block Diagram of the NMU

The calibration procedure is almost the same of the Guardian meter, with the addition of a fourth command for the calculation of the peak detector calibration coefficients, since this system does not use the ADE7880 for this purpose, but other hardware. The current to be applied for this passage is 100 A though all the six Rogowski coils.
In Figure 4.19 it is schematized in a simplified way how the firmware works and what are the main scheduled operations carried out.

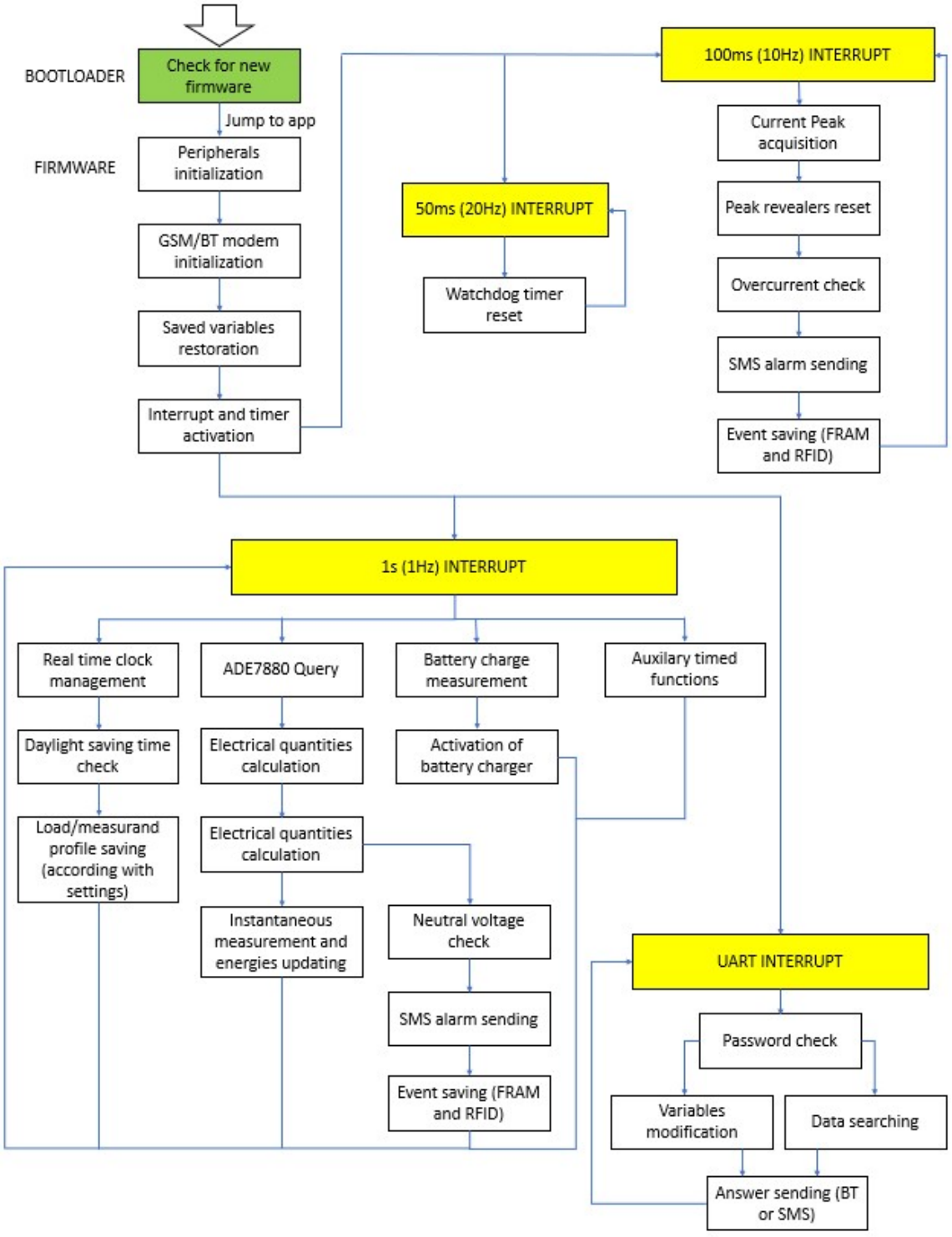

Figure 4.19 – Firmware flow diagram

In case of event (over-current, voltage unbalance or cabinet opening), the device does these operations:

1) Sending an SMS reporting the event (communicating the device ID, the GPS coordinate, the type of event and the parameters measured)
2) Storing the event in the internal flash
3) Storing the event in the EEPROM memory of the internal NFC tag

Since in case of overcurrent the secondary substation circuit breaker could intervene interrupting the power supply, the device is provided of a 300 mAh backup battery to guarantee the correct operation for at least 2 hours.
Furthermore, thanks to the NFC tag it is possible to download all the events without the NMU turned on. This is particularly useful in case the interruption lasting for long time, helping also in this case to find faster the branch involved in a fault.
The commands implemented for the control of the device are the following:

- Set the device ID
- Set the GPS coordinate
- Synchronize the internal real time clock
- Visualize the alarms (from the auto-diagnosis systems)
- Visualize all the instantaneous parameters (with a refresh time of 1 s)
- Visualize the totalizers (with a refresh time of 1 s)
- Download the profiles
- Set the over-current thresholds (for line A and for line B)
- Set the voltage unbalance threshold
- Download the events
- Erase the memories
- Update the firmware

The commands can be sent through a specified Android application (Figure 4.20) in two difference ways:

- locally via Bluetooth communication
- remotely, sending the commands via SMS (the application provide to decode the answers of the NMU, in order to display them correctly)

All the data downloaded in the smartphone or tablet can be exported in .csv format to allow, for example, a post-elaboration.

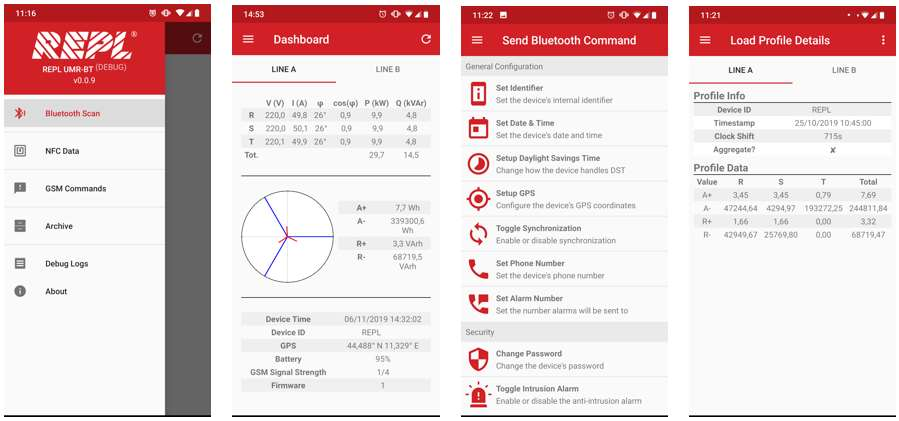

Figure 4.20 – Android application screenshots

Furthermore, if the customer wants store automatically all the data in a central server, it is possible to adding a new feature loading an extended version of the firmware and installing a webserver and a MySQL database on a mainframe, allowing the NMU to communicate with a central database.

In fact, the MySQL structure allow to save neatly huge amount of data, that can be downloaded and managed easily through the open-source "phpMyAdmin" interface (Figure 4.21), accessible with all type of browser from all type of devices and, if the server is connected to internet, from everywhere.

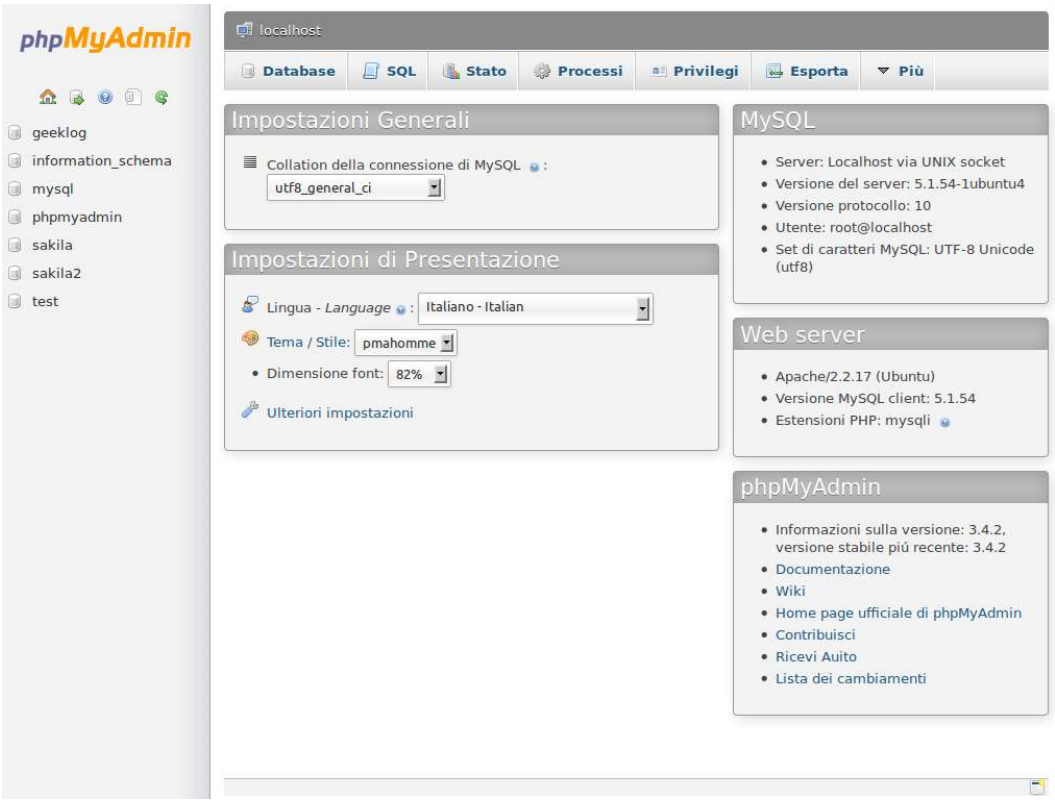

Figure 4.21 – phpMyAdmin interface

Since it is very difficult for the NMU communicate directly with the MySQL server for uploading measurement data, a webserver is used as an interface. In this, some webpages developed in PHP language with the code for SQL communication are uploaded, allowing:

- the connection with the database
- the creation and the erasing of the tables
- the uploading of the measurement data

Therefore, periodically (for the measurement and energy profiles) or when an event occurs, the NMU loads these webpages through their URLs and its GSM/GPRS modem, communicating:

- the IP address of the MySQL server
- the authentication data
- the device information
- the measurement data

In this way, it is possible to store the measurements of all NMU installed in the LV network in a single central server, in order to monitor the network efficiently.

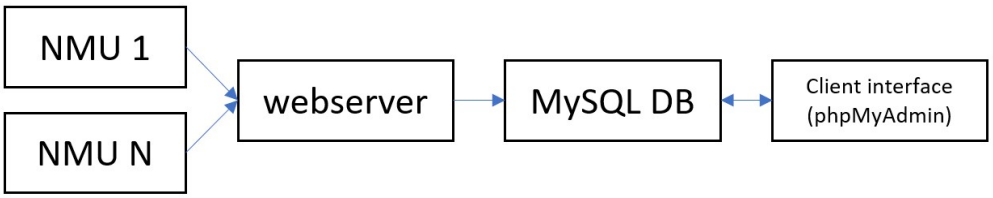

Figure 4.22 – Block diagram of the system for central server storage

4.2.3 Metrological characterization

4.2.3.1 Measure of instantaneous parameters

To evaluate the instrument performance in measurements of instantaneous electrical parameters, the following test points were considered to simulate more load conditions and different situations:

Test point	Voltage [V]	Current [A]	Power factor	Frequency [Hz]
1	230 (RST)	100 (RST)	1	50
2	230 (RST)	100 (RST)	0.5L	50
3	230 (RST)	100 (RST)	0.8C	50
4	207 (RST)	100 (RST)	1	50
5	207 (RST)	100 (RST)	0.5L	50
6	207 (RST)	100 (RST)	0.8C	50
7	253 (RST)	100 (RST)	1	50
8	253 (RST)	100 (RST)	0.5L	50
9	253 (RST)	100 (RST)	0.8C	50
10	230 (RST)	100 (RST)	1	49
11	230 (RST)	100 (RST)	0.5L	49
12	230 (RST)	100 (RST)	0.8C	49
13	230 (RST)	100 (RST)	1	51
14	230 (RST)	100 (RST)	0.5L	51
15	230 (RST)	100 (RST)	0.8C	51
16	230 (RS)	100 (RST)	1	50
17	230 (RT)	100 (RST)	1	50
18	230 (RST)	20 (RST)	0.9L	50
19	230 (RST)	5 (RST)	0.9L	50

Table 4.16 – Test point

In order to carry out the tests, the setup represented in the Figure 4.23 was used, powering the "device under test" and generating the reference signals thought the electrical power standard Fluke 6105A [30] (table 4.17) and the transconduttance amplifier Fluke 55120A [31] (that working as slave unit, allowing to reach the nominal current of 100 A).

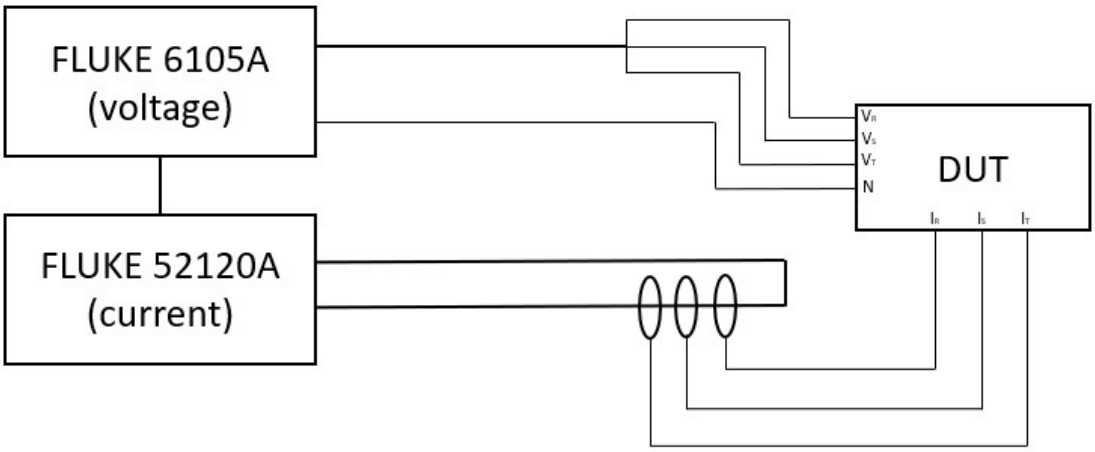

Figure 4.23 – test setup

Maximum voltage output	1008 V
Voltage output uncertainty	60 ppm of output + 3.2 mV (96% confidence level)
Maximum current output (with 55120A)	120 A
Current output uncertainty (with 55120A)	0.015% of the output + 0.006% of full scale (99% confidence level)
Phase resolution	0.001°
Maximum phase error	0.003° at 50 Hz (96% confidence level)

Table 4.17 – electrical standard characteristics

For each test point, 100 measurement are registered (through the Android Application). To characterize the performance, the average values of the measured parameters have been computed. The results are summarized in the following tables.

TEST POINT 1										
	Voltage		**Current**		**phase disp.**		**Active power**		**Reactive power**	
phase	$\overline{x}$ [V]	$\sigma/\overline{x}$	$\overline{x}$ [A]	$\sigma/\overline{x}$	$\overline{x}$ [rad]	$\sigma/\overline{x}$	$\overline{x}$ [W]	$\sigma/\overline{x}$	$\overline{x}$ [VAr]	$\sigma/\overline{x}$
1	229.41	0.00045	99.45	0.00057	0.00352	0.0030	22816	0.00075	80.2	0.0030
2	229.57	0.00040	99.94	0.00053	0.00242	0.0029	22942	0.00072	55.6	0.0029
3	229.76	0.00044	100.76	0.00058	0.00377	0.0028	23151	0.00062	87.2	0.0029

Table 4.18 – results related to test point 1

TEST POINT 2										
	Voltage		**Current**		**phase disp.**		**Active power**		**Reactive power**	
phase	$\overline{x}$ [V]	$\sigma/\overline{x}$	$\overline{x}$ [A]	$\sigma/\overline{x}$	$\overline{x}$ [rad]	$\sigma/\overline{x}$	$\overline{x}$ [W]	$\sigma/\overline{x}$	$\overline{x}$ [VAr]	$\sigma/\overline{x}$
1	229.48	0.00042	100.61	0.00055	1.050	0.0029	11472	0.00525	20024	0.0019
2	229.51	0.00047	100.60	0.00058	1.049	0.0029	11493	0.00539	20023	0.0020
3	229.67	0.00041	99.53	0.00055	1.050	0.0027	11357	0.00494	19837	0.0018

Table 4.19 – results related to test point 2

TEST POINT 3										
	Voltage		Current		phase disp.		Active power		Reactive power	
phase	$\overline{x}$ [V]	$\sigma/\overline{x}$	$\overline{x}$ [A]	$\sigma/\overline{x}$	$\overline{x}$ [rad]	$\sigma/\overline{x}$	$\overline{x}$ [W]	$\sigma/\overline{x}$	$\overline{x}$ [VAr]	$\sigma/\overline{x}$
1	229.51	0.00044	100.71	0.00058	0.647	0.0030	18443	0.00161	13933	0.0027
2	229.60	0.00037	100.65	0.00053	0.647	0.0027	18438	0.00150	13930	0.0023
3	229.69	0.00045	100.36	0.00057	0.647	0.0028	18392	0.00167	13896	0.0023

Table 4.20 – results related to test point 3

TEST POINT 4										
	Voltage		Current		phase disp.		Active power		Reactive power	
phase	$\overline{x}$ [V]	$\sigma/\overline{x}$	$\overline{x}$ [A]	$\sigma/\overline{x}$	$\overline{x}$ [rad]	$\sigma/\overline{x}$	$\overline{x}$ [W]	$\sigma/\overline{x}$	$\overline{x}$ [VAr]	$\sigma/\overline{x}$
1	206.43	0.00046	100.55	0.00057	0.00314	0.0029	20756	0.00074	65.1	0.0030
2	206.55	0.00041	100.15	0.00057	0.00191	0.0028	20687	0.00062	39.5	0.0029
3	206.88	0.00043	98.85	0.00056	0.00422	0.0026	20450	0.00072	86.4	0.0027

Table 4.21 – results related to test point 4

TEST POINT 5										
	Voltage		Current		phase disp.		Active power		Reactive power	
phase	$\overline{x}$ [V]	$\sigma/\overline{x}$	$\overline{x}$ [A]	$\sigma/\overline{x}$	$\overline{x}$ [rad]	$\sigma/\overline{x}$	$\overline{x}$ [W]	$\sigma/\overline{x}$	$\overline{x}$ [VAr]	$\sigma/\overline{x}$
1	206.42	0.00040	99.42	0.00058	1.050	0.0028	10202	0.00518	17805	0.0018
2	206.69	0.00046	99.34	0.00054	1.050	0.0030	10212	0.00556	17813	0.0019
3	206.83	0.00042	99.95	0.00057	1.051	0.0027	10258	0.00508	17946	0.0017

Table 4.22 – results related to test point 5

TEST POINT 6										
	Voltage		Current		phase disp.		Active power		Reactive power	
phase	$\overline{x}$ [V]	$\sigma/\overline{x}$	$\overline{x}$ [A]	$\sigma/\overline{x}$	$\overline{x}$ [rad]	$\sigma/\overline{x}$	$\overline{x}$ [W]	$\sigma/\overline{x}$	$\overline{x}$ [VAr]	$\sigma/\overline{x}$
1	206.47	0.00040	100.49	0.00059	0.646	0.0028	16557	0.00156	12502	0.0025
2	206.51	0.00041	99.99	0.00058	0.646	0.0027	16488	0.00147	12432	0.0025
3	206.71	0.00045	100.50	0.00061	0.647	0.0029	16567	0.00160	12533	0.0026

Table 4.23 – results related to test point 6

TEST POINT 7										
	Voltage		Current		phase disp.		Active power		Reactive power	
phase	$\overline{x}$ [V]	$\sigma/\overline{x}$	$\overline{x}$ [A]	$\sigma/\overline{x}$	$\overline{x}$ [rad]	$\sigma/\overline{x}$	$\overline{x}$ [W]	$\sigma/\overline{x}$	$\overline{x}$ [VAr]	$\sigma/\overline{x}$
1	252.61	0.00044	99.70	0.00058	0.00313	0.0029	25184	0.00074	78.7	0.0029
2	252.61	0.00043	100.75	0.00057	0.00283	0.0028	25449	0.00070	72.1	0.0029
3	252.62	0.00045	99.23	0.00057	0.00400	0.0026	25068	0.00070	100.2	0.0027

Table 4.24 – results related to test point 7

TEST POINT 8										
	Voltage		Current		phase disp.		Active power		Reactive power	
phase	$\overline{x}$ [V]	$\sigma/\overline{x}$	$\overline{x}$ [A]	$\sigma/\overline{x}$	$\overline{x}$ [rad]	$\sigma/\overline{x}$	$\overline{x}$ [W]	$\sigma/\overline{x}$	$\overline{x}$ [VAr]	$\sigma/\overline{x}$
1	252.63	0.00043	99.41	0.00057	1.050	0.0028	12489	0.00516	21789	0.0019
2	252.72	0.00042	100.73	0.00056	1.049	0.0027	12675	0.00496	22077	0.0019
3	252.61	0.00045	99.23	0.00059	1.051	0.0026	12434	0.00486	21766	0.0017

Table 4.25 – results related to test point 8

TEST POINT 9										
	Voltage		Current		phase disp.		Active power		Reactive power	
phase	$\overline{x}$ [V]	$\sigma/\overline{x}$	$\overline{x}$ [A]	$\sigma/\overline{x}$	$\overline{x}$ [rad]	$\sigma/\overline{x}$	$\overline{x}$ [W]	$\sigma/\overline{x}$	$\overline{x}$ [VAr]	$\sigma/\overline{x}$
1	252.47	0.00044	100.11	0.00054	0.646	0.0031	20168	0.00163	15233	0.0028
2	252.69	0.00043	99.74	0.00061	0.646	0.0030	20118	0.00169	15178	0.0026
3	252.61	0.00043	99.49	0.00057	0.647	0.0032	20041	0.00176	15165	0.0027

Table 4.26 – results related to test point 9

TEST POINT 10										
	Voltage		Current		phase disp.		Active power		Reactive power	
phase	$\overline{x}$ [V]	$\sigma/\overline{x}$	$\overline{x}$ [A]	$\sigma/\overline{x}$	$\overline{x}$ [rad]	$\sigma/\overline{x}$	$\overline{x}$ [W]	$\sigma/\overline{x}$	$\overline{x}$ [VAr]	$\sigma/\overline{x}$
1	229.52	0.00044	99.41	0.00063	0.00346	0.0033	22818	0.00076	79.0	0.0033
2	229.61	0.00046	100.02	0.00060	0.00298	0.0031	22966	0.00076	68.5	0.0030
3	229.73	0.00043	100.46	0.00058	0.00433	0.0028	23080	0.00075	99.9	0.0030

Table 4.27 – results related to test point 10

TEST POINT 11										
	Voltage		Current		phase disp.		Active power		Reactive power	
phase	$\overline{x}$ [V]	$\sigma/\overline{x}$	$\overline{x}$ [A]	$\sigma/\overline{x}$	$\overline{x}$ [rad]	$\sigma/\overline{x}$	$\overline{x}$ [W]	$\sigma/\overline{x}$	$\overline{x}$ [VAr]	$\sigma/\overline{x}$
1	229.54	0.00040	99.14	0.00059	1.051	0.0028	11298	0.00514	19743	0.0018
2	229.63	0.00045	100.69	0.00063	1.049	0.0029	11519	0.00543	20048	0.0017
3	229.70	0.00045	99.29	0.00057	1.050	0.0029	11336	0.00527	19790	0.0019

Table 4.28 – results related to test point 11

TEST POINT 12										
	Voltage		Current		phase disp.		Active power		Reactive power	
phase	$\overline{x}$ [V]	$\sigma/\overline{x}$	$\overline{x}$ [A]	$\sigma/\overline{x}$	$\overline{x}$ [rad]	$\sigma/\overline{x}$	$\overline{x}$ [W]	$\sigma/\overline{x}$	$\overline{x}$ [VAr]	$\sigma/\overline{x}$
1	229.54	0.00042	100.65	0.00059	0.646	0.0028	18427	0.00159	13916	0.0025
2	229.53	0.00045	99.05	0.00058	0.646	0.0029	18145	0.00157	13697	0.0026
3	229.66	0.00044	100.21	0.00057	0.647	0.0029	18360	0.00155	13876	0.0027

Table 4.29 – results related to test point 12

TEST POINT 13										
	Voltage		Current		phase disp.		Active power		Reactive power	
phase	$\overline{x}$ [V]	$\sigma/\overline{x}$	$\overline{x}$ [A]	$\sigma/\overline{x}$	$\overline{x}$ [rad]	$\sigma/\overline{x}$	$\overline{x}$ [W]	$\sigma/\overline{x}$	$\overline{x}$ [VAr]	$\sigma/\overline{x}$
1	229.54	0.00040	100.10	0.00060	0.00357	0.0029	22967	0.00078	81.9	0.0030
2	229.50	0.00043	99.40	0.00055	0.00212	0.0027	22812	0.00075	48.4	0.0029
3	229.70	0.00043	100.45	0.00055	0.00406	0.0029	23073	0.00072	93.6	0.0031

Table 4.30 – results related to test point 13

TEST POINT 14										
	Voltage		Current		phase disp.		Active power		Reactive power	
phase	$\overline{x}$ [V]	$\sigma/\overline{x}$	$\overline{x}$ [A]	$\sigma/\overline{x}$	$\overline{x}$ [rad]	$\sigma/\overline{x}$	$\overline{x}$ [W]	$\sigma/\overline{x}$	$\overline{x}$ [VAr]	$\sigma/\overline{x}$
1	229.53	0.00042	100.16	0.00064	1.050	0.0029	11423	0.00535	19950	0.0019
2	229.75	0.00043	100.64	0.00058	1.050	0.0027	11500	0.00499	20059	0.0018
3	229.66	0.00045	100.56	0.00062	1.051	0.0030	11466	0.00571	20047	0.0019

Table 4.31 – results related to test point 14

TEST POINT 15										
	Voltage		Current		phase disp.		Active power		Reactive power	
phase	$\overline{x}$ [V]	$\sigma/\overline{x}$	$\overline{x}$ [A]	$\sigma/\overline{x}$	$\overline{x}$ [rad]	$\sigma/\overline{x}$	$\overline{x}$ [W]	$\sigma/\overline{x}$	$\overline{x}$ [VAr]	$\sigma/\overline{x}$
1	229.50	0.00044	100.76	0.00060	0.647	0.0029	18450	0.00147	13941	0.0027
2	229.65	0.00040	98.89	0.00058	0.645	0.0029	18134	0.00162	13670	0.0025
3	229.64	0.00044	99.71	0.00057	0.647	0.0030	18268	0.00168	13805	0.0026

Table 4.32 – results related to test point 15

TEST POINT 16										
	Voltage		Current		phase disp.		Active power		Reactive power	
phase	$\overline{x}$ [V]	$\sigma/\overline{x}$	$\overline{x}$ [A]	$\sigma/\overline{x}$	$\overline{x}$ [rad]	$\sigma/\overline{x}$	$\overline{x}$ [W]	$\sigma/\overline{x}$	$\overline{x}$ [VAr]	$\sigma/\overline{x}$
1	229.55	0.00041	98.94	0.00056	0.00385	0.0029	22702	0.00072	87.4	0.0029
2	229.50	0.00044	99.67	0.00060	0.00193	0.0029	22874	0.00074	44.2	0.0029
3	229.82	0.00044	99.30	0.00057	0.00379	0.0031	22822	0.00074	86.4	0.0032

Table 4.33 – results related to test point 16

TEST POINT 17										
	Voltage		Current		phase disp.		Active power		Reactive power	
phase	$\overline{x}$ [V]	$\sigma/\overline{x}$	$\overline{x}$ [A]	$\sigma/\overline{x}$	$\overline{x}$ [rad]	$\sigma/\overline{x}$	$\overline{x}$ [W]	$\sigma/\overline{x}$	$\overline{x}$ [VAr]	$\sigma/\overline{x}$
1	229.46	0.00040	100.39	0.00059	0.00330	0.0029	23025	0.00072	76.1	0.0030
2	229.61	0.00041	99.83	0.00062	0.00301	0.0028	22922	0.00077	68.9	0.0029
3	229.64	0.00042	100.01	0.00063	0.00363	0.0026	22965	0.00075	83.4	0.0028

Table 4.34 – results related to test point 17

TEST POINT 18										
	Voltage		Current		phase disp.		Active power		Reactive power	
phase	$\overline{x}$ [V]	$\sigma/\overline{x}$	$\overline{x}$ [A]	$\sigma/\overline{x}$	$\overline{x}$ [rad]	$\sigma/\overline{x}$	$\overline{x}$ [W]	$\sigma/\overline{x}$	$\overline{x}$ [VAr]	$\sigma/\overline{x}$
1	229.55	0.00042	20.41	0.00060	0.454	0.0030	4207	0.00112	2056	0.0027
2	229.55	0.00044	20.18	0.00054	0.453	0.0029	4165	0.00106	2027	0.0026
3	229.90	0.00045	19.81	0.00059	0.455	0.0028	4090	0.00098	2002	0.0027

Table 4.35 – results related to test point 18

TEST POINT 19										
	Voltage		Current		phase disp.		Active power		Reactive power	
phase	$\overline{x}$ [V]	$\sigma/\overline{x}$	$\overline{x}$ [A]	$\sigma/\overline{x}$	$\overline{x}$ [rad]	$\sigma/\overline{x}$	$\overline{x}$ [W]	$\sigma/\overline{x}$	$\overline{x}$ [VAr]	$\sigma/\overline{x}$
1	229.49	0.00044	4.57	0.00059	0.454	0.0029	941	0.00091	460.2	0.0029
2	229.62	0.00046	4.59	0.00059	0.452	0.0029	948	0.00101	461.1	0.0028
3	229.73	0.00045	4.63	0.00059	0.454	0.0030	955	0.00094	467.0	0.0030

Table 4.36 – results related to test point 19

4.2.4.2 Measure of energies

With the same setup, the energy metering performance evaluation is carried out considering these points (20 measurement for each test point have been registered):

Test point	Voltage [V]	Current [A]	Power factor	Frequency [Hz]	Time [h]
20	230 (RST)	80 (RST)	1	50	2
21	230 (RST)	80 (RST)	0.5L	50	2
22	230 (RST)	80 (RST)	0.8C	50	2

Table 4.37 – test points

The results are summarized in the following tables.

TEST POINT 20				
	active energy		reactive energy	
phase	$\overline{x}$ [Wh]	$\sigma/\overline{x}$	$\overline{x}$ [VArh]	$\sigma/\overline{x}$
1	36320	0,00076	114	0,0030
2	36548	0,00066	77	0,0029
3	36238	0,00063	135	0,0029

Table 4.38 – results related to test point 20

TEST POINT 21				
	active energy		reactive energy	
phase	$\overline{x}$ [Wh]	$\sigma/\overline{x}$	$\overline{x}$ [VArh]	$\sigma/\overline{x}$
1	18047	0,00499	31496	0,0016

2	18451	0,00506	32129	0,0018
3	18253	0,00554	31853	0,0019

Table 4.39 – results related to test point 21

TEST POINT 22				
	active energy		reactive energy	
phase	$\overline{x}$ [Wh]	$\sigma/\overline{x}$	$\overline{x}$ [VArh]	$\sigma/\overline{x}$
1	29689	0,00139	22448	0,0025
2	28938	0,00161	21805	0,0025
3	29161	0,00141	22034	0,0023

Table 4.40 – results related to test point 22

4.2.4.3 Metrological performance vs temperature

All the test described previously are carried out at standard ambient temperature (25 ± 2 °C).
Since the temperature inside the street electrical cabinet changes almost as the outdoor temperature, some metrological tests were carried out using the thermal chamber, to evaluate the performance in measurement of the instantaneous parameters at the extremes of the operational temperature range (-10 °C / +55 °C). The test setup used is described in the Figure 4.24, and the test points are collected in table 4.41.
100 measurement for each test point have been registered.

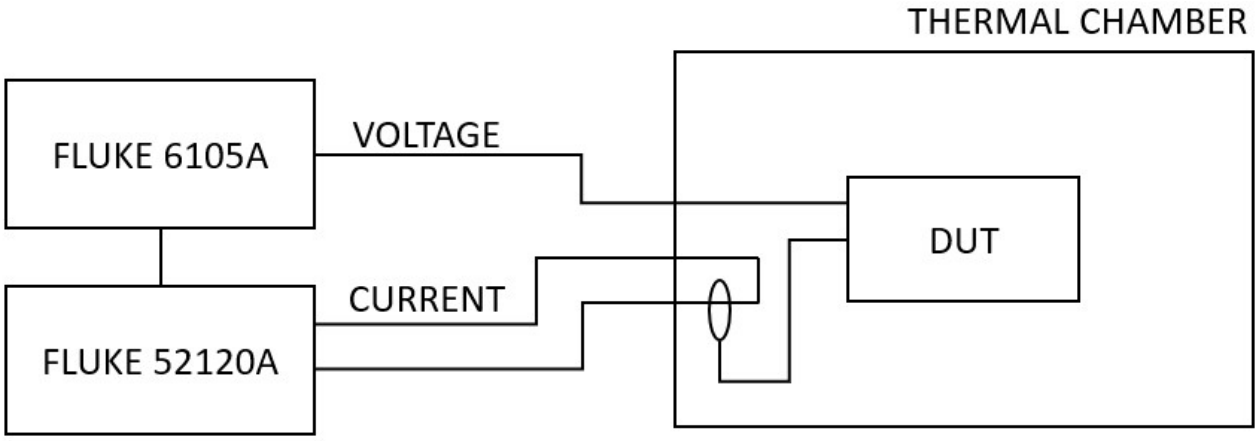

Figure 4.24 – test setup

TEST POINT	Voltage [V]	Current [A]	Power factor	Frequency [Hz]	Temperature [°C]
23	230	100	1	50	-10
24	230	100	0.5L	50	-10
25	230	100	0.8C	50	-10
26	230	100	1	50	55
27	230	100	0.5L	50	55
28	230	100	0.8C	50	55

Table 4.41 – test points

Obviously, I have waited the thermal regime (about 2 hours from the temperature changing) before starting tests. In the following tables are collected the results.

TEST POINT 23										
	Voltage		Current		phase disp.		Active power		Reactive power	
phase	$\overline{x}$ [V]	$\sigma/\overline{x}$	$\overline{x}$ [A]	$\sigma/\overline{x}$	$\overline{x}$ [rad]	$\sigma/\overline{x}$	$\overline{x}$ [W]	$\sigma/\overline{x}$	$\overline{x}$ [VAr]	$\sigma/\overline{x}$
1	230.05	0.00043	99.04	0.00054	0.00333	0.0027	22785	0.00062	75.8	0.0028
2	230.07	0.00042	100.29	0.00062	0.00326	0.0030	23072	0.00080	75.1	0.0032
3	230.05	0.00040	100.65	0.00060	0.00394	0.0029	23154	0.00073	91.2	0.0030

Table 4.42 – results related to test point 23

TEST POINT 24										
	Voltage		Current		phase disp.		Active power		Reactive power	
phase	$\overline{x}$ [V]	$\sigma/\overline{x}$	$\overline{x}$ [A]	$\sigma/\overline{x}$	$\overline{x}$ [rad]	$\sigma/\overline{x}$	$\overline{x}$ [W]	$\sigma/\overline{x}$	$\overline{x}$ [VAr]	$\sigma/\overline{x}$
1	230.08	0.00042	100.50	0.00057	1.05088	0.0027	11488	0.00515	20067.5	0.0016
2	230.17	0.00047	99.89	0.00052	1.04905	0.0029	11459	0.00532	19932.5	0.0020
3	230.04	0.00047	99.45	0.00054	1.05096	0.0030	11364	0.00549	19855.9	0.0020

Table 4.43 – results related to test point 24

TEST POINT 25										
	Voltage		Current		phase disp.		Active power		Reactive power	
phase	$\overline{x}$ [V]	$\sigma/\overline{x}$	$\overline{x}$ [A]	$\sigma/\overline{x}$	$\overline{x}$ [rad]	$\sigma/\overline{x}$	$\overline{x}$ [W]	$\sigma/\overline{x}$	$\overline{x}$ [VAr]	$\sigma/\overline{x}$
1	230.12	0.00044	99.04	0.00057	0.64704	0.0029	18185	0.00171	13739.5	0.0024
2	230.15	0.00044	100.21	0.00058	0.64729	0.0027	18398	0.00153	13907.7	0.0024
3	229.83	0.00045	100.62	0.00056	0.64753	0.0030	18445	0.00165	13950.4	0.0026

Table 4.44 – results related to test point 25

TEST POINT 26										
	Voltage		Current		phase disp.		Active power		Reactive power	
phase	$\overline{x}$ [V]	$\sigma/\overline{x}$	$\overline{x}$ [A]	$\sigma/\overline{x}$	$\overline{x}$ [rad]	$\sigma/\overline{x}$	$\overline{x}$ [W]	$\sigma/\overline{x}$	$\overline{x}$ [VAr]	$\sigma/\overline{x}$
1	229.39	0.00043	98.39	0.00056	0.00365	0.0027	22569	0.00068	82.4	0.0027
2	229.59	0.00040	99.20	0.00059	0.00294	0.0029	22776	0.00069	67.0	0.0029
3	229.33	0.00042	99.46	0.00056	0.00362	0.0029	22809	0.00071	82.6	0.0030

Table 4.45 – results related to test point 26

TEST POINT 27										
	Voltage		Current		phase disp.		Active power		Reactive power	
phase	$\overline{x}$ [V]	$\sigma/\overline{x}$	$\overline{x}$ [A]	$\sigma/\overline{x}$	$\overline{x}$ [rad]	$\sigma/\overline{x}$	$\overline{x}$ [W]	$\sigma/\overline{x}$	$\overline{x}$ [VAr]	$\sigma/\overline{x}$
1	229.43	0.00043	100.38	0.00056	1.05061	0.0030	11447	0.00550	19984.0	0.0020
2	229.35	0.00044	100.08	0.00055	1.05061	0.0029	11409	0.00547	19917.2	0.0018

3	229.49	0.00044	101.25	0.00061	1.05050	0.0029	11551	0.00508	20160.8	0.0021

Table 4.46 – results related to test point 27

TEST POINT 28										
	Voltage		Current		phase disp.		Active power		Reactive power	
phase	$\overline{x}$ [V]	$\sigma/\overline{x}$	$\overline{x}$ [A]	$\sigma/\overline{x}$	$\overline{x}$ [rad]	$\sigma/\overline{x}$	$\overline{x}$ [W]	$\sigma/\overline{x}$	$\overline{x}$ [VAr]	$\sigma/\overline{x}$
1	229.34	0.00043	98.70	0.00062	0.64669	0.0028	18065	0.00147	13638.9	0.0027
2	229.43	0.00044	99.12	0.00056	0.64653	0.0029	18150	0.00153	13698.8	0.0026
3	229.52	0.00042	100.92	0.00056	0.64784	0.0030	18470	0.00171	13977.8	0.0026

Table 4.47 – results related to test point 28

4.2.4.3 Metrological performance with realistic distorted voltages and currents

As described in the previous chapters, the huge dissemination of distorting loads in the network increase the harmonic contents of the voltage and current waveform close to the acceptable limits.
To evaluate the performance of the NMU as energy meter in these scenarios, some test similar of those described in the 5.3 paragraph (for revenue energy meters) were carried out. These are:

- Changing random harmonic tests: the total voltage and current RMS values are imposed to 230 V and 80 A respectively (PF = 0,9L). The harmonic content is automatically changed every ten minutes from the 2° order to the 25° order, considering the limits described in the EN 50160 and imposing the THD to 8. The test duration is 4 hours (the test was repeated 20 times).

- Fixed random harmonic tests: the total voltage and current RSM values are imposed to 230 V and 80 A respectively. The harmonic content is random and fixed for all the duration of the test (considering the limits described in the EN 50160 and imposing the THD to 8). The test duration is 4 hours (the test was repeated 20 times).

The test setup is the same of the Figure 4.23, with the addition of the connection (though GPIB interface) between the calibrator and a laptop. In fact, to automatically change the harmonic content, a LabView software was developed to control the laboratory equipment.
The results of the tests are:

TEST POINT 29				
	active energy		reactive energy	
phase	$\overline{x}$ [Wh]	$\sigma/\overline{x}$	$\overline{x}$ [VArh]	$\sigma/\overline{x}$
1	66861	0.00102	32661	0.0029
2	67201	0.00108	32750	0.0028
3	66003	0.00099	32282	0.0028

Table 4.48 – results related to test point 29

TEST POINT 30				
	active energy		reactive energy	
phase	$\overline{x}$ [Wh]	$\sigma / \overline{x}$	$\overline{x}$ [VArh]	$\sigma / \overline{x}$
1	65617	0.00104	32073	0.0026
2	66782	0.00097	32514	0.0031
3	65506	0.00089	32053	0.0028

Table 4.49 – results related to test point 30

4.2.4.4 Evaluation of the results

As for the Guardian Meter, the results of each test point can be:

- Compliant with the specification: the average value and its confidence interval are entirely inside the acceptable range
- Undetermined: part of the confidence interval is inside the acceptable range and part it is outside
- Not compliant with the specification: the average value and its confidence interval are outside the acceptable range

A coverage factor k = 2 was considered for the confidence interval calculation.
The acceptable range are summarized in the following table:

Parameter	Rated value	Declared accuracy	Acceptable interval
Voltage	230 V	0.4 %	± 0.92 V
Current	100 A	1.5 %	± 1.5 A
Active power	23000 W	2 %	± 460 W
Reactive power	23000 VAr	2 %	± 460 VAr
Active energy	36800 Wh	2 %	± 736 Wh
Reactive energy	36800 VArh	2 %	± 736 VArh
Active energy (harmonic test)	73600 Wh	2 %	± 1472 Wh
Reactive energy (harmonic test)	73600 VArh	2 %	± 1472 VArh

Table 4.49 – acceptable range

All measurement results are compliant with the specification, therefore, the accuracy performance declared are confirmed.

5. Scientific outcomes of the development work

The R&D work for the development and metrological characterization of the new monitoring systems (described in the previous chapter) led to several scientific outcomes. The most significant are reported in this chapter.
In particular, the next sections describe:

- A proposal of a low-cost acquisition board for sampling signals synchronous with the power line.
- A proposal of a set of tests to characterize monitoring systems for LV networks.
- A proposal of new tests to evaluate monitoring systems and energy meters when the voltages and the currents are distorted.

5.1 Accuracy verification of a Low cost PLL-Based Acquisition system

The device under test described in this paragraph is a first prototype of the Guardian Meter (paragraph 5.1) in which, before choosing to use the ADE7880 DSP for acquisition of the signals, it was used the ADC implemented in the microcontroller for signals acquisition, timing the conversion with an external PLL circuit synchronized with the line frequency (in order to avoid the leakage phenomenon).
Thanks to the good performances demonstrated, this solution has found application also as low-cost acquisition board for laboratory and in-field use, very useful for the acquisition of signals with an unstable frequency [97].

5.1.1 Introduction

When measurement acquisition is concerned, a variety of expensive acquisition systems are available on the market to fulfil all kind of final applications. A first application classification can be made on the basis of the measurement campaign location: in-field or laboratory campaign. At the one hand, when measurements are performed inside a laboratory, the working conditions are typically good enough to obtain satisfactory results. On the other hand, in-field measurements require all kinds of precautions to avoid any possible disturbances introduced by the non-controlled environment. For example, a frequent problem faced in-field is the not known frequency of the measured signal. In addition, focusing on measurements on power systems, frequency is a quantity that varies continuously in the allowed range 50 Hz ± 1 % [32]. Hence, the stability required by any acquisition system is not guaranteed.
A second classification, instead, can be made on the economical availability for the application. For Transmission System Operators (TSOs), for example, it is easier to invest money in expensive measurement equipment to monitor their networks. On the contrary, Distribution System Operators (DSOs) are forced to contain spending and to find new cheaper solutions to obtain the same results (as the one proposed in [33-34]). DSOs issues are mainly due to the meshed characteristic of a Medium or Low-Voltage (MV and LV) network. In fact, the presence of thousands of nodes, limits the spread of expensive monitoring solutions, with the effect of a limited monitored portion of grid, except for the critical nodes.
In light of the aforementioned, I and my research group propose a simple acquisition system to answer both the criticalities arose in this Section: adaptability for in-field operations and inexpensiveness for laboratory purposes or for being implemented inside low-cost application

spreadable in the distribution networks. Different works can be found in the literature presenting low-cost solution for either power systems [36-37] or biomedical purposes [38-39]. In [40] instead, the low-cost acquisition board has been already implemented in a smart meter and controlled via LabView software. However, among them, none used a Phase Locked Loop-based (PLL) hardware to prevent spectral leakage phenomenon, although it is a well-known and scientifically tackled topic [41-42].
In this paragraph I want to evaluate the performance of the prototype including a very critical aspect when power systems supply is concerned: the off-nominal, sinusoidal or distorted conditions. Such a non-ideal status of the supply voltage could cause serious damages to the equipment; therefore, its study is mandatory. Consequently, this topic is tackled in almost all power systems research areas: electric machines [44, 45], insulating materials [46], and metering [47]. Furthermore, the study providing a full comparison among off-the-shelf data acquisition systems (DAQ) and the proposed one considering the existing reference literature [48-50] and the related Standard [51] was been completed. Such a comparison is provided for both technical and economic point of view. Tests aimed at assessing the performance of the proposed solution but, at the same time to confront it with expensive but common DAQs available on the market.

5.1.2 Spectral leakage

As already introduced in the previous Section, spectral leakage phenomenon becomes an issue during a signal sampling. Therefore, let us briefly recall this critical concept [40].

5.1.2.1 Definition

Be $s_P(t)$ a periodic signal of period T limited by the *Nth* harmonic. For sampling such a signal, a train of pulses $i(t)$ of period T_s with *2N+1* samples is used:

$$i(t) = \sum_{k=-N}^{N} \delta(t - kT_s) \tag{5.1}$$

Hence, the sampled signal p in the time and in the frequency domain results:

$$p(t) = s_p(t) \cdot i(t) \tag{5.2}$$

And

$$P(j\omega) = S_p(j\omega) * I(j\omega) \tag{5.3}$$

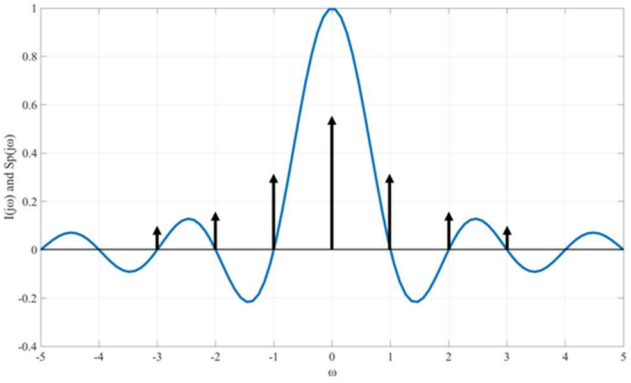

Figure 5.1 $I(j\omega)$ and $S_p(j\omega)$ when the synchronous sampling condition is met

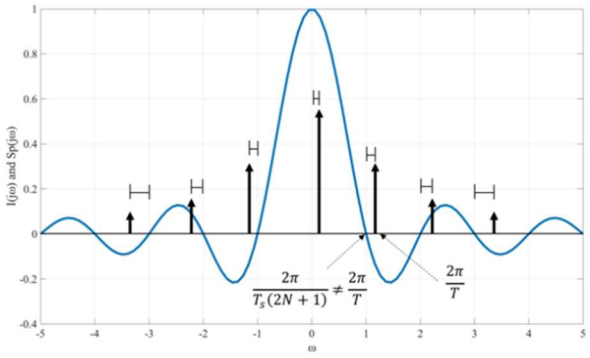

Figure 5.2 $I(j\omega)$ and $S_p(j\omega)$ when the synchronous sampling condition is not met

respectively. Being $S_P j\omega)$ and $I(j\omega)$ the Fourier transform of $s_P t)$ and $i(t)$, respectively. Due to its expression:

$$I(j\omega) = \frac{sin\ \frac{\omega}{2}T_s(2N+1)\Big)}{sin\left(\frac{\omega}{2}T_s\right)} \tag{5.4}$$

$I(j\omega)$ is zero for $\omega_0(k) = \frac{2\pi k}{T_s(2N+1)}$ with k an integer, different from 2N+1.
When the synchronous sampling condition is met, the observation window and the signal period correspond. Moreover, all the s_P (t) harmonic components lay under the main lobe pick or in correspondence of the zero crossings (see Fig. 5.1). Hence, the signal has been correctly acquired and the leakage phenomenon avoided. However, the sampling condition is not always verified, especially in in-field measurement campaigns, because:

- Typically, the signal period is unknown.
- When it is known, the sampling clock rarely has sufficient resolution.
- Finally, when there is a sufficient resolution, the signal period is not stable during all the measurement time window.

Hence, the non-synchronous condition results in a discrepancy between the $I(j\omega)$ zeros and $P(j\omega)$ harmonics
position (see Fig. 5.2). Then, at each convolution step, the harmonic component of the sampled signal the $P(j\omega)$ is related to the $S_P(j\omega)$ by:

$$P\left(\frac{2\pi k}{T_s(2N+1)}\right) = \alpha S_p\left(j\frac{2\pi k}{T}\right) + \sum_{h\neq k}\beta_h S_p\left(j\frac{2\pi k}{T}\right) \tag{5.5}$$

In this expression, the first term is due to the fact that the component of $S_P(j\omega)$ laying under the main lobe, is not perfectly centred. Normalizing $I(j\omega)$, α is a multiplication factor comprised between 0 and 1 which considers the lobe shape and the decentralization of the aforementioned component, quantified as:

$$\Delta\omega = 2\pi\left[\frac{1}{T_s(2N+1)} - \frac{1}{T}\right] \tag{5.6}$$

As for the second term of (5.5), it depends only on the non-correspondence of the harmonics with the zeros of $I(j\omega)$. Each component is weighted by a coefficient β_h which depends on $\Delta\omega$ and on the lobes shape. Going in much detail in the coefficients analysis, during synchronous sampling they are $\alpha = 1$ and $\beta_h = 0\ \forall h$ and therefore $P(j\omega) = S_P(j\omega)$. Instead, when $\alpha < 1$ it is referred as short-range leakage due to dispersion in the main lobe. Finally, when $\beta M \neq 0$ it is referred as long-range leakage due to dispersion in the external lobes. In both cases, it is $P(j\omega) \neq S_P(j\omega)$ and this is usually referred to as leakage error.

5.1.2.1 Methods for leakage error reduction

Due to the effects on the leakage presence during a measurement campaign, some countermeasures need to be taken in advance. The main methods used for such a purpose, and fully describe in the literature [41-43], are:

- Windowing
- Time or frequency interpolation
- PLL hardware synchronization

Among the three, the third one has been adopted in the proposed low-cost acquisition board and detailed in the following Sections.

5.1.3 Acquisition board

The PLL-based acquisition board (Acquisition System, AS from here on out) essentially consists in the following main components: a comparator, a PLL, an adder, a microcontroller with integrated ADC and a personal computer. In Fig. 5.3, a schematic representation of the acquisition systems is shown.

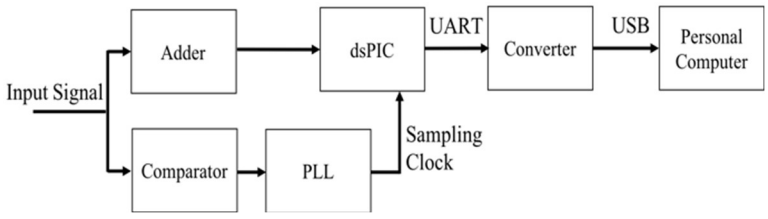

Figure 5.3 Schematic representation of Acquisition System proposed

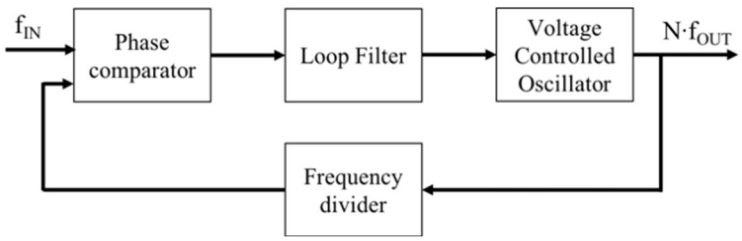

Figure 5.4 PLL general schematic representation

Starting from the input signal, two main branches can be noted. The bottom chain is aimed at generating the sampling clock:

- A comparator transforms the input signal in a square-wave with a frequency f equal to the input signal one.
- A PLL takes the f frequency signal as input and provides a sampling clock signal at a Nf frequency. It provides output for inputs up to 150 Hz, hence enough when considering the power frequency values (50 Hz) adopted in the tests.
- Such output is given to the DSPIC microcontroller as described in the following. A general structure of the PLL is shown in Fig. 5.4 with the blocks commonly required for its implementation: the phase comparator for the input frequency detection and the voltage-controlled oscillator, that provides a new output frequency.

The upper chain of Fig. 5.3 instead, contains:

- An adder block to obtain a completely positive output.
- The microcontroller STM32L452, whose characteristics are listed in Table 5.1. The choice has been supported to extend the range of off-the-shelf tested products. A feature of the adopted microcontroller is the oversampling. It allows to increase the measurement accuracy by acquiring 1 sample each X values (averaging them). However, by considering the results described in the following and the increase of the measurement time window (not always possible in in-field application), such a technique has not been used. The micro samples the positive input signal with a sampling frequency provided by the PLL output: $f_s = Nf$. The sampled signal, can be either stored in the microcontroller memory and then processed, for example, through the Discrete Fourier Transform (DFT), or simply sent as output and processed successively. In this case the latter applies: the output of the STM32 is then transmitted via UART communication interface and then converted to an USB one to store data on a personal computer (PC).

For the sake of clarity, in Fig. 5.5 a block diagram of the acquisition stage of the microcontroller is presented. In the Figure, just one channel has been detailed (4 identical channels). Each of them has its dedicated sample&hold circuit, allowing the simultaneous acquisitions.

Architecture	32-bit	**Max CPU speed**	60 MHz
Memory	512 kB	**SRAM**	52 kB
Temperature Range	-40 to 125 °C	**Operating and Input Voltage**	3 to 3.6 V_{PP}
ADC resolution		12 bits	

Table 5.1 – microcontroller characteristics

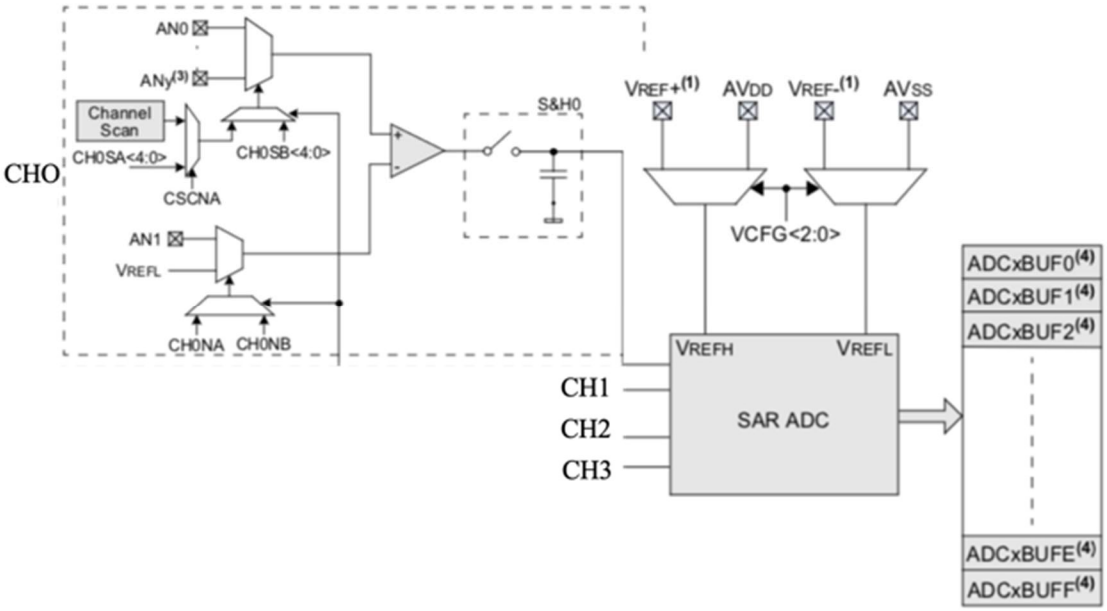

Figure 5.5 - Block diagram of the microcontroller acquisition stage

5.1.4 System Evaluation Tests

Several tests have been developed and performed to assess the AS performance and compare them with off-the-shelf systems. Before detailing them, the instrumentation of the different setups is described.

5.1.4.1 Setup

The instrumentation adopted consists of:

- Fluke Calibrator 6105A (max values 1000 V, 120 A) provides the supply voltage either with a 50 Hz sinusoid or with non-sinusoidal inputs. The latter includes possible frequency variations or harmonic superimposition. It features a 42 ppm accuracy in the voltage range tests (1 - 23 V) described in the following. Moreover, it has been used for testing all the DUTs, hence its uncertainty does not contribute to assess variations among them.
- NI 9215 and NI 9239 (cDAQ controlled), these 2 common acquisition board have been chosen to compare the AS results with. Their specifications are listed in Table 5.2 and 5.3, respectively.

In light of the aforementioned, four tests have been run:

- an amplitude characterization;
- an amplitude vs. frequency characterisation;
- an amplitude vs. harmonics components characterization.
- windowing test

Tests have been performed on all the devices under test: the AS and the two NI DAQs, with the setup shown in Fig. 5.6, valid for the four tests.

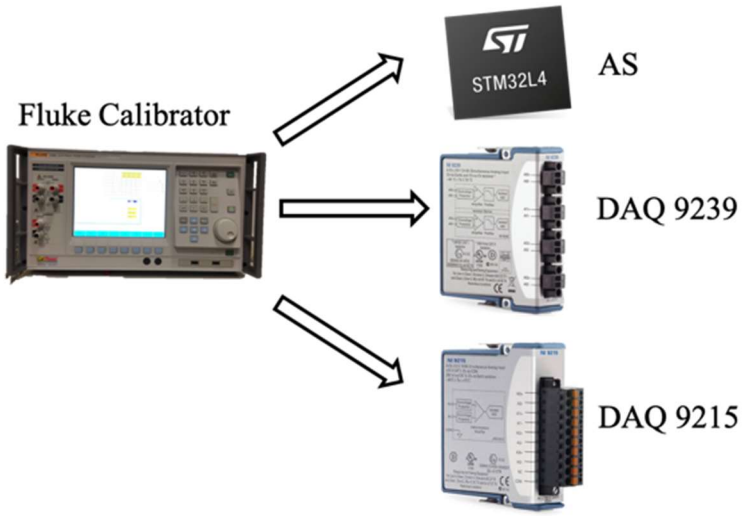

Figure. 5.6 - Automatic measurement setup for the tests performed with the 3 Device Under Test (DUT)

Architecture	24-bit	**Max input signal**	±10 V
Sample rate	50 kS/s/ch	**Simultaneous channels**	YES
ADC	Delta Sigma	**Temperature range**	-40 to 70 °C
Gain Error	0.03 %	**Offset Error**	0.008 %

Table 5.2 – Main characteristics of the NI 9239

Architecture	16-bit	**Max input signal**	±10 V
Sample rate	100 kS/s/ch	**Simultaneous channels**	YES
ADC	SAR	**Temperature range**	-40 to 70 °C
Gain Error	0.02 %	**Offset Error**	0.014 %

Table 5.3 – Main characteristics of the NI 9215

5.1.4.2 Amplitude characterization

It consists in the Fluke Calibrator feeding each device under test (DUT) with a 50-Hz sinusoidal signal. The AS measured the rms value of the waveforms acquired in a range of 0.1 – 1 V rms (i.e. max 2.83 V_{PP}) with a 0.05 V step. As for the two DAQs, a 0.7 – 7 V range has been used with 0.3 V steps. This, to guarantee the same full-scale working condition of the three DUTs. For all the devices, in each step, mean value and standard deviation of the mean of the rms values acquired have been computed. To equalize the results, aside of the capabilities of each device, DUTs only stored the waveforms leaving all the computations to a common software (LabView 2016).

5.1.4.3 Amplitude vs. Frequency characterization

The frequency characterization test setup is the same of Fig. 5.5. The Calibrator feeds the DUT with a sinusoidal signal with an amplitude of 1 V rms. The frequency varies in the range 48.5 to 51.5 Hz with steps of 0.05 Hz. Such interval, according to [32], contains the thresholds within systems with synchronous connection to an interconnected system have to being fed with for the 99.5 % of the time. One hundred sequences of 10 periods for the AS and 200 ms for the DAQ have been acquired as suggested in [13]. All the instruments are connected to a PC which sets the Calibrator and stores the acquired waveforms. The rms values of the components, at tested frequencies, are then computed by applying the same Discrete Fourier Transform algorithm to all the sequences of samples.

5.1.4.4 Amplitude vs. Harmonic components characterization

This third test aimed at completing the power quality tests started with the previous one. To this purpose, according to [32], DUTs have been fed with a signal consisting of the fundamental signal (50 Hz) plus 1 odd harmonic in the range (34-56). Even harmonics have not been considered for the sake of brevity but also because not significant in most of the application concerning Distribution Networks. The amplitude of the superimposed harmonics has been chosen as the maximum value allowed by [32] and detailed in the results Section. Also for this test 100 sequences of 10 periods have been collected, using 1 V rms as amplitude value for the fundamental signal. Then, rms value of the composed signal has been calculated together with its standard deviation. By following the same measurement procedure two more tests have been done concerning harmonics.
First test consists of the same test above described but setting a 30 ° initial phase on the harmonics waveforms. Again, harmonics up to the 25th have been tested and 100 measurements acquired
Second test consists in the simultaneous application of the 3rd, 5th and 7th harmonic on the fundamental signals (7 V and 1 V, rms, for the DAQ and the AS, respectively). Their amplitudes have been selected according to [1], which limits the THD to 5 %. Hence 2.5 %, 3 % and 2.5 % of the applied voltage have been used as values for the 3rd, 5th and 7th harmonic, respectively. Then 100 measurements of the voltage amplitude have been acquired.

5.1.4.5 Windowing test

This last test aimed at verifying a second method for the leakage phenomenon reduction, as mentioned above: the windowing. To this purpose, the 3 DUTs have been used to acquire the same number of samples of the previous tests. Then, trough LabView software, a digital cosine window of the second order, the Hanning, has been applied to the acquired samples.

5.1.5 Results

This Section contains all the tests results. Subsection 5.1.5.1 aims at evaluating the performance of the AS proposed. Subsection 5.1.5.2 instead presents a full comparison among the 3 DUTs analysed in this work.

5.1.5.1 AS evaluation

1) Amplitude

Table 5.4 lists the results of the amplitude characterization performed using the Calibrator. The Table contains the reference voltage value V_{Cal}, the mean value (100 measurements) of the rms voltages measured with or without the PLL block of the AS, V_{Ma} and V_{Mb}, respectively. Both quantities are provided along with their standard uncertainty evaluated with type A method, σ_{Ma} and σ_{Mb}, respectively. From the Table it can be noted that in the case of measurement without PLL, the uncertainty associated is at least one order of magnitude lower than the one of measurements performed with PLL. Furthermore, results in Table 5.4 represents a calibration curve for the developed AS, which can be linearized by applying a regression technique that provides a straight line crossing the axes origin. Hence, it is possible to define the deviation of the calibration curve from the ideal one by means of the gain error *k* and the non-linearity error δ:

$$k = \frac{g - g_n}{g} \tag{5.7}$$

$$\delta = \frac{max\{|V_{M,i} - gV_{Cal,i}|\}}{max\{V_{M,i}\}} \tag{5.8}$$

In (5.7), g is the angular coefficient of the line which linearizes the calibration curve, whereas g_n is the slope (which is unity in suitable coordinates) of the ideal characteristic. As for V_M it refers to both the voltages measured by the AS, V_{Ma} and V_{Mb}. The application of the above method provides $k = 0.010009\ \%$ and $\delta = 0.026829\ \%$ for V_{Ma} and $k = 0.018726\ \%$ and $\delta = 0.027047\ \%$ for V_{Mb}. The 2 parameters highlight that the developed AS features a remarkable linearity over the whole working range, with or without PLL, when the signal is a 50 Hz frequency stable signal.

Reference	***With PLL***		***Without PLL***	
V_{Cal} [V]	V_{Ma} [V]	σ_{Ma} [V]	V_{Mb} [V]	σ_{Mb} [V]
0.1	0.10028	$4\cdot 10^{-5}$	0.09975	$3\cdot 10^{-5}$
0.15	0.15006	$2\cdot 10^{-5}$	0.14994	$4\cdot 10^{-5}$
0.2	0.19997	$3\cdot 10^{-5}$	0.20007	$3\cdot 10^{-5}$
0.25	0.24997	$4\cdot 10^{-5}$	0.25016	$4\cdot 10^{-5}$
0.3	0.300010	$9\cdot 10^{-6}$	0.30027	$4\cdot 10^{-5}$
0.35	0.35007	$1\cdot 10^{-5}$	0.35003	$3\cdot 10^{-5}$
0.4	0.400111	$9\cdot 10^{-6}$	0.40033	$4\cdot 10^{-5}$
0.45	0.450142	$9\cdot 10^{-6}$	0.45008	$5\cdot 10^{-5}$
0.5	0.500184	$8\cdot 10^{-6}$	0.50014	$4\cdot 10^{-5}$
0.55	0.55002	$9\cdot 10^{-5}$	0.55016	$4\cdot 10^{-5}$
0.6	0.600141	$9\cdot 10^{-6}$	0.60015	$4\cdot 10^{-5}$
0.65	0.650123	$8\cdot 10^{-6}$	0.65025	$6\cdot 10^{-5}$
0.7	0.700071	$8\cdot 10^{-6}$	0.70021	$6\cdot 10^{-5}$
0.75	0.750069	$9\cdot 10^{-6}$	0.75016	$6\cdot 10^{-5}$
0.8	0.800090	$6\cdot 10^{-6}$	0.80014	$5\cdot 10^{-5}$
0.85	0.850065	$7\cdot 10^{-6}$	0.85004	$7\cdot 10^{-5}$
0.9	0.899986	$9\cdot 10^{-6}$	0.90014	$5\cdot 10^{-5}$

0.95	0.950005	$8\cdot 10^{-6}$	0.95004	$6\cdot 10^{-5}$
1	1.00007	$1\cdot 10^{-5}$	1.00008	$6\cdot 10^{-5}$

Table 5.4 – Amplitude characterization results

2) Frequency

Frequency test results are reported in Fig. 5.7. They confirm the choice of using an architecture PLL-based. In fact, in the graph, the dotted line represents the 1 V rms acquisition when the PLL is activated, while the other line represents the case when it is not. Close to the frequency of interest (50 Hz) also the latter solution presents good results, but as soon as the frequency changes the measurement goodness drops. Moreover, comparing the standard deviation of the mean between the two cases, it results that with PLL it is 100 times lower than of the second case (10^{-6} vs. 10^{-4}). This is already an effect of the leakage error that, for the same length of the sequence and for the same frequency, leads to different RMS values depending on the sampling starting instant. For sure, this further effect could be reduced if the acquisitions are triggered.

As a final comment on Fig. 5.7, around 50.05 it could seem that there is a drop in the quantity measured by the AS. However, such values, considered the full scale of the Figure, have the same variation from 1 V rms as the other ones but with an opposite sign.

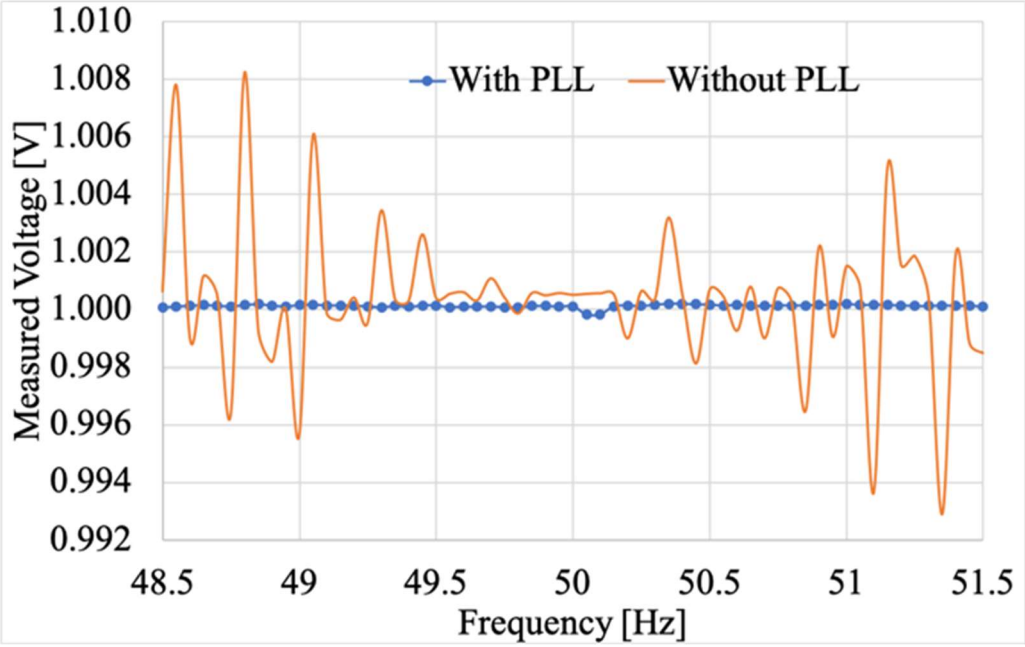

Figure 5.7 - AS Frequency characterization results either when the PLL feature is activated or not

3) Harmonics

As mentioned above, different harmonics have been superimposed (one at the time) to the fundamental signal at 50 Hz. The amplitudes *p (%)* of the harmonics, with respect to the fundamental signal (1 V rms), are listed in Table 5.5. To improve the readability of the results, the Table contains also the total rms value of the voltage V_T (not the single harmonic component) that the Calibrator is providing at its terminals. Such quantity (the reference value) and the results from the acquisitions, with or without PLL, are reported in the histogram of Fig. 5.8. It is interesting to highlight the higher

discrepancy between the results with PLL and the reference value than of the one without PLL (although the absolute value of the difference is limited in amplitude).

Harmonics Superimposition		
Harmonic order [-]	*p [%]*	V_T *[V]*
3	5.0	1.00124922
5	6.0	1.00179838
7	5.0	1.00124922
9	1.5	1.00011249
11	3.5	1.00061231
13	3.0	1.0004499
15	0.5	1.0000125
17	2.0	1.00019998
19	1.5	1.00011249
21	0.5	1.0000125
23	1.5	1.00011249
25	1.5	1.00011249

Table 5.5 – list of harmonics superimposed to the fundamental

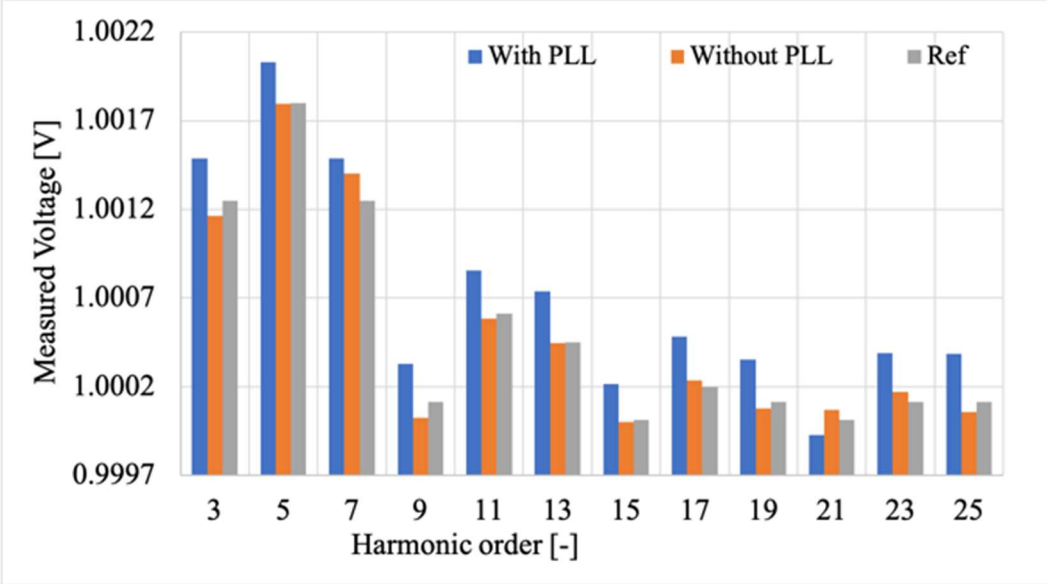

Fig. 5.8 AS Harmonic characterization results either when the PLL feature is activated or not

5.1.5.2 Data acquisition systems comparison

In this final subsection, the 3 different DUTs are compared to determine their performance.

1) Amplitude

For the sake of brevity, the amplitude comparison is provided through the use of the two parameters defined above: the gain and non-linearity error (k and δ). All the values are reported in Table 5.6 . As

it appears from the Table, both AS parameters are definitely consistent with the ones of the NI DAQs. Moreover, all the 3 devices present a remarkable behaviour on the full range considered.

Parameter	AS	NI 9239	NI9215
k [%]	0.010009	-0.015130	-0.003350
δ [%]	0.026829	0.005568	0.015278

Table 5.6 – DUT comparison of the amplitude

2) Frequency

Moving to frequency comparison, the results of the test are shown in Fig. 5.9. These results do not include anymore the solution of AS without PLL because it has already been demonstrated its inefficiency with respect to the PLL solution. In the figure, the solid line represents the 9215, the dashed one the 9239, while the proposed solution is represented by dotted line. From the results it is evident the stability vs. frequency of the proposed acquisition board in all the considered range. The differences among the 3 DUTs, considering their overall little variation in the y axis, can be further highlighted from Fig. 5.10. It contains the standard deviation of the mean for the 3 DUTs in all the frequencies range. The AS provide figures two order of magnitude lower than the other two DAQs (10^{-6} vs. 10^{-4}). A further comment can be made focusing on the two NI DAQs. Both present a quite stable behaviour, the 9215 less than the 9239, on the overall range of frequency expect for some points. In particular, 48.55 Hz for the 9239 and 51.45 for the 9215. These two critical points deserved a particular attention and have been tackled in the next subsection.

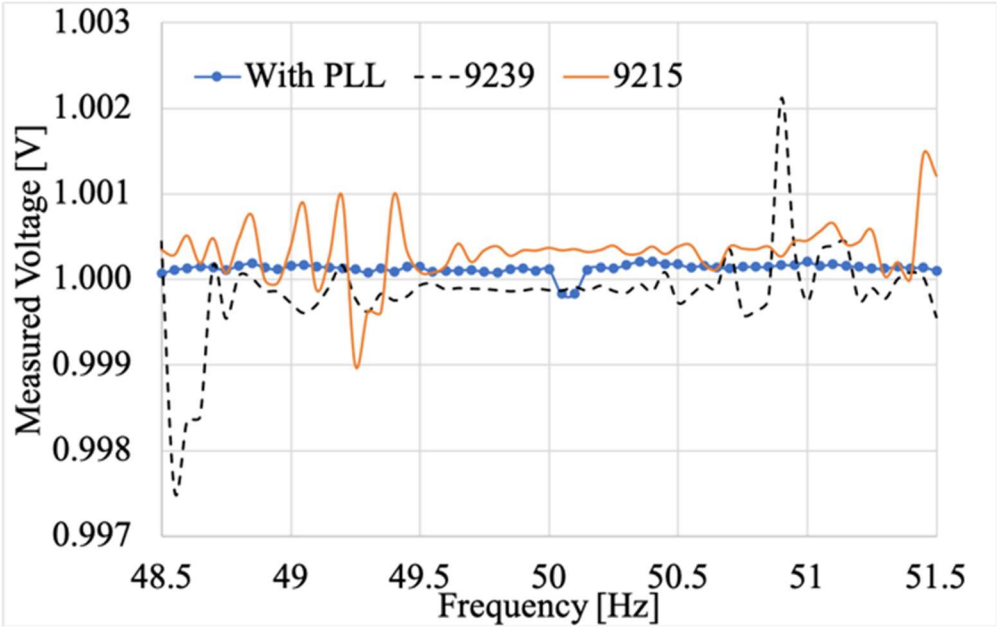

Figure 5.9 - AS Frequency characterization results comparison among the DUTs

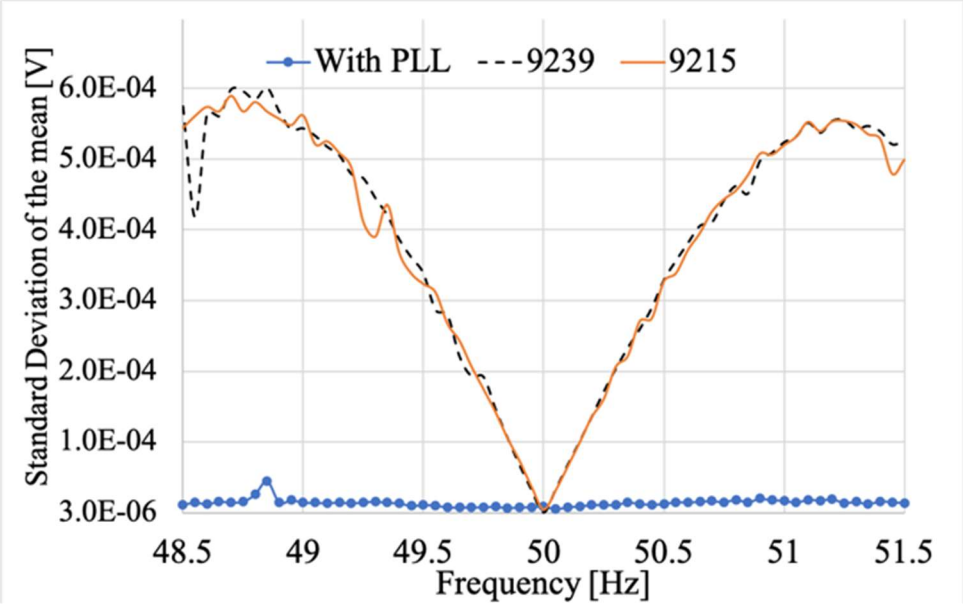

Figure 5.10 - Comparison of the standard deviation obtained from the frequency characterisation, for the 3 DUTs

3) Harmonics

Last comparison concerns the harmonic superimposition on the fundamental signal (50 Hz). Referring to the harmonics' values of Table 5.2, the full comparison among the DUTs is presented in Fig. 5.11. For this analysis the test results of the AS without PLL has been maintained, as explained above, for its consistence with the other results. In fact, it can be seen from the figure that the PLL solution and the 9215 DAQ suffer the most by the harmonics presence, with respect of the 9239 one. In Fig. 5.12, the results of the same test, but with a 30° phase shift of the harmonic waveform, are presented. From the graph it can be noted that the PLL-based proposed solution suffers more than the DAQ from the phase shift. This is confirmed also by comparing Fig. 5.11 with Fig. 5.12. In fact, the variation of the AS measurement is higher compared to the reference one. However, the absolute variation of the results from the reference is limited and still acceptable for the DUTs (max two per thousand), but in particular for the AS. This is due to its limited cost and particular field of application, where inexpensiveness and accuracy have almost the same weight.

As for the multiple harmonics test, results are listed in Table 5.7. At a glance, it emerges that the AS results are 1 order of magnitude worse than the DAQs ones. However, the variation is in the order of 1 per thousand of the reference value (1 V rms), hence a satisfactory results.

To complete the harmonics analysis, the two critical frequencies aforementioned have been used to run another harmonic test. Such test is identical to the one performed at 50 Hz, and it is aimed at discovering if 48.55 and 51.45 Hz are really critical points for the 9239 and 9215 DAQs, respectively. Fig. 5.13 and 5.14 show the results of this tests. The yellow column in Fig. 5.13 represents the measured voltage by the 9239 DAQ when the fundamental frequency is 48.55 Hz. The behaviour confirms what preannounced: at that frequency the DAQ cannot follow the reference value shown in grey. For the other DUTs instead, the selected frequency does not cause any change in their behaviour.

The same conclusion can be made focusing on Fig. 5.14. In this case is the DAQ 9215 whose presenting some issues with the frequency 51.45 Hz. One more time, the rms values measured are completely different from the reference one, while for the other DUTs this is not happening. The main

explanation of these critical behaviour at those frequency can be associated to the different internal architecture of the two DAQs.
Moving to the multiple harmonics presence effects on the measured voltage, results of this test are presented in Table 5.7. It contains the mean value (of 100 measurements) and the associated standard deviation of the mean for the 3 DUTs. Values have been normalized to 1 for the sake of comparison. As it can be seen from the Table, the harmonic presence is not significantly affecting the 3 DUTs. In addition, the AS result is fully comparable with the DAQs, hence implementable also in power quality applications.

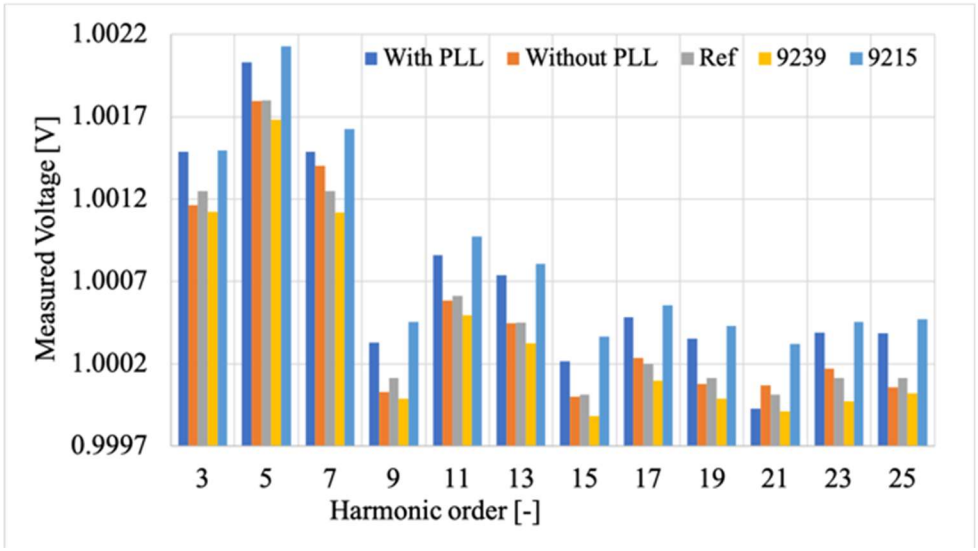

Figure 5.11 - Harmonic characterization results comparison among the DUTs at 50 Hz fundamental frequency

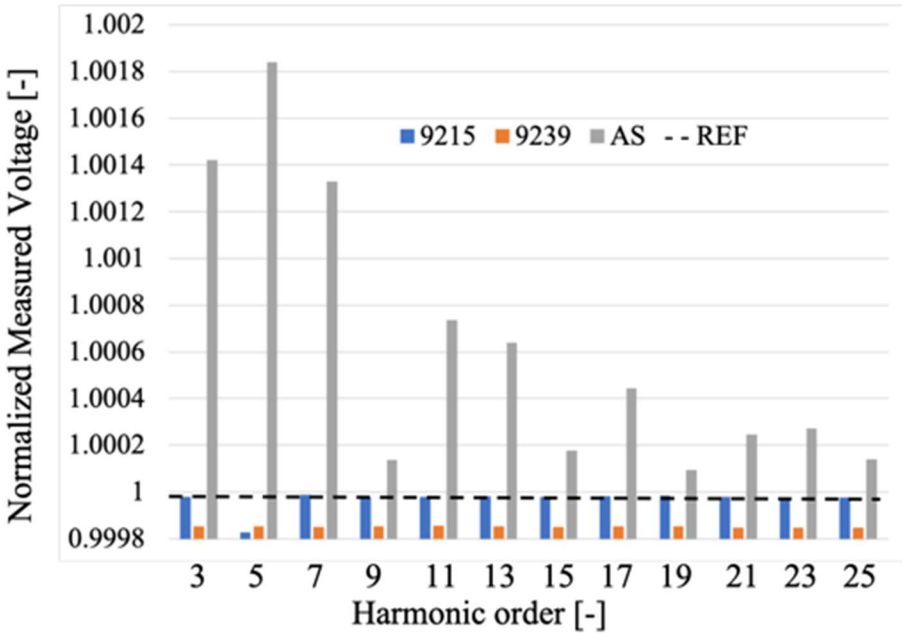

Figure 5.12 - Harmonic characterization (with 30 ° phase shift) results comparison among the DUTs at 50 Hz fundamental frequency

Reference voltage 1 V		
DUT	**Measured Voltage [V]**	**Std. Deviation of the mean[V]**
AS	1.00124	$8 \cdot 10^{-5}$
NI9239	0.9998367	$3 \cdot 10^{-7}$
NI9215	0.999981	$3 \cdot 10^{-6}$

Table 5.7 – DUT comparison of the multiple harmonics presence test results

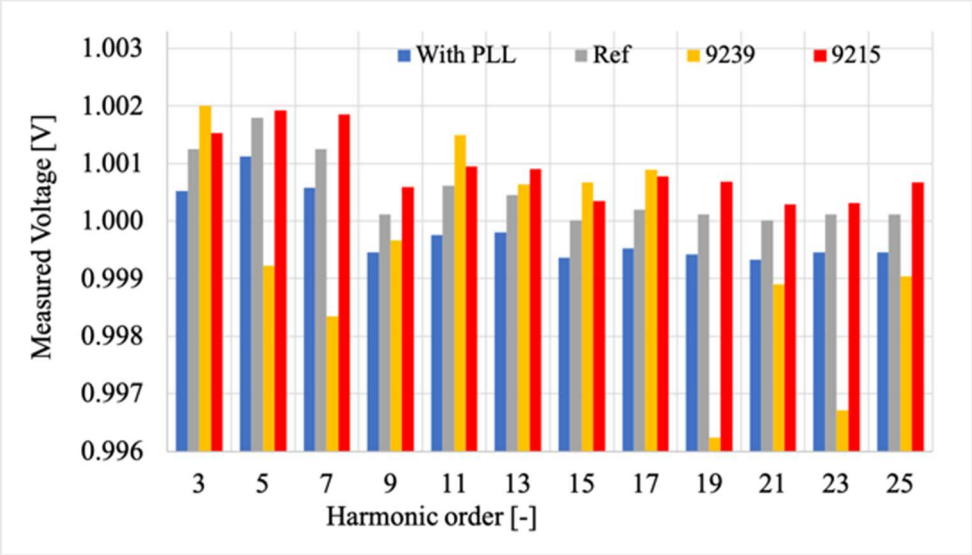

Figure 5.13 - Harmonic characterization results comparison among the DUTs at 48.55 Hz fundamental frequency

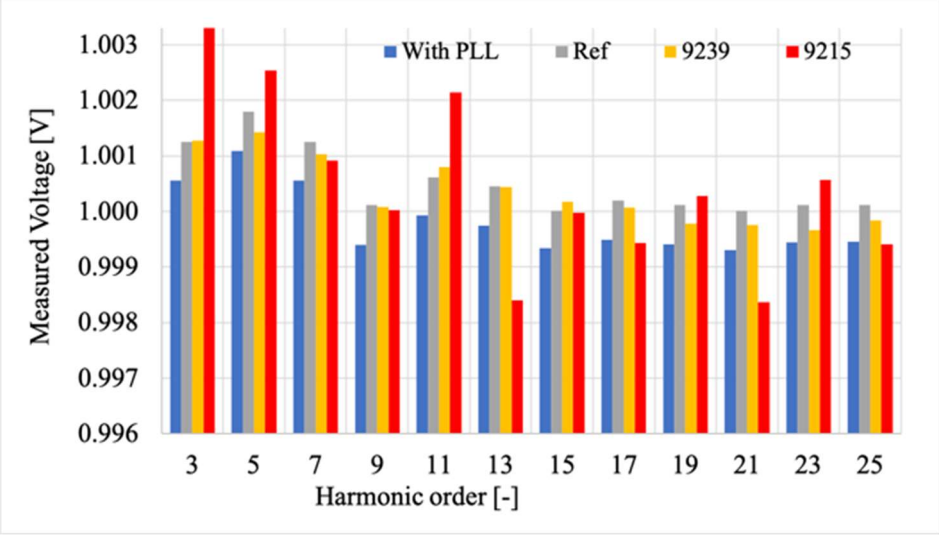

Figure 5.14 - Harmonic characterization results comparison among the DUTs at 51.45 Hz fundamental frequency

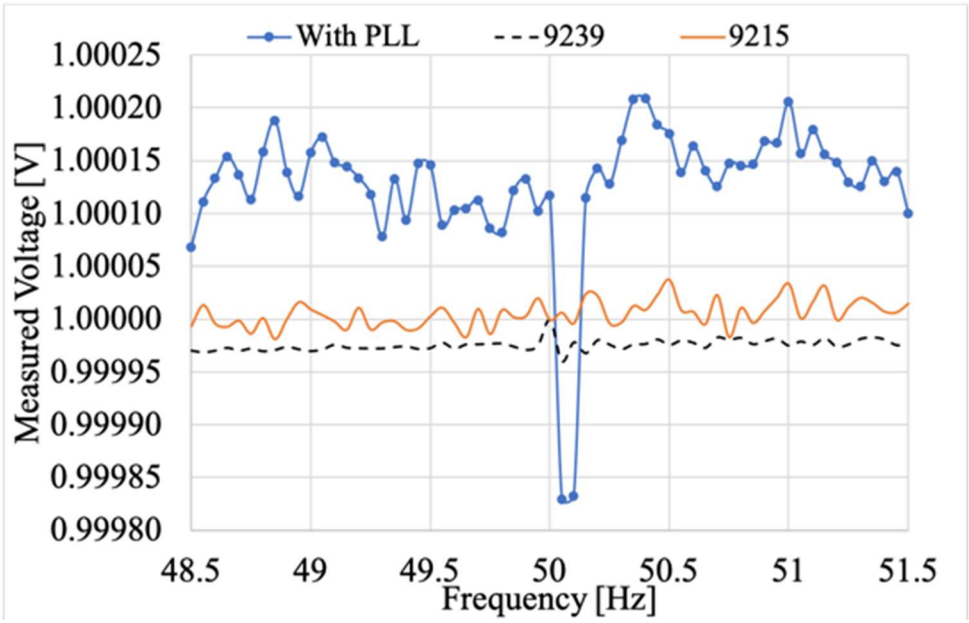

Figure 5.15 - Results of the windowing application results comparison among the DUTs

4) Windowing

In this subsection the results of a Hanning window application on the acquired data is presented. The results are summarised in Fig. 5.14. From the graph it is clear that the window improved dramatically the results of the measurements performed with the two DAQs (9239 and 9215), which are now stable along the overall range of frequencies. Moreover, the standard deviation of the mean associated to the windowed measurements dropped from 10^{-4} to 10^{-6} for both the acquisition boards 9239 and 9215. The results of the proposed solution have been added to the graph to compare its performance in case of windowing. As it can be seen, the AS present high variation with respect of the DAQs, however, the absolute value of these variations is very limited and in the order of $1 \cdot 10^{-5}$. Such value, considering the price of the AS proposed, is very satisfactory and acceptable with respect to the expensive solutions.

5.1.5.3 Economic analysis

To better detail the advantages of the proposed solution, in this subsection a brief economic analysis is provided. By starting from the NI-DAQ board, their average cost is around 1600 € (including board and chassis). Of course, the costs can be slightly reduced if lower accuracy and features are accepted by the user. As for the proposed AS, the evaluation board plus the ST has a single unit cost of 13 €. By adding the PLL and the electronic components added to run the board, an overall cost of 20-22 € is obtained.

In light of the aforementioned cost, some comments arise. The AS it is suitable for two different purposes:

- It is a convenient solution to be implemented inside a laboratory to extend the instrument portfolio of a research group. This without renouncing to the accuracy aspects, as shown in the previous sections.
- Low-cost applications. DSOs and electrical utilities require, for MV and in particular LV networks, inexpensive solutions. Hence, the AS has been completed with chassis and connectors to evaluate its cost impact on a complete measurement system installable in-field.

The overall amount reached the 50 € for a single unit, hence by considering the economy of scale the cost can be halved.

Of course, the analysis might be extended to all kind of acquisition systems available on the market. For example, a compact RIO-based solution costs around 3000 € hence, even if with much higher performance, not comparable with the proposed solution. Furthermore, to my knowledge, one of the cheapest DAQ plus PLL solution available on the market costs 400 €. Therefore, in the overall, the presented comparison tackles a wide scenario of off-the-shelf, expensive or not products, leading to the conclusion that the AS proposed might be well-implemented in multifold applications.

5.1.6 Conclusions

Different applications require different acquisition systems. In particular, in-field or low-cost measurements can be performed only with equipment fulfilling some basic requirements. With this purpose, the paragraph presents a low-cost PLL-based acquisition system solution stressed with all the power quality limits (frequency and harmonics) as defined in the EN 50160. Furthermore, a full comparison among off-the-shelf data Acquisition boards is provided to assess the performance and limitations of the proposed solution. The results, and the <40 € price, confirms its applicability in both laboratory and low-cost distributed network applications. In fact, the proposed system performances are always comparable with the one of common but expensive off-the-shelf systems.

5.2 Performance evaluation of an energy meter for low-voltage system monitoring

5.2.1 The energy meter

The energy meter under test described in this paragraph is an intermediate version of the Guardian Meter (similar to the last one, but with a different model of DSP, different Rogowski Coils, different functions implemented for the measurement evaluation and other minor hardware differences).

The main characteristics regarding the measuring system are:

- Three Rogowski coils featuring: nominal ratio 1000 A/100 mV @ 50 Hz, accuracy 1 %, non-linearity 0.2 %, frequency range 20 Hz – 5 kHz.
- Three resistive voltage dividers having nominal ratio 230 V/ 115 mV and made by resistors with 0.1 % tolerance.
- A conditioning circuit which, among other things, implements a second order antialiasing filter (cut-off frequency set at 4 kHz) for each of the six input channels. The bandwidth of the system is then limited to 4 kHz, sufficient by considering that the power quality frequency range is up to 2.5 kHz.
- A commercial high-accuracy multifunctional energy metering IC. Such a device can operate simultaneous sampling at 8 kSa/s on its six input channels and measure several electrical parameters (for example voltage and current RMS, active and reactive energy and power, harmonics, etc.) with an accuracy up to 0.1 %.
- A 32-bit microcontroller which communicates with the energy metering IC via I2C, stores the measurements in its internal flash memory and makes them available via Bluetooth or USB port.
- Rated voltage: 230 V
- Rated Current: 200 A

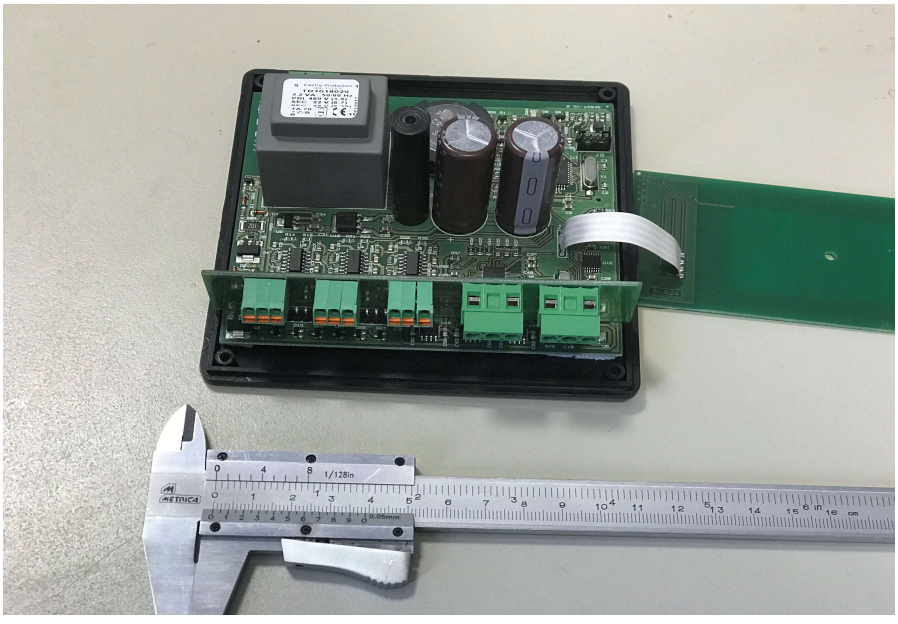

Figure 5.16 – prototype of Guardian meter

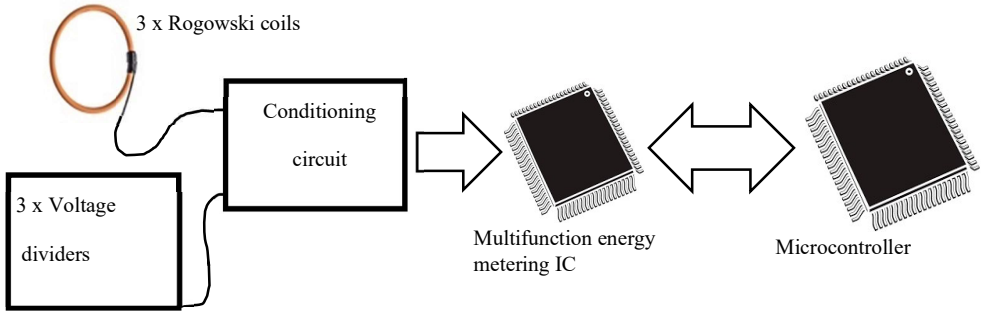

Figure 5.17 - Schematic representation of the designed energy meter

5.2.2 Measurement setup

In order to evaluate the performance of the above-described energy meter, the measurement setup reported in Fig. 5.18 has been implemented. It consists of:

- The energy meter under test (EUT).
- A Fluke 6105A Electrical Calibrator with the Fluke 52120A Transconductance Amplifier.
- A personal computer (PC) running a proper software developed under NI Labview environment and connected to the calibrator via IEEE 488 and to the EUT via USB port.

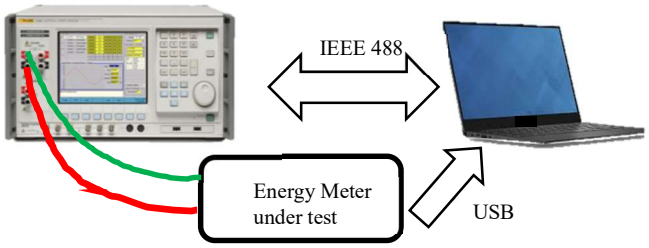

Figure 5.18 - Schematic representation of the measurement setup

The calibrator can provide sinusoidal voltage and current up to 1008 V and 21 A RMS, respectively, in the frequency range 16 Hz ⊚ 850 Hz [30]. The use of the external transconductance amplifier allows to extend the current range up to 120 A [31]. Moreover, it is also possible to set the phase shift between voltage and current with a resolution of 0.001 °. The uncertainty on this angle is 0.003 ° (96 %-confidence level) at 50 Hz. Additional 0.006 ° must be considered, as in this case, when the external transconductance amplifier is used. As for the uncertainty affecting voltage and current, the manufacturer states that it is no more than 60 ppm of output plus 3.2 mV for voltage (96 %-confidence level) and no more than 0.015 % of output plus 0.006 % of range (99 %-confidence) for the current provided by the transconductance. All the above specifications refer to the case of sinusoidal, 50 Hz waveform. The software running on the PC first controls the calibrator by setting

the desired values of voltage, current, frequency and angle. Then, it waits a few seconds to allow all the transients to be ended and starts to read via USB port the measurements performed by the EUT.

5.2.3 Results and discussion

Aim of the experimental activity is to verify the performances of the energy meter depending on the actual network operating conditions, besides to evaluate the uncertainty affecting each measurement of a given quantity. In this connection, all the parameters that can be set in the calibrator (voltage, current, frequency and phase angle) have been considered as influence quantities and their range of variation has been chosen according to what is defined by the international Standards for instruments transformers [11,20,21,57,58]. In particular, the following values have been selected:

- Voltage RMS: 80%, 100% and 120% of the rated RMS voltage (230 V).
- Current RMS: 5%, 20%, 100% and 120% of the rated RMS current (200 A).
- Frequency: 47 Hz, 49.5 Hz, 50 Hz, 50.5 Hz, 52 Hz.
- Phase angle: 60°, 36.870°, 25.842°, 0°, which corresponds to power factors 0.5, 0.8, 0.9 and 1, respectively.

The combination of the above values gives rise to 240 different working conditions. For each of them, 100 measurements of voltage and current RMS U and I, active and apparent power P and S have been performed and stored for each of the three phases of the energy meter, which have been all connected to the same source. Moreover, two turns of cable around the Rogowski coils allow to get an equivalent current of 240 A, as requested. Mean values and standard deviations have been computed and, in order to simplify the comparisons, normalized to the values obtained under rated working conditions (230 V, 200 A, 50 Hz, unity power factor) which have been taken as reference and whose mean values U , I, P and S have been to set to 1 p.u. (per unit). The first observation that can be drawn from the obtained results is that the contribution of random effects can be considered negligible. In fact, the relative standard deviations result lower than 10^(-3) in all the 240 situations tested.
As for the performance under different working conditions, for the sake of brevity only the analysis of the variations of the active power versus voltage, current, frequency and power factor are reported in the paragraph. In each of these analysis, the quantities that aren't varied are kept constant to their rated values. Fig. 5.19a to 5.19d graphically shown the above relationships for phase #1 and can be considered as a sort of calibration curves. From such figures, it can be learned that the performances seem very good as far as the variation of voltage, current and frequency is concerned. As for the power factor, it appears as the active power is slightly overestimated and that such a behaviour is more marked for lower power factor. This can be easily explained if a constant phase error occurs in the measurement of voltage and current phasors. In fact, according to the cosine function, a given difference between actual and estimated phase leads to variation of the cosine that gets higher as the angle gets wider. To numerically quantify the performances, the calibration curves of Fig. 5.19a, b and d are then linearized by applying a regression technique, which provides a straight line crossing the axes origin; this way it is possible to define the deviation of the calibration curve from the ideal characteristic by means of the well-known following indexes:

$$k = \frac{g - g_n}{g_n} \tag{5.9}$$

$$\delta = \frac{max\{|y_i - g x_i|\}}{y_{FS}} \tag{5.10}$$

In (5.9), g is the angular coefficient of the best fit line y=gx, which linearizes the calibration curve, whereas g_n is the slope of the ideal characteristic. In (5.10), y_i is the generic measurement of the EUT, whereas x_i denotes the reference measurement. In the end, y_{FS} refers to the maximum of y_i. Let us refer to k and δ as gain error and the non-linearity error, respectively. As for data in Fig. 5.19c, given that it is expected that the ideal curve is horizontal (and hence g_n=0), two different indexes are used:

$$\alpha = \frac{1}{N}\sum_{i=1}^{N}(y_i - x_i) \tag{5.11}$$

$$\beta = \frac{max\{|y_i - x_i|\}}{y_{FS}}, \tag{5.12}$$

where N is the number of measurements. The higher is α, the more biased are the measurements provided by the energy meter with respect to reference ones. The lower is β, the lower is the difference between actual and reference measurements. Table 5.8 shows the value of the above indexes for the case depicted in figures 5.19a-d. Such numbers confirm the previous considerations: the measured active power exhibits a very good linearity vs. voltage, current and frequency. On the contrary, when the power factor is considered, the effect of a constant phase error makes such relationship non-linear. Very similar results hold for the other two phases.

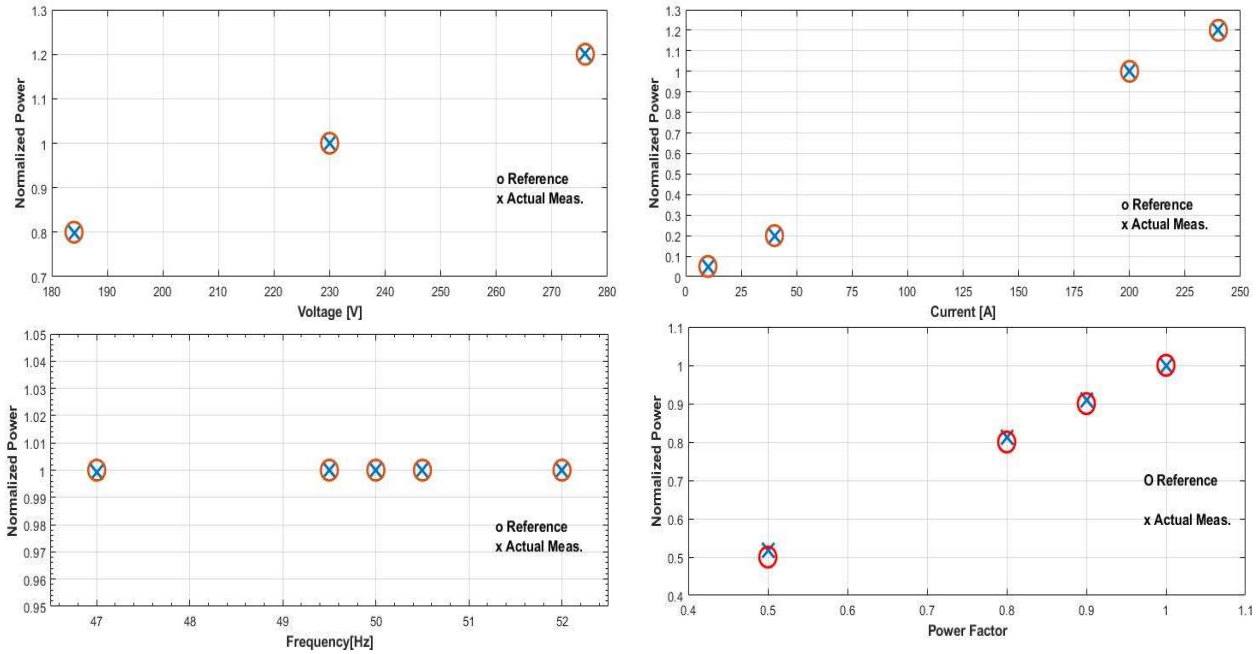

Figure 5.19 - Calibration curves of active power vs. voltage (a), current (b), frequency (c) and power factor (d)

	k(%)	δ (%)	α(%)	β(%)
vs. voltage	0.0097	0.054	-	-
vs. current	0.014	0.019	-	-
vs. frequency	-	-	0.067	0.060
vs. power factor	0.95	1.12	-	-

Table 5.8 Indexes of the calibration curves of the active power

5.2.4 Conclusions

This paragraph has presented the design and the performance of an intermediate version of the Guardian Meter, an energy meter developed for some European utilities mainly to compare its measurements with the ones provided by energy meter installed by the costumers and to monitor the main electrical parameters of the network.
The main characteristics of the system are its high accuracy, its capability to be installed during network operation, the possibility to be both remotely and locally controlled vie PLC and Bluetooth, respectively. Experimental results, aiming at verifying the metrological performance of the system, confirm that the abovementioned specifications have been successfully met by the developed system.

5.3 Testing of electrical energy meters subject to realistic distorted voltages and currents

On the basis of the tests for the NMU described in the paragraph 5.2.4.2, I and my research group have developed a procedure to evaluate the performance of standard revenue energy meters (compliant with the standard IEC 50470) when the voltage and current waveforms are distorted. Our method, illustrated in the next paragraph, is thought to simulate the worst conditions to which the meters can be subjected when they are connected to the LV network [99].

5.3.1 Introduction

As introduced in the previous chapters, the observability of the distribution network (low and medium voltage, LV and MV) is becoming a key-factor after the huge revolution of the grid towards the smart grid concept [59–63]. Effective control stability of the network and fair energy billing [64–66] are possible when accurate measurements of the energy consumed/generated by users/producers are collected by energy meters (EM). In addition, the knowledge of such critical quantities can be used to run several algorithms used to manage and control the network [67–70]. However, the measurement process performed by EMs is affected by the spread among the network of renewable energy resources and non-linear loads, which worsen the electric power quality (PQ), and hence the quantities to be measured by EMs.

Nowadays, electronic EMs are replacing the old electromechanical induction meters, even if their behaviour is acceptable with medium–low levels of PQ [71]. The reason is that EMs are preferred because they enable utilities and consumers to perform "smart" operations, such as remote readings, computation of many power quality parameters, managing real-time pricing, and smart load control [72]. Consequently, with the increase of complex operations demanded of EMs, due to the variety of algorithms and technology that can be implemented, their behaviour in all possible operating conditions should be assessed even with regards to the applicable standards [73–75]. To this purpose, the literature offers a variety of works on the topic. In [76], EMs' response to harmonic active power components up to 3 kHz was tested. In [71], a calibration procedure for EMs based on the generation of random non-sinusoidal signals, while in [77], a portable instrument for on field EM calibration was developed. In [78,79], a metrological characterization of EMs for non-sinusoidal reactive energy was presented. Finally, [80,81] dealt with the testing of one EM (under non-sinusoidal conditions) and proposed a new set of tests, respectively.

The aim of this activity is to contribute, in a different way, to the definition of test signals to be applied to the energy meters. The idea came from the current literature and the standards in which the described signals are stressing specific situations that may happen during the network operation. However, to my knowledge, none of them tackled the issue from a more realistic point of view. Therefore, the goal of the presented research is to propose a possible procedure based on test waveforms that try to emulate, as far as possible and with a simple methodology, the daily behaviour of the network.

Support to this choice is given by the current literature which is facing the same issue of providing actual or more realistic waveforms to the devices under test. For example, [24–26] was done on current transformers, while in [85,86] for the voltage ones.

Starting from the standards [9,11], realistic test waveforms have been designed and applied to three different Measuring Instruments Directive-compliant class B single-phase EMs. In particular, EMs

rated as Measuring Instruments Directive (MID) class B have been chosen because it is the same as the new revenue meters deployed by the main Italian distribution system operators [87]. Then, the meters accuracy was evaluated through the error index defined in the standards.

5.3.2 Regulatory context

The reference documents for EMs, detailed in [88], are (i) the European Directive 2014/32/EU [33], also known as Measuring Instruments Directive, which concern all the measuring instruments; (ii) the EN 50,470 series [90–92] that is the harmonized standard in force for electricity metering equipment; (iii) the IEC 62052 [93] and IEC 62053 [94,95] with modifications in order to be compliant with the MID. This work concerns the three accuracy classes C, B, and A, which are described in the EN 50470-3 [92]. Nevertheless, some electronic energy meters are marked also with the IEC accuracy class: in particular, the IEC 62053-22 and 62053-21 define four accuracy classes: 0.2S, 0.5S, 1, 2 [94,95]. Thus, it is interesting to compare the accuracy requirement of the two standard families, as it has been already carried out in [88]. For the sake of brevity, only some of the main aspects are reported here, focusing mainly on the harmonic disturbance-related aspects.
The accuracy classes defined by both the standards families are based on the percentage error *e%*:

$$e\% = \frac{E_m - E_t}{E_t} \cdot 100 \tag{5.13}$$

where E_t is the reference energy with traceable uncertainty and E_m is the energy registered by the meter. In Table 5.9, the percentage error limits for the accuracy classes prescribed by EN 50470-3 are listed as function of the load, current, and power factor (PF). The current ranges are in per-unit with base quantity I_{ref} , as the rated current. Adopting the same notation, Table 5.10 presents the percentage error limits prescribed in IEC 62053-21 and IEC 62053-22. Note that, (i) classes 0.5S, 1, 2 are comparable, respectively, to classes C, B, and A; (ii) there is no accuracy prescriptions for class 2 meters if a capacitive load is present; therefore, not exceeding the class B and A limits ensure that class 1 and 2 limits are not exceeded. (iii) concerning the classes C and 0.5S, one class does not cover the other: class 0.5S applies accuracy constraints on a current range below the lower limit identified by the class C. Nevertheless, class C demands a smaller percentage error for currents $\geq 0.1\ I_{ref}$ and $PF \neq 1$. The reference conditions at which the accuracy class percentage error limits are defined are the same for the comparable classes (1 and B, 2 and A, 0.5S and C).

	EN 50470					
	Class A		**Class B**		**Class C**	
	Power Factor					
$i=I/I_{ref}$ [p.u.]	1	0.8 cap, 0.5 ind	1	0.8 cap, 0.5 ind	1	0.8 cap, 0.5 ind
$0.03 \leq i \leq 0.05$					± 1.0	
$0.05 \leq i \leq 0.1$	± 2.5		± 1.5		± 1.0	
$0.1 \leq i \leq 0.2$	± 2.0	± 2.0	± 1.0	± 1.0	± 0.5	± 0.5
$0.2 \leq i \leq 5$	± 2.0	± 2.0	± 1.0	± 1.0	± 0.5	± 0.5

Table 5.9 - Percentage error limits defined by EN 50470

	IEC 62053							
	Class 2		Class 1		Class 0.5S		Class 0.2S	
	Power Factor							
$i=I/I_{ref}$ [p.u.]	1	0.5 ind	1	0.8 cap, 0.5 ind	1	0.8 cap, 0.5 ind	1	0.8 cap, 0.5 ind
0.01 ≤ i ≤ 0.02					± 1.0		± 0.4	
0.02 ≤ i ≤ 0.03					± 1.0	± 1.0	± 0.4	± 0.5
0.03 ≤ i ≤ 0.05					± 1.0	± 1.0	± 0.4	± 0.5
0.05 ≤ i ≤ 0.1	± 2.5		± 1.5		± 0.5	± 1.0	± 0.2	± 0.5
0.1 ≤ i ≤ 0.2	± 2.0	± 2.5	± 1.0	± 1.5	± 0.5	± 0.6	± 0.2	± 0.3
0.2 ≤ i ≤ 5[a]	± 2.0	± 2.0	± 1.0	± 1.0	± 0.5	± 0.6	± 0.2	± 0.3

Table 5.10 - Percentage error limits defined by IEC 62053-21, -22

Considering the standards' part concerning the evaluation of how the influence quantities impact the accuracy, it can be found that the IEC 62053-22 does not prescribe the "DC and even harmonics" and "odd harmonics" tests. However, the most noticeable difference introduced by the MID is the definition of the composite error e_c:

$$e_c=\sqrt{e^2(I, \cos\phi)+\delta^2(T, I, \cos\phi)+\delta^2(U, I, \cos\phi)+\delta^2(f, I, \cos\phi)} \tag{5.14}$$

where:

- I and $\cos\varphi$ are, respectively, the current magnitude and the power factor that fully describe a certain load;
- $e(I, \cos\varphi)$ is the percentage error at reference conditions, in presence of the load described by I and $\cos\varphi$;
- $\delta(T, I, \cos\varphi)$ is the additional error due to the temperature variation, in presence of the load described by I and $\cos\varphi$;
- $\delta(U, I, \cos\varphi)$ is the additional error due to the voltage variation at the same load, in presence of the load described by I and $\cos\varphi$;
- $\delta(f, I, \cos\varphi)$ is the additional error due to the variation of frequency, in presence of the load described by I and $\cos\varphi$.

The composite error e_c contemporarily considers multiple effects on the accuracy class and it shall not exceed the maximum permissible errors (MPE) detailed in Table 5.15 of the EN 50470-3 standard [92].

Focusing on the tests for the EM calibration in presence of harmonic disturbances, three different categories of disturbances can be found in the standards EN 50470-3 and IEC 62053-21: (i) harmonic components in the current and voltage circuits; (ii) DC and even harmonics in the current circuit; (iii) odd harmonics in the current circuit. In the IEC 62053-22 only test, (i) is defined. Moreover, a test for current sub-harmonics is prescribed, but it will not be discussed since it deals with a case that is not under the scope of this work. The additional percentage error limits admitted for the above tests are listed in Table 5.11.

Disturbance	Value of Current	*PF*	Limits of Additional Percentage Error for Meters of Class Index ± [%]						
			A	**B**	**C**	**2**	**1**	**0.5S**	**0.2S**
Harmonic components in the current and voltage circuits	0.5 I_{max}	1 [a]	1.0	0.8	0.5	1.0	0.8	0.5	0.4
DC and even harmonics in the a.c. current circuit	$\frac{I_{max}}{\sqrt{2}}$	1	6.0	3.0	1.5	6.0	3.0	-	-
Odd harmonics in the a.c. current circuit	0.5 I_{ref}	1	6.0	3.0	1.5	6.0	3.0	-	-

Table 5.11 - Additional percentage error limits for the harmonic disturbance tests regarding the accuracy classes A, B, C (EN 50470-3) and 2, 1, 0.5S, 0.2S (IEC 62053-21, -22)

The peculiarity of all the harmonic disturbance tests for the active EMs calibration is the fact that a standard test waveform has been chosen, distinguished by a very specific harmonic content. For instance, in the disturbance category (i) the voltage and current waveforms are both formed by a fundamental and a 5th harmonic component, but with different Total Harmonic Distortion factor (THD): 10% for the voltage and 40% for the current. The fundamental and the 5th component of voltage are in phase at the positive zero crossing and the current components are in phase with the same-order voltage components. As for the disturbance category (ii), the standards establish a half-wave rectified current waveform, composed just by even harmonics with a THD ≈ 87%, while for the disturbance category (iii), a phase-fired alternate current waveform, made by odd harmonics and characterized by a THD ≈ 113% is defined. In Figure 5.20 and 5.21 the time-domain signal and the magnitude spectrum of the mentioned test waveforms are depicted, respectively.

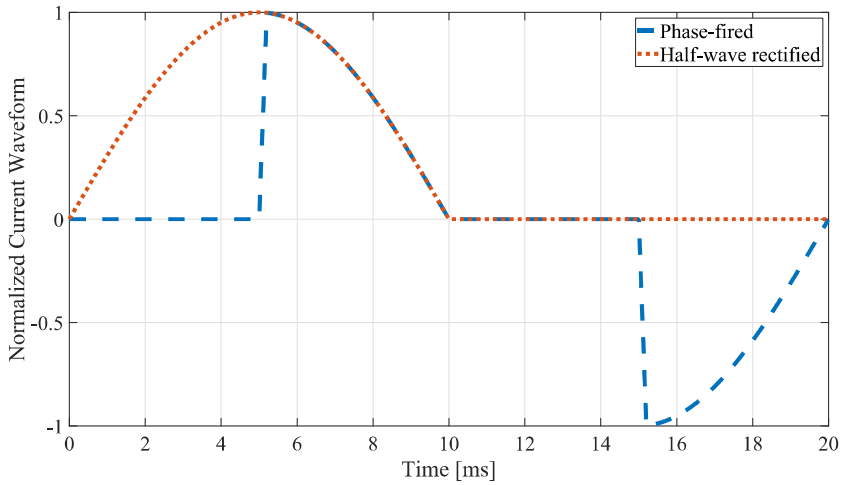

Figure 5.20 - Odd and even harmonic disturbance tests waveforms defined in EN 50470-3 and IEC 62053-21

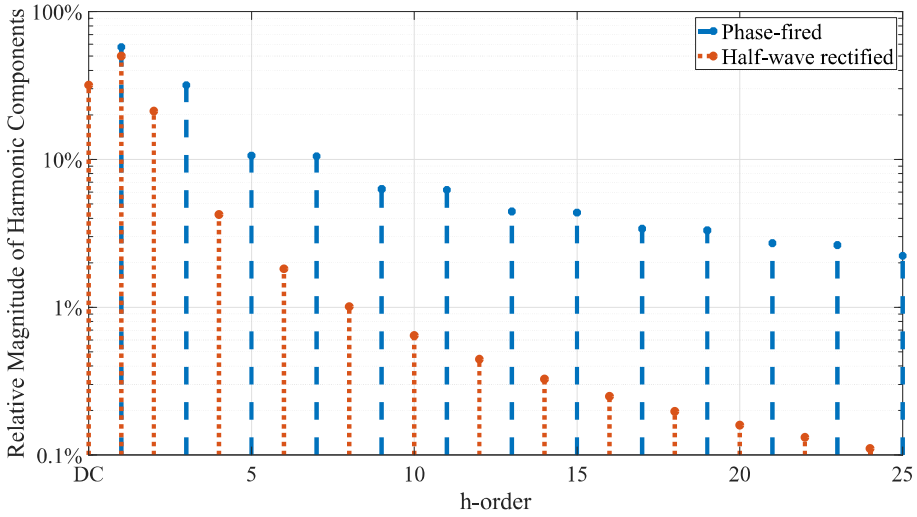

Figure 5.21 - Odd and even harmonic disturbance tests waveforms magnitude spectra defined in EN 50470-3 and IEC 62053-21.

5.3.3 Measurement system description

The experimental tests were carried out by means of the test setup illustrated in Figure 5.22, analogous to the one presented in [88], except for an additional energy meter under test (EMUT) connected in series to the current circuit and in parallel to the voltage one.

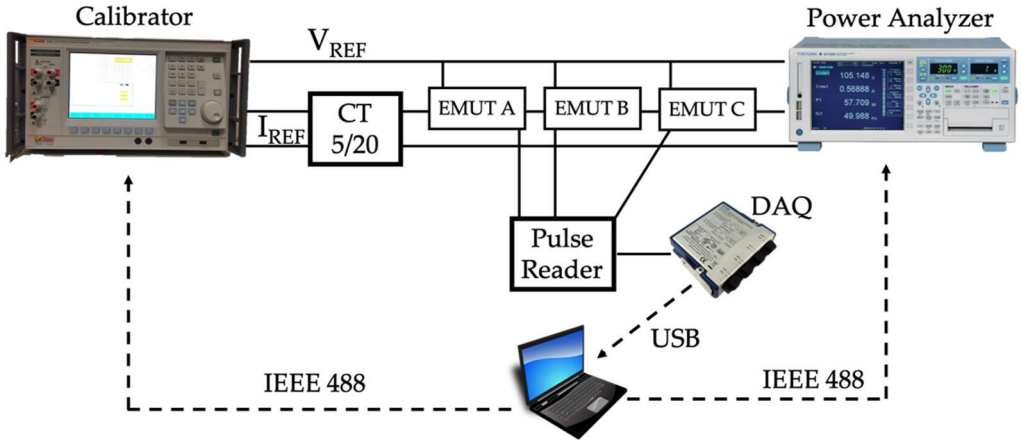

Figure 5.22 - Adopted measurement setup for testing the 3 off-the-shelf energy meters (Ems)

Since full information concerning the test setup can be found in [88], in the following just a brief summary of the employed equipment is reported and the specifications of the new EMUT are listed. A Fluke 6105A calibrator provided the reference voltage and current inputs. The voltage is directly applied across the EMUTs terminals, while the current is stepped-up by means of a 5 VA 5:20 current transformer (CT), feeding the EMUTs. A high-accuracy power analyzer Yokogawa WT3000E, of which accuracy is ± (0.01% of reading + 0.03% of range + 0.02% of time reading), served as reference for the active energy measurement. The three EMUTs, identified as EMUT A, B, and C, are single-phase MID class B compliant, according to the standard EN 50470-3. In spite of the same rated voltage U_n = 230 V and the same rated current I_{ref}= 5 A, the EMUT C maximum current I_{max} is 100 A (I_{max}= 45 A for EMUT A, I_{max} = 40 A for EMUT B) and it is equipped with a static pulsed test output at 1000 impulses per unit of energy (imp/kWh). The three test outputs have been connected to a

pulse reader, made of three signal conditioning circuits based on a photodetector (for EMUT A) and two pull-up resistors (one for EMUT B and one for the EMUT C), cascaded with logical ports acting as voltage regulators to obtain 0–5 V at the output. These three signals at the output have been acquired through a NI9239 24-bit Data Acquisition board (DAQ) connected to a host PC running the test automation.

5.3.4 Experimental tests

The tests proposed in this paragraph are aimed at evaluating the EMs behaviour when the voltage and the current are not sinusoidal. It should be highlighted that they are not only distorted waveforms, but they are also distinguished by a realistic harmonic content for an LV distribution network, considering the limits defined in the standards [9,11]. Three different tests were carried out, all of them are based on the setup sketched in Figure 5.21:

- sinusoidal waveform test (calibration measurement);
- fixed random harmonics test;
- random time-varying harmonics test.

In these three tests, detailed in the following, the calibrator generated a sinusoidal current and voltage at f_r=50 Hz. Only in the last two tests, an additional harmonic content up to the 25th harmonic was superimposed to the 50 Hz components. The relative phase displacement between voltage and current was set equal to zero for all the frequency components (pure resistive load), to focus only on the effect of the harmonic content on the active energy measurements performed by the EMs. This scenario is meaningful since the loads' power factor is very close to 1 in typical LV power networks. The current from the calibrator I_p has been stepped-up to I_s by a factor of 4 through the CT and then fed to the EMUTs. The potential of the secondary winding of the CT has been raised to U in order to obtain a phantom power supply for the EMUTs. The active energies E_{mA}, E_{mB}, and E_{mC} measured by EMUT A, EMUT B, and EMUT C, respectively, are compared against E_t, the energy measured by the reference power analyzer. The synchronization of the readings from the EMUTs and the power analyzer was implemented by starting the pulse counter acquisition in parallel with the energy computation performed by the power analyzer. The active energy readings were triggered when the electrical quantities provided by the calibrator were already in steady state. A detailed analysis on the "pulse reader + DAQ" system properties is conducted in the Appendix A section.

5.3.4.1 Sinusoidal current and voltage-calibration measurement

The first test consisted of providing a sinusoidal current (I_p= 5 A, rms) and a sinusoidal voltage (U=230 V, rms) by means of the Fluke 6105A to carry out the calibration of the EMUT C at nominal conditions and to check its measurement repeatability. Note that this operation had been already performed for EMUTs A and B in [88]. The time duration of this calibration test is about 8 hours in order to replicate the same conditions under which EMUT A and B were subjected to. Note also that such a long-duration test makes negligible the contribution to uncertainty due to the test output reading compared to the overall energy measured by the EMUT. The chosen value for I_s is 20 A since it lays between I_{ref} and I_{max} for all the three EMUTs and also because it is representative of a typical current intensity at the node where the EMs are installed in residential applications. This calibration procedure was repeated 8 times. For each repetition, the calibration coefficient $K_{EM\,C}$ was computed as:

$$K_{EM\,C} = \frac{E_{mC}}{E_t} \tag{5.14}$$

where E_{mC} is the active energy reading from EMUT C and E_t is the corresponding reading of the reference instrument. Afterwards, the computations of the mean value $\overline{K}_{EM\,C}$ and of the standard deviation of the mean $\sigma_{K_{EM\,C}}$ were carried out by evaluating the 8 values obtained by each test repetition.

The coefficient $\overline{K}_{EM\,C}$ and the ones computed in [88], $\overline{K}_{EM\,A}$ and $\overline{K}_{EM\,B}$, for EMUT A and B, respectively, have been then used to correct the E_m in all the following tests (see Section 5.2 and 5.3). The correction is performed through:

$$E^*_{m\,i} = \frac{E_{m\,i}}{\overline{K}_{EM\,i}} \tag{5.15}$$

where: i = A, B and C; $E^*_{m\,i}$ is the EMUT i's corrected active energy reading. This procedure allows assessing the effect of the considered harmonic disturbances by means of the additional percentage error $e_i^*\%$:

$$e_i^*\% = \frac{E^*_{m\,i} - E_t}{E_t} \cdot 100 \tag{5.16}$$

5.3.4.2 Fixed random harmonics

In the second test, two sets of current and voltage harmonics were randomly generated, complying with the limits prescribed by [11] for the voltage harmonics up to the 25th order in LV systems. Each voltage harmonic component was drafted from a uniform distribution that ranges from 0 to the corresponding limit presented in the EN 50160 standard. Since a pure resistive load was assumed, as mentioned above, the current harmonic relative amplitudes were analogous to the voltage ones and the overall rms value was set to I_p= 5 A. The THD of the waveforms obtained according to the described procedure were 6.2% and 5.4%, which are realistic values for current and voltage distortion according to those highlighted in the standard [9]. The experiment based on the test waveform with THD = 6.2% will be addressed as ↯1, while the one based on the test waveform with THD = 5.4% as ↯2. The magnitude spectra of the waveforms are represented in Figure 5.23 and are normalized to the 50 Hz component magnitude. The time duration of this test is about 8 h. Finally, the effects of the fixed random harmonic are evaluated by applying Equations (4) and (5).

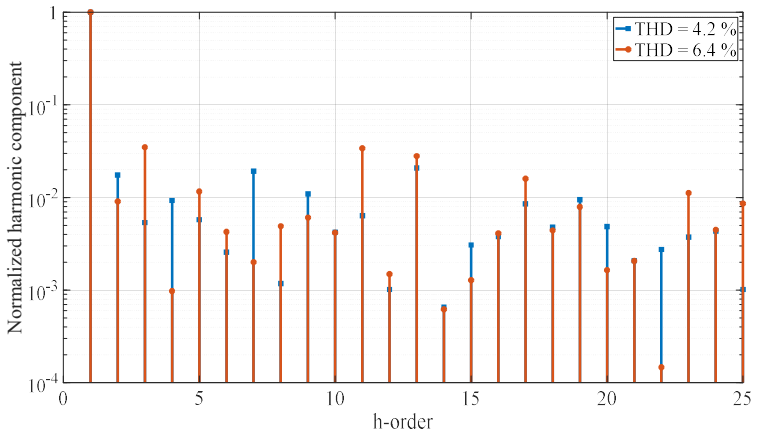

Figure 5.23 - Normalized harmonic components randomly generated for the "Fixed random harmonics" tests ↯1 (THD = 6.2%) and test ↯2 (THD = 6.4%). THD, Total Harmonic Distortion.

5.3.4.3 Random time-varying harmonic distorsion

The third test's objective is to simulate a realistic scenario in which the energy meters are subjected to a harmonic distortion that changes unpredictably over time. To achieve this, a distorted voltage and current waveforms both generated with the same technique, illustrated in Section 5.2, were applied for a short time interval (about 10 min). After that, another random waveform was applied, and so on for about 8.5 h. This operation was repeated 7 times. Finally, the effects of the random time-varying harmonic distortions are evaluated by applying Equations (4) and (5).

5.3.5 Experimental results

5.3.5.1 Sinusoidal current and voltage-calibration measurement

In Table 5.12, the data from the EMUT C calibration is reported, whereas the summary of the EMUTs' A and B results obtained in [88] are listed in Table 5.13. The percentage error $e_C\%$ has been computed according to Equation (1) and $K_{EM\,C}$ according to Equation (3). Note that, even for EMUT C, the standard deviation $\sigma_{K_{EM\,C}}$, associated to the computed average calibration coefficient, is very limited compared to the related average value $\overline{K}_{EM\,C}$ and consistent with the ones obtained for EMUT A and EMUT B in [32] and reported in Table 5.13 for the sake of readability. This result means that the EMUT A, EMUT B, and EMUT C calibration measurements are distinguished by a good repeatability (all obtained standard deviations are at least 5000 times lower than the measured quantity). Finally, a check of the accuracy class has been conducted, and since the percentage error is about 0.70%, the EMUT C has been proved to be widely compliant with the declared class (as for the EMUTs A and B).

	E_t [Wh]	E_{mC} [Wh]	$K_{EM\,C}$	$e_C\%$ [%]
	36416.0	36648	1.00637	0.64
	36419.5	36658	1.00655	0.65
	36420.8	36660	1.00657	0.66
	36423.7	36663	1.00657	0.66
	36407.3	36657	1.00686	0.69
	36406.6	36658	1.00696	0.70
	36406.7	36662	1.00701	0.70
	36406.9	36662	1.00701	0.70
$\overline{K}_{EM}$			1.00674	
$\sigma_{K_{EM}}$			$9\cdot10^{-5}$	

Table 5.12 - EMUT C calibration at nominal sinusoidal conditions.

	EMUT A	EMUT B
	0.9983	1.00892
$\sigma_{K_{EM}}$	$2\cdot10^{-5}$	$4\cdot10^{-5}$

Table 5.13 - EMUTs A and B calibration at nominal sinusoidal conditions.

5.3.5.2. Fixed random harmonics

In Table 5.14, the readings and the additional percentage errors e_i^*% (i = A, B, and C) regarding the active energy measurements for the two fixed random harmonics tests are collected. The standard uncertainty $u_{ei\,\%}$ of each additional percentage error computed for this test is shown in the top row of Table 5.15.

.

	THD [%]	E_t [Wh]	E^*_{mA} [Wh]	E^*_{mB} [Wh]	E^*_{mC} [Wh]	e^*_A% [%]	e^*_B% [%]	e^*_C% [%]
↯1	6.2	36529.1	36528.3	36476.8	36516.0	0.00	−0.15	−0.04
↯2	6.4	36532.2	36539.2	36476.8	36512.0	0.02	−0.16	−0.06

Table 5.14 - EMUTs additional percentage error at random distorted current and voltage condition

		$u_{eA\%}$ [%]	$u_{eB\%}$ [%]	$u_{eC\%}$ [%]
Fixed random harmonics	#1	0.09	0.09	0.09
	#2			
Random time-varying harmonics	#1	0.2	0.2	0.2
	#2			
	#3			
	#4			
	#5			
	#6			
	#7			

Table 5.15 - Evaluation of Standard Uncertainty for the EMUTs additional percentage errors.

Examining also the e_i^*% values in Table 5.14, it can be noticed that: first, the magnitude of EMUT B's percentage error is greater than $u_{eB\%}$ by around 2 times; second, the values of e_A^*% and e_C^*% are of the same order of magnitude of (and even smaller than) $u_{eA\%}$ and $u_{eC\%}$. Given that, the analysis of the presented values is carried out according to the following considerations. Thanks to the average calibration coefficient $\overline{K}_{EM\,C}$ definition, it is possible to express the additional percentage error e_i^*% (I = A, B, C) by Equation (5). e_i^*% is equal to zero (within the limits of the variation associated with $\overline{K}_{EM\,C}$) if $E^*_{m\,i}$ (I = A, B, C) is measured in conditions analogous to the ones of the calibration procedure. When the current and voltage distortion is introduced, the root mean square (RMS) values are the same as the ones related to the sinusoidal quantities used for the calibration. The reference energy meter is assumed to not present a significantly different behaviour in the distorted conditions, given its wide bandwidth. Therefore, any value of the e_i^*% different from zero observed in distorted conditions may be attributed to a performance downgrade of the EMs in these conditions. But first, the uncertainty associated to e_i^*% must be considered: if its confidence interval does not include zero, then it is reasonable to state that the EMs' behaviour have been affected by the introduced distortion; otherwise, if the interval includes zero, the impact of the distortion is not observable and nothing can be stated. Finally, the confidence interval has been computed as a double-sided interval centered in e_i^*% by means of the standard uncertainty.
According to the analysis above, only EMUT B shows a slight influence due to the fixed random harmonic presence, given that the relative confidence intervals are [−0.24%, −0.06%] and [−0.25%, −0.07%].

5.3.5.3 Random time-varying harmonic distorsion

In Table 5.16, there are listed the observed maximum and minimum THD values of the generated current and voltage waveforms for each test sequence.

Sequence	THD min [%]	THD max [%]
#1	3.5	6.9
#2	3.5	6.9
#3	3.8	7.0
#4	3.8	7.0
#5	3.2	6.9
#6	6.2	7.0
#7	3.7	7.5

Table 5.16 - THD range maximum and minimum values with random time-varying harmonic distorted current and voltage distortion.

For each sequence, the E^*_{mi} values, the reference energy readings E_t and the $e_i^*\%$ are shown in Table 5.17, while the standard uncertainties $u_{ei\,\%}$ of the additional percentage errors $e_i^*\%$ are reported in the bottom row of Table 5.15.

Sequence	E_t [Wh]	E^*_{mA} [Wh]	E^*_{mB} [Wh]	E^*_{mC} [Wh]	$e_A^*\%$ [%]	$e_B^*\%$ [%]	$e_C^*\%$ [%]
#1	38075.1	38201.9	38060.6	38075.5	0.3	0.0	0.0
#2	38067.3	38196.0	38060.6	38078.5	0.3	0.0	0.0
#3	38059.4	38192.0	38060.6	38067.5	0.3	0.0	0.0
#4	38061.8	38177.2	38060.6	38082.4	0.3	0.0	0.1
#5	38053.8	38167.3	38060.6	38068.5	0.3	0.0	0.0
#6	38050.9	38160.4	38060.6	38072.5	0.3	0.0	0.0
#7	38051.4	38107.9	38060.6	38079.5	0.1	0.0	0.0

Table 5.17 - EMUTs additional percentage error with random time-varying harmonic distorted current and voltage distortion.

The random current and voltage distortion variations lead to percentage error variations that are not significative for EMUT B and C: as a matter of fact, the $u_{ei\,\%}$ values define confidence intervals including zero (see observations in Section IV B). On the contrary, EMUT A exhibits a [0.1%, 0.5%] confidence interval of $e_i^*\%$ for the sequences #1 to #5. Then, it can be concluded that the effect of the test scenario where the harmonic distortion of the current and the voltage waveforms randomly evolves over the time is not negligible for the EMUT A. Finally, observing Table 5.17, one could question the fact that the uncertainties relative to the percentage errors in the random time-varying harmonic test are higher than the ones in the fixed random harmonic test. This results from the test setup. In order to change the harmonic content of the voltage and current waveforms, the calibrator outputs must be set on standby and the active energy cannot be measured during the transients between the standby and operational states because they would pollute the measurement.

Therefore, considering that each harmonic configuration shall be applied for about 10 min, the present test results in performing about 50 different measurements and then to sum the readings of each measurement. Hence, the uncertainty of the $e_i^*\%$ relative to the cumulative readings is higher than the uncertainty obtained in the fixed random harmonic cases. However, even if this uncertainty is twice the one in the fixed random harmonics case, it is still possible to observe whether the EMUTs' behaviour is affected. Of course, the variation of the measured quantity must be evaluated against its confidence interval in order to judge the experimental result.

5.3.6 Conclusions

The energy meter performances are affected by the spread of new actors among the grid, which degrade the overall power quality and the quantities to be measured. This challenging scenario and the need of more and more network observability demand new testing procedures to be developed. To this purpose, three off-the-shelf energy meters have been tested by applying distorted current and voltage waveforms. Their behaviour has been assessed computing the index prescribed by the standards to verify whether distorted conditions affect the energy meters accuracy. From the results it is possible to conclude that (i) the adopted waveforms and the measurement setup implemented allow appreciating small variations in the energy meters accuracy; (ii) not all the energy meters are affected by distorted conditions. Therefore, considering the test waveforms prescribed by the standards and the results herein presented, it can be concluded that the standards should improve in terms of incorporating more realistic test waveforms to better assess the energy meters' behaviour in realistic conditions.

6. Conclusions

This thesis provides to the reader the main concepts to understand why the monitoring of the electrical networks, with a particular attention to the low-voltage ones, is important for the assessment of the power quality and for the advent of smart grids.
In fact, after the description of the foundations on the measurement uncertainty assessment, chapter two introduces the concepts of smart grid and power quality, which are intimately connected. This chapter also introduces low-voltage monitoring systems and describes the main functions desired by DSOs for the real-time control of the networks.
Finally, chapters 4 and 5 show the 3 years PhD course results: the former describes the research and development work carried out thanks to the collaboration between the University of Bologna and REPL Italia srl, and the latter describes the scientific implications related to the R&D work.
The main topics treated can be here recapped, starting from the problems emerged to which I tried to find a possible solution:

- Need to increase the power quality and to reduce the number and the duration of interruptions of service.
- Difficulty in the monitoring of the low-voltage networks, whose topology is often not known.
- Lack in the market of complete low-cost solutions that could help the DSOs in the real-time monitoring of the LV networks

Therefore, two different devices were developed to answer to requests from the DSOs:

- The Guardian Meter: small and low-cost monitoring system for street electrical cabinets installation, able to acquire voltages and currents for the calculation of the main electrical parameters, in order to check their variations over time identifying possible problems in a specific point of the grid (as under-loader lines, over-loaded lines, unbalanced loads, non-technical losses, etc.).
  Thanks to the integrated PLC modem, the device can use the existent communication network for the revenue energy meter management to transmit data remotely.
- The Network Monitoring Unit: evolution of the Guardian Meter with additional alarm functions (over-current, unbalanced voltages), safety functions (check of the state of closure of the electrical cabinets) and power quality monitoring functions (THDv and THDi calculation and monitoring of the interruptions). Regarding the communication, the integrated GSM modem allows the remote device management though almost all smartphones.

The specifications of both solutions were elaborated after a careful analysis from the DSOs, who collaborated during the research and development phase.
The R&D work led also to some interesting scientific outcomes:

- A proposal of a design for the realization of a low-cost board for the acquisition of signal characterized by a not stable frequency, timing the conversions with a cheap PLL circuit (in order to avoid the leakage phenomenon during the Fourier analysis).
- A proposal of a procedure for the metrological characterization of the low-voltage monitoring systems.
- A proposal of a new set of tests for the evaluation of the energy meter in presence of harmonic distortion.

In conclusion, it can be affirmed that this thesis provides some ideas both for the designing of innovative devices that can help DSOs in managing networks and for the development of new standards or for the updating of the existing ones.

7. Bibliography

[1] BIPM JCGM 100:2008, "Evaluation of measurement data – Guide to the expression of uncertainty in measurement (GUM)", GUM 1995 with minor corrections (2008)

[2] BIPM JCGM 101:2008, "Evaluation of measurement data – Supplement 1 to the Guide to the expression of uncertainty in measurement – Propagation of distributions using a Monte Carlo method"

[3] C. Cecati, G. Mokryani, A. Piccolo, P. Siano, "An overview on the smart grid concept", IECON 2010 - 36th Annual Conference on IEEE Industrial Electronics Society, USA, November 2010

[4] European Technology Platform Smart Grids, "Strategic Deplomen Document for European´s Electricity Networks of the Future", Draft for 3rd General Assembly, Belgium, October 2008

[5] L. Peretto, "The role of measurements in the smart grid era", IEEE Instrumentation & Measurement Magazine, vol. 13, n. 3, pp 22-25, June 2010

[6] B.Subhash, V.Rajagopal, "Overview of smart metering system in a smart grid scenario", 2014 power and energy systems: towards sustainable energy, India, April 2014

[7] 6th CEER benchmarking report on the quality of electricity and gas supply – 2016

[8] A. Kusko, M.T. Thompson, "Power quality in electrical systems", McGraw-Hill, 2007

[9] IEEE 519, "Recommend practices and requirements for harmonic control in electric power systems"

[10] E. Gunther, "Harmonic, and interharmonic measurement according to IEEE 519 and IEC 61000-4-7", 2005/2006 IEEE/PES Transmission and Distribution Conference and Exhibition, USA, May 2006

[11] IEC 50160:2010, "Voltage characteristics of electricity supplied by public electricity networks"

[12] T. Short, "Distribution Reliability and Power Quality". CRC Press, 2006.

[13] IEC 61000-4-30:2015, "testing and measurement techniques – power quality measurement methods"

[14] IEC 61000-4-7:2002, "Testing and measurement techniques . General guide on harmonics and interharmonics measurements and instrumentation, for power supply systems and equipment connected thereto"

[15] G. Iuculano, D. Mirri, "Misure elettroniche", Cedam, 2004

[16] P. Malcovati, "appunti di Misure elettriche", 2014

[17] G. Pasini, "appunti di Misure elettriche", 2014

[18] LEM "Isolated current and voltage transducers Characteristics - Applications – Calculations", 3rd edition

[19] IEC 61869-1:2007, “Instrument transformers - Part 1: General requirements”

[20] IEC 61869-10:2017, “Instrument transformers - Part 10: Additional requirements for low-power passive current transformers”

[21] IEC 61869-11, “Instrument transformers - Part 11: Additional requirements for low power passive voltage transformers”

[22] STmicroelectronics, “STM32F101xC STM32F101xD STM32F101xE datasheet”

[23] Analog device, “ADE7880 datasheet”

[24] Analog device, “AN-1171 Application note - Calibrating a Three-Phase Energy Meter Based on the ADE7880”

[25] M. Huczala, T. Lukl, J. Misurec, “Capturing energy meter data over secured power line”, 2006 International Conference on Communication Technology, China, November 2006

[26] IEC 60870-5-102, “Telecontrol equipment and systems - Part 5: Transmission protocols - Section 102: Companion standard for the transmission of integrated totals in electric power systems”

[27] IEC 61010-1:2010, “Safety requirements for electrical equipment for measurement, control, and laboratory use - General requirements”

[28] IEC 61010-2-30:2010, “Safety requirements for electrical equipment for measurement, control, and laboratory use - Particular requirements for testing and measuring circuits”

[29] STmicroelectronics, “STM32F411xC STM32F411xE datasheet”

[30] Fluke Calibration, “Electrical Power Quality Calibrator” 6105A datasheet, Sept. 2009.

[31] Fluke Calibration, “Transconductance Amplifier” 52120A datasheet, Sept. 2012

[32] EN 50160:2011, “Voltage characteristics of electricity supplied by public electricity networks”, European committee for standardization, Brussels, 2017.

[33] A. Mingotti, L. Peretto, R. Tinarelli, “An equivalent synchronization for phasors measurements in Power Networks”, Proceedings of IEEE International Workshop on Applied Measurements for Power Sytstem (AMPS), Liverpool, Sept. 2017.

[34] A. Mingotti, L. Peretto, R. Tinarelli, “Uncertainty Analysis of an Equivalent Synchronization Method for Phasor Measurements”, IEEE Transaction on Instrumentation and Measurement, vol. 67, n. 10, pp. 2444-2452, April 2018.

[35] L. Bartolomei, A. Mingotti, L. Peretto, R. Tinarelli, P. Rinaldi, “Accuracy verification of PLL-based acquisition system for low-cost applications”, Proceedings of IEEE International Workshop on Applied Measurements for Power Sytstem (AMPS), Bologna, Sept. 2018.

[36] S. Sousa, M. Onofre, T. Antunes, C. Branco, J. Maia, J. I. Rocha, V. F. Pires, "Implementation of a low cost data acquisition board for photovoltaic arrays analysis and diagnostic", International Conference on Renewable Energy Reasearch and Applications, Madrid, Oct. 2013.

[37] Y. C. Chen, H. Y. Shen, H. Y. Chen, C. H. Hsu, "Low Cost Arduino DAQ Development and Implementation on an Android App for Power Frequency Measurement", International Symposium on Computer, Consumer and Control, Xi'an, July 2016.

[38] A. E. Beltràn, "Low-cost acquisition and development board. An open source hardware proposal", Symposium of Signals, Images and Artificial Vision, Bogota, Sept. 2013.

[39] R. Barioul, S. F. Ghribi, O. Kanoun, "A low cost signal acquisition board design for myopathy's EMG database construction", 13th International Multi-Conference on Systems, Signals & Devices, Leipzig, Mar. 2016.

[40] C. C. Inwai, J. Mungkornassawakul, "A Smart Recording Power Analyzer Prototype Using LabVIEW and Low-Cost Data Acquisition (DAQ) in Being a Smart Renewable Monitoring System", IEEE Green Technologies Conference, Denver, April 2013.

[41] M. Jalalifar, G. S. Byun, "A Wide-Range Low-Power PLL-Based PI Multiphase Generator Using Adaptive Frequency Tracking Technique", IEEE Transaction on Circuits and Systems II: Express Briefs, early access, 2017.

[42] L. Zheng, S. Quan, L. Huang, K. Yang, Y. Xiong, J. Quan, "Research on frequency conversion PLL for three-phase unbalanced and harmonic power system", 32nd Youth Academic Annual Conference of Chinese Association of Automation, Hefei, May 2017.

[43] L. Bartolomei, A. Mingotti, L. Peretto, R. Tinarelli, P. Rinaldi, G. Pasini, L. Puddu, "Performance evaluation of an energy meter for low-voltage system monitoring", Proceedings of International Measurement Confederation (IMEKO), Belfast, Sept 2018.

[44] C. Thanga Raj, P. Agarwal, S. P. Srivastava, "Performance analysis of a three-phase squirrel-cage induction motor under unbalanced sinusoidal and balanced non-sinusoidal supply voltages", International Conference on Power Electronics, Drives and Energy Systems, 2006.

[45] B. Suechoey, S. Tadsuan, C. Thammarat, M. Leelajindakraireak, "Estimation of core loss transformer under non-sinusoidal voltage supply", IEEE Internation Conference on Power System Technology, vol. 1, pp. 511-516, 2004.

[46] W. G. Ariastina, T. R. Blackburn, "PD distribution in aged oil insulation using non sinusoidal voltage supply", IEEE 9th International Conference on the Properties and Applications of Dielectric Materials, pp. 517-520, 2009.

[47] P. Tenti, A. Costabeber, P. Mattavelli, F. P. Marafao, H. K. M. Paredes, "Load characterization and revenue metering under non-sinusoidal and asymmetrical operation", IEEE Transaction on Instrumentation and Measurement, vol. 63, n. 2, pp. 422-431, Feb. 2014.

[48] G. D'Antona, A. Ferrero, R. Ottoboni, "Improvement of metrological performance for low-cost DSP-based board with analog interface circuit", IEEE Transaction on Instrumentation and Measurement, vol. 48, n. 6, pp. 1278-1281,1999.

[49] D. W. Braudaway, "Uncertainty specification for data acquisition (DAQ) devices", IEEE Transaction on Instrumentation and Measurement, vol. 55, n. 1, pp. 74-78, 2006.

[50] F. Alegria, P. Girao, V. Haasz, A. Serra, "Performance of data acquisition systems from the user's point of view", IEEE Transaction on Instrumentation and Measurement, vol. 53, n. 4, pp. 907-914, 2004.

[51] EN 62008:2005, "Performance characteristics and calibration methods for digital data acquisition systems and relevant software", European committee for standardization, Brussels, 2018.

[52] G. D'Antona, A. Ferrero, Digital Signal Processing for Measurement Systems: Theory And Applications, Springer Verlag, 2010.

[53] V. Matthews, D. Youn, "Spectral leakage suppression properties of linear and quadratic windowing", IEEE Transactions on Acoustics, Speech and Signal Processing, vol. 32, n. 5, pp. 1092-1095, Oct. 1984.

[54] T. Claeys, D. Vanoost, J. Peuteman, G. A. E. Vandenbosch, D. Pissoort, "An Iterative Interpolated DFT to Remove Spectral Leakage in Time-Domain Near-Field Scanning", IEEE Transactions on Electromagnetic Compatibility, vol. 60, n. 1, pp. 202-210, May 2017.

[55] F. J. Harris, "On the use of windows for harmonic analysis with the discrete Fourier transform", Proceedings of IEEE, vol. 66, n. 1, pp. 51-83, Jan 1968

[56] Semiconductor CMOS Micropower-SCHS043B, Texas Instruments Dallas, Texas 75265, Data sheet, July 2003.

[57] IEC 61869-2:2011, "Instrument transformers - Part 2: Additional requirements for current transformers", International Standardization Organization, Geneva, Switzerland, 2011.

[58] IEC 61869-3:2011, "Instrument transformers - Part 3: Additional requirements for inductive voltage transformers", International Standardization Organization, Geneva, Switzerland, 2011.

[59] Qianjun, Y.; Guichu, W.; Fenqun, Y.; Hongyan, X. Design and applications of intelligent low voltage distribution system based on ZigBee. In Proceedings of the International Conference on Electronics, Communications and Control, Ningbo, China, 9–11 September 2011.

[60] Löf, A.; Repo, S.; Pikkarainen, M.; Lu, S.; Pöhö, T. Low voltage network monitoring in RTDS environment. In Proceedings of the IEEE PES ISGT Europe, Lyngby, Denmark, 12–15 October 2013.

[61] Lu, S.; Repo, S.; Della Giustina, D.; Figuerola, F.A.C.; Löf, A.; Pikkarainen, M. Real-Time Low Voltage Network Monitoring—ICT Architecture and Field Test Experience. IEEE Trans. Smart Grid 2015, 6, 2002-2012.

[62] Mingotti, A.; Ghaderi, A.; Mazzanti, G.; Peretto, L.; Tinarelli, R.; Valtorta, G.; Danesi, S. Low-cost monitoring unit for MV cable joints diagnostics. In Proceedings of the 9th IEEE International Workshop on Applied Measurements for Power Systems (AMPS 2018), Bologna, Italy, 26–28 September 2018.

[63] Mingotti, A., Ghaderi, A., Peretto, L., Tinarelli, R., & Lama, F. (2018). Test setup design, and calibration for tan delta measurements on MV cable joints. Paper presented at the 9th IEEE International Workshop on Applied Measurements for Power Systems, AMPS 2018 – Proceedings.

[64] Farhangi, H. The path of the smart grid. IEEE Power and Energy Magazine 2010, 8, 18-28.

[65] Sanchez, R.; Iov, F.; Kemal, M.; Stefan, M.; Olsen, R. Observability of low voltage grids: Actual DSOs challenges and research questions. In Proceedings of the 52nd International Universities Power Engineering Conference (UPEC), Heraklion, Greece, 28–31 August 2017.

[66] Al-Wakeel, A.; Wu, J.; Jenkins, N. State estimation of medium voltage distribution networks using smart meter measurements. Applied Energy 2016, 184, 207-218.

[67] Mingotti, A.; Peretto, L.; Tinarelli, R. A Novel Equivalent Power Network Impedance Approach for Assessing the Time Reference in Asynchronous Measurements. In Proceedings of the 2017 IEEE International Instrumentation and Measurement Technology Conference, I2MTC, Torino, Italy, 22–25 May 2017; pp. 624–629.

[68] Nasrollahi, S.; Sardarabadi, A.; Khoshian, Y.; Gharib, A. A novel hybrid algorithm for reconfiguration problem of the distribution networks. In Proceedings of the 22nd International Conference and Exhibition on Electricity Distribution, Stockholm, Sweden, 10–13 June 2013.

[69] Liu, Y.; Wang, Z.; Meng, X.; Sheng, W. Distribution network planning considering distributed generations based on genetic algorithm. In Proceedings of the IEEE Power Engineering and Automation Conference, Wuhan, China, 8–9 September 2011.

[70] Zhang, J.; Huang, T.; Zhang, H. The Reactive Power Optimization of Distribution Network Based on an Improved Genetic Algorithm. In Proceedings of the IEEE/PES Transmission & Distribution Conference & Exposition: Asia and Pacific, Dalian, China, 18 August 2005.

[71] Ferrero, A.; Faifer, M.; Salicone, S. On Testing the Electronic Revenue Energy Meters. IEEE Transactions on Instrumentation and Measurement 2009, 58, 3042-3049.

[72] Sun, Q.; Li, H.; Ma, Z.; Wang, C.; Campillo, J.; Zhang, Q.; Wallin, F.; Guo, J. A Comprehensive Review of Smart Energy Meters in Intelligent Energy Networks. IEEE Internet of Things Journal 2016, 3, 464-479.

[73] Cetina, R.Q.; Roscoe, A.J.; Wright, P.S. A review of electrical metering accuracy standards in the context of dynamic power quality conditions of the grid. In Proceedings of the 2017 52nd International Universities Power Engineering Conference (UPEC), Heraklion, Greece, 28–31 August 2017.

[74] Ferrero, A.; Peretto, L.; Sasdelli, R. Revenue metering in the presence of distortion and unbalance: myths and reality. In Proceedings of the 8th International Conference on Harmonics and Quality of Power. Proceedings (Cat. No.98EX227), Athens, Greece, 14–16 October 1998; pp. 42–47

[75] Bernieri, A.; Betta, G.; Ferrigno, L.; Laracca, M. Electrical energy metering in compliance with recent european standards. In Proceedings of the 2012 IEEE International Instrumentation

and Measurement Technology Conference Proceedings, Graz, Austria, 13–16 May 2012; pp. 1541–1545.

[76] Novotny, J.; Drapela, J.; Topolanek, D.Frequency response of revenue meters in measured active energy. In Proceedings of the 2016 17th International Conference on Harmonics and Quality of Power (ICHQP), Belo Horizonte, Brazil, 16–19 October 2016; pp. 524–529.

[77] Femine, A.D.; Gallo, D.; Landi, C.; Luiso, M. Advanced Instrument for Field Calibration of Electrical Energy Meters. IEEE Transactions on Instrumentation and Measurement 2009, 58, 618-625.

[78] Cataliotti, A.; Cosentino, V.; Nuccio, S. Static Meters for the Reactive Energy in the Presence of Harmonics: An Experimental Metrological Characterization. IEEE Transactions on Instrumentation and Measurement 2009, 58, 2574-2579.

[79] Cataliotti, A.; Cosentino, V.; Lipari, A.; Nuccio, S. Metrological Characterization and Operating Principle Identification of Static Meters for Reactive Energy: An Experimental Approach Under Nonsinusoidal Test Conditions. IEEE Transactions on Instrumentation and Measurement 2009, 58, 1427-1435.

[80] Gallo, D.; Landi, C.; Pasquino, N.; Polese, N. A New Methodological Approach to Quality Assurance of Energy Meters under Nonsinusoidal Conditions. IEEE Transactions on Instrumentation and Measurement 2007, 56, 1694-1702.

[81] Georgakopoulos, D.; Wright, P.S. Calibration of energy and power meters under non-sinusoidal conditions. IEE Proceedings Science, Measurement and Technology 2006, 153, 241-247.

[82] Mingotti, A.; Peretto, L.; Tinarelli, R.; Zhang, J. Use of COMTRADE Fault Current Data to Test Inductive Current Transformers. In Proceedings of the IEEE Workshop on Metrology for Industry 4.0 and IoT, Naples, Italy, 4–6 June 2019.

[83] Rietveld, G.; Sloot, W.; So, E.; Guo, X.; Mubarak, F.; de Geus, J.; van Halm, F.; Wismans, B.; Bruijns, S.; Koers, F.; et al. Performance evaluation of HV CTs subjected to actual operating conditions in substations and its impact on smart metering infrastructure within smart grids. In Proceedings of the IEEE Power and Energy Society General Meeting, San Diego, CA, USA, 22–26 July 2012.

[84] So, E.; Arseneau, R.; Bennett, D.; Frigault, M. A current-comparator-based system for calibrating high voltage conventional and non-conventional current transformers under actual operating conditions of high voltage and distorted current waveforms up to 100 kV and 2000 A. In Proceedings of the CPEM 2010 Daejeon, South Korea, 13–18 June 2010.

[85] Mahesh, G.; George, B.; Jayashankar, V.; Kumar, V.J. Instrument transformer performance under distorted-conditions. In Proceedings of the IEEE INDICON 2004 First India Annual Conference, Kharagpur, India, 20–22 December 2004.

[86] Lei, T.; Cristaldi, L.; Faifer, M.; Ottoboni, R.; Toscani, S.; Cherbaucich, C.; Mazza, P. Behavior of voltage transformers under distorted conditions. In Proceedings of the International Instrumentation and Measurement Technology Conference, Taipei, Taiwan, 23–26 May 2016.

[87] Dichiarazione di Conformità Alla Direttiva 2014/53/UE “RED”, e-Distribuzione S.p.A. 2017.

[88] Bartolomei, L.; Cavaliere, D.; Mingotti, A.; Peretto, L.; Tinarelli, R. Testing of Electrical Energy Meters in Off-Nominal Frequency Conditions. In Proceedings of the 2019 IEEE 10th International Workshop on Applied Measurements for Power Systems (AMPS), Aachen, Germany, 25–27 September 2019.

[89] EU Directive on Measuring Instruments (MID); 2014/32/EU; European Parliament and of the Council: Brussels, Belgium, 2014.

[90] Electricity Metering Equipment (A.C.)—Part 1: General Requirements, Tests and Test Conditions—Metering Equipment (Class Indexes A, B and C); EN 50470-1:2006+A1:2018; CENELEC: Brussels, 2018.

[91] Electricity Metering Equipment (A.C.)—Part 2: Particular Requirements—Electromechanical Meters for Active Energy (Class Indexes A and B); EN 50470-2:2006+A1:2018; CENELEC: Brussels, 2018.

[92] Electricity Metering Equipment (A.C.)—Part 3: Particular Requirements—Static Meters for Active Energy (Class Indexes A, B and C); EN 50470-3:2006+A1:2018; CENELEC: Brussels, 2018.

[93] Electricity Metering Equipment (AC)—General Requirements, Tests and Test Conditions—Part 11: Metering Equipment; IEC 62052-11:2003+A1:2016; IEC: Geneva, Switzerland, 2016.

[94] Electricity Metering Equipment (A.C.)—Particular Requirements—Part 21: Static Meters for Active Energy (Class 1 and 2); IEC 62053-21:2003/A1:2016; IEC: Geneva, Switzerland, 2016.

[95] Electricity Metering Equipment (A.C.)—Particular Requirements—Part 21: Static Meters for Active Energy (Class 0, 2S and 0, 5S); IEC 62053-22:2003+A1:2016; IEC: Geneva, Switzerland, 2016.

[96] Electricity Metering Equipment (A.C.)—Particular Requirements—Part 31: Pulse output Devices for Electromechanical and Electronic Meters (Two Wires only); IEC 62053-31:1998; IEC: Geneva, Switzerland, 1998.

[97] Bartolomei L., Mingotti A., Peretto L., Tinarelli R., Rinaldi P., “Performance Evaluation and Comparison of a Low-Cost, PLL-Based Acquisition System under Off-Nominal Conditions”, IEEE Transactions on Instrumentation and Measurement, 2020

[98] Bartolomei L., Mingotti A., Pasini G., Peretto L., Rinaldi P., Tinarelli R., Puddu L. “Performance evaluation of an energy meter for low-voltage system monitoring”, Journal of Physics: Conference Series, 2018

[99] Bartolomei L., Cavaliere D., Mingotti A., Peretto L., Tinarelli R., “Testing of electrical energy meters subject to realistic distorted voltages and currents”, Energies, 2020

8. LIST OF FIGURES

Fig. 2.1. Automation functions of a smart grid

Fig. 2.2. RGDM

Fig. 2.3. Smart terminations

Fig. 2.4. Smart termination installed in a MV/LV substation

Fig. 2.5. Example of a fault in the LV network

Fig. 2.6. Inter-harmonic limit values

Fig. 2.7. Voltage dip

Fig. 2.8. Voltage swell

Fig. 2.9. Notching

Fig. 2.10. Interruption

Fig. 3.1. Scheme for current measurement through a shunt

Fig. 3.2. Commercial current transformer

Fig. 3.3. Equivalent scheme of a transformer

Fig. 3.4. CT vectorial diagram

Fig. 3.5. Rogowski coil

Fig. 3.6. Commercial openable Rogowski coils

Fig. 3.7. Hall element

Fig. 3.8. Scheme of the open-loop Hall effect current sensor

Fig. 3.9. Scheme of the closed-loop Hall effect current sensor

Fig. 3.10. Types of dividers expected by the IEC 61869-11 standard

Fig. 3.11. Surface-mounted resistors

Fig. 3.12. Scheme of Hall effect voltage sensor

Fig. 3.13. Commercial Hall effect voltage sensor

Fig. 4.1. Development procedure

Fig. 4.2. Street electrical cabinets

Fig. 4.3. “Inside” an electrical cabinet

Fig. 4.4. Guardian Meter

Fig. 4.5. Openable Rogowski coil
Fig. 4.6. Hypothetical situation of connections between customers and substations
Fig. 4.7. Block diagram (Guardian Meter)
Fig. 4.8. Measurement profile
Fig. 4.9. Energy profile
Fig. 4.10. Calibration setup
Fig. 4.11. Window for PLC communication
Fig. 4.12. Scheme of automatic system for meters reading
Fig. 4.13. Possible phase displacement for the carrier in 8-PSK modulation
Fig. 4.14. Evaluation of the results (Guardian Meter characterization)
Fig. 4.15. NMU first prototype
Fig. 4.16. NMU final version
Fig. 4.17. Openable Rogowski coil and voltage plug
Fig. 4.18. Block Diagram of the NMU
Fig. 4.19. Firmware flow diagram (NMU)
Fig. 4.20. Android application screenshots (NMU)
Fig. 4.21. PhpMyAdmin interface
Fig. 4.22. Block diagram of the system for central server storage
Fig. 4.23. Test setup (metrological characterization of the NMU)
Fig. 5.1. I(jω) and S_p (jω) when the synchronous sampling condition is met
Fig. 5.2. I(jω) and S_p (jω) when the synchronous sampling condition is not met
Fig. 5.3. Schematic representation of Acquisition System proposed
Fig. 5.4. PLL general schematic representation
Fig. 5.5. Block diagram of the microcontroller acquisition stage
Fig. 5.6. Automatic measurement setup for the tests performed with the 3 Device Under Test (DUT)
Fig. 5.7. AS Frequency characterization results either when the PLL feature is activated or not
Fig. 5.8. AS Harmonic characterization results either when the PLL feature is activated or not
Fig. 5.9. AS Frequency characterization results comparison among the DUTs

Fig. 5.10. Comparison of the standard deviation obtained from the frequency characterisation, for the 3 DUTs

Fig. 5.11. Harmonic characterization results comparison among the DUTs at 50 Hz fundamental frequency

Fig. 5.12. Harmonic characterization (with 30 ° phase shift) results comparison among the DUTs at 50 Hz fundamental frequency

Fig. 5.13. Harmonic characterization results comparison among the DUTs at 48.55 Hz fundamental frequency

Fig. 5.14. Harmonic characterization results comparison among the DUTs at 51.45 Hz fundamental frequency

Fig. 5.15. Results of the windowing application results comparison among the DUTs

Fig. 5.16. prototype of Guardian meter

Fig. 5.17. Schematic representation of the designed energy meter

Fig. 5.18. Schematic representation of the measurement setup

Fig. 5.19. Calibration curves of active power vs. voltage (a), current (b), frequency (c) and power factor (d)

Fig. 5.20. Odd and even harmonic disturbance tests waveforms defined in EN 50470-3 and IEC 62053-21

Fig. 5.21. Odd and even harmonic disturbance tests waveforms magnitude spectra defined in EN 50470-3 and IEC 62053-21.

Fig. 5.22. Adopted measurement setup for testing the 3 off-the-shelf energy meters (Ems)

Fig. 5.23. Normalized harmonic components randomly generated for the “Fixed random harmonics” tests ↯1 (THD = 6.2%) and test ↯2 (THD = 6.4%). THD, Total Harmonic Distortion.

9. LIST OF TABLES

Tab. 2.1. Voltage harmonic limit values

Tab. 2.2. Current harmonic limit values

Tab. 2.3. Interharmonic limit values

Tab. 2.4. Harmonic limit values

Tab. 3.1. Current transformer ratio and phase errors

Tab. 4.1. Frequency ranges for PLC communication

Tab. 4.2. Test points (metrological characterization Guardian Meter – instantaneous parameters)

From Tab. 4.3 to Tab. 4.10 Results (metrological characterization Guardian Meter – instantaneous parameters)

Tab. 4.11. Test points test points (metrological characterization Guardian Meter – energies)

From Tab 4.12 to Tab 4.14. Results (metrological characterization Guardian Meter – energies)

Tab. 4.15. Reference values (Guardian Meter metrological characterization)

Tab. 4.16. Test points (NMU metrological characterization – instantaneous parameters)

Tab. 4.17. Electrical standard characteristics

From Tab 4.18 to Tab 4.36. Results (NMU metrological characterization – instantaneous parameters)

Tab. 4.37. Test points (NMU metrological characterization – energies)

From Tab 4.38 to Tab 4.40. Results (NMU metrological characterization – energies)

Tab. 4.41. Test points (NMU - Metrological performance vs temperature)

From Tab 4.42 to Tab 4.47. Results (NMU - Metrological performance vs temperature)

From Tab 4.48 to Tab 4.49. Results (NMU – harmonic distortion tests)

Tab. 4.49. Acceptable range (NMU)

Tab. 5.1. Microcontroller characteristics (AS)

Tab. 5.2. Main characteristics of the NI 9239

Tab. 5.3. Main characteristics of the NI 9215

Tab. 5.4. Amplitude characterization results

Tab. 5.5. List of harmonics superimposed to the fundamental

Tab. 5.6. DUT comparison of the amplitude

Tab. 5.7. DUT comparison of the multiple harmonics presence test results

Tab. 5.8. Indexes of the calibration curves of the active power

Tab. 5.9. Percentage error limits defined by EN 50470

Tab. 5.10. Percentage error limits defined by IEC 62053-21, -22

Tab. 5.11. Additional percentage error limits for the harmonic disturbance tests regarding the accuracy classes A, B, C (EN 50470-3) and 2, 1, 0.5S, 0.2S (IEC 62053-21, -22)

Tab. 5.12. EMUT C calibration at nominal sinusoidal conditions.

Tab. 5.13. EMUTs A and B calibration at nominal sinusoidal conditions.

Tab. 5.14. EMUTs additional percentage error at random distorted current and voltage condition

Tab. 5.15. Evaluation of Standard Uncertainty for the EMUTs additional percentage errors.

Tab. 5.16. THD range maximum and minimum values with random time-varying harmonic distorted current and voltage distortion.

Tab. 5.17. EMUTs additional percentage error with random time-varying harmonic distorted current and voltage distortion.

10. LYST OF ACRONYSM

GUM	Guide to the expression of uncertainty in measurements
LV	Low-voltage
PLC	Power line communication
MTBF	Mean time between failures
MTTR	Mean time to repair
RGDM	Rivelatore di guasto direzionale e misura
THD	Total harmonic distortion
CEER	Council of European Energy Regulators
IEEE	Institute of Electrical and Electronics Engineers
IEC	International Electrotechnical Commission
PCC	Point of common coupling
RMS	Root mean square
SAIDI	System average interruption duration index
SAIFI	System average interruption frequency index
ENS	Energy not supplied
MAIFI	Momentary average interruption duration index
UTC	Coordinated universal time
CT	Current transformer
DSO	Distribution system operator
IC	Integrated circuit
DSP	Digital signal processor.
RTC	Real time clock
DUT	Device under test
NMU	Network monitoring unit
NFC	Near field communication
SMS	Short message service
MCU	MicroController unit

EEPROM	Electrically erasable programmable read-only memory
GPS	Global positioning system
GSM	Global system for mobile communication
GPRS	General packet radio service
PLL	Phase-locked loop
ADC	Analog to digital converter
TSO	Transmission system operator
AS	Acquisition system
USB	Universal serial bus
UART	Universal asynchronous receiver-transmitter
DFT	Discrete Fourier transform
PC	Personal computer
NI	National Instruments
EMUT	Energy meter under test
MID	Measuring instruments directive